



GlobAlbedo Final Product Validation Report

Author: J-P. Muller

TITLE: GlobAlbedo Final Validation Report

Document Number: GlobAlbedo_FVR_V1.2 Date 16/07/13

Distribution:

ESA	O. Leonard	<input checked="" type="checkbox"/>
	S. Pinnock	<input checked="" type="checkbox"/>
University College London	J-P. Muller	<input checked="" type="checkbox"/>
	T. Kennedy	<input checked="" type="checkbox"/>
	P. Lewis	<input checked="" type="checkbox"/>
	S. Kharbouche	<input checked="" type="checkbox"/>
	D. Fisher	<input checked="" type="checkbox"/>
Swansea	P. North	<input checked="" type="checkbox"/>
	A. Heckel	<input checked="" type="checkbox"/>
Free University of Berlin	J. Fisher	<input checked="" type="checkbox"/>
	L.Guanter	<input checked="" type="checkbox"/>
Brockmann Consult	C. Brockmann	<input checked="" type="checkbox"/>
	O. Danne	<input checked="" type="checkbox"/>
	N. Fomferra	<input checked="" type="checkbox"/>

Author:

Date:

Manager/Project Office

Date:

PA:

Date:



Title: GlobAlbedo Final Validation Report

Doc. No. GlobAlbedo_FVR_V1.2

CHANGE RECORD

ISSUE	DATE	PAGES CHANGED	COMMENTS
1.0	26/6/13	First issue	First issue
1.1	7/7/13	Response to RIDs of 3/7/13	CCN aspects removed. Figures 4,5,6,46,47,62,66 verified as being present. Added new section 11.1 on artifacts
1.2	16/7/13	Further response to RIDs	Updated time series plots with EPS versions

CONTRIBUTORS

Author Names	Organisation
J.-P. Muller, N. Shane, G. Lopez, D. Fisher, S. Kharbouche	UCL MSSL
O. Danne, C. Brockmann, U. Krämer, M. Zühlke,	Brockmann Consult
A. Heckel, P. North	Swansea University
C. Domenech, L. Guanter, J. Fischer	Freie Universität Berlin
Z. Wang and C. Schaaf	Boston University (data contributions)
Alessandro Cescatti	JRC Ispra Fluxnet*Database

**This work used tower albedometer data acquired by the FLUXNET community and in particular by the following networks: AmeriFlux (U.S. Department of Energy, Biological and Environmental Research, Terrestrial Carbon Program (DE-FG02-04ER63917 and DE-FG02-04ER63911)), AfriFlux, AsiaFlux, CarboAfrica, CarboEuropeIP, Carboltaly, CarboMont, ChinaFlux, Fluxnet-Canada (supported by CFCAS, NSERC, BIOCAP, Environment Canada, and NRCan), GreenGrass, KoFlux, LBA, NECC, OzFlux, TCOS-Siberia, USCCC.*

We acknowledge the financial support to the tower albedometer data harmonization provided by CarboEuropeIP, FAO-GTOS-TCO, iLEAPS, Max Planck Institute for Biogeochemistry, National Science Foundation, University of Tuscia, Université Laval and Environment Canada and US Department of Energy and the database development and technical support from Berkeley Water Center, Lawrence Berkeley National Laboratory, Microsoft Research eScience, Oak Ridge National Laboratory, University of California - Berkeley, University of Virginia.



1 Executive Summary

Validation of EO products is usually defined as the assessment with respect to independent data such as upscaled ground measurements and other EO datasets. In the case of the GlobAlbedo products, validation has been performed both of albedo and of intermediate products in the processing chain to ensure that a full audit trail can be established so that any errors or artefacts seen further down the chain can be traced back to their origin. These intermediate products include (a) AATSR forward-to-nadir co-registration (part of CCN1); (b) AATSR nadir-to-MERIS co-registration and subsequent geocoding of AATSR products (part of CCN1); (c) sensor inter-calibration coefficients used for narrowband-to-broadband conversion to ensure that all the BBDRs are consistent; (d) pixel classification into cloud or snow to ensure that snow pixels are included in the final GlobAlbedo product; (e) Aerosol Optical Depth (AOD) derived from the input sensors to ensure that consistent atmospheric correction will be performed; (f) BBDRs to ensure that the BBDRs were consistent and finally; (e) the DHR and BHR and the derived Blue Sky Albedo (BlueSA) when data on atmospheric transmission is available. Here the AOD is taken from VEGETATION-AOD retrievals. A summary of the results is here presented based on the year 2005 for these intermediate products and for 2007 for a new sea-ice mask developed within the GlobAlbedo CCN-1.

Extensive worldwide inter-comparisons of the automated AATSR nadir-to-forward co-registration (see ATBD D-20 for algorithm description) and AATSR nadir-to-MERIS co-registration is demonstrated with the former being shown to be pixel-level accuracy and the latter accurate to sub-pixel. However, results are shown for looking at the impact of AATSR nadir and forward on the resultant albedo which suggests that AATSR forward is too resolution and will have a deleterious impact on spatial resolution of the final GlobAlbedo product. This suggests that it might be possible to consider inclusion of AATSR nadir in future.

The radiometric inter-sensor calibration coefficients are similar to the ones that have been generated by RAL for previous years using different numbers of pixels. The values are within each other's error bars and so are considered to be consistent. Inter-comparison of MERIS and VGT BBDRs do indicate that for one tile, VGT have higher BBDR values than MERIS but for all other tiles examined they are within each others' uncertainty estimates. Agreement is slightly worse in the NIR of VIS or SW.

An assessment of the cloud detection method using the Pixel identification method (IDEPIX) provided realistic results for various atmospheric conditions and allowed for adequate classification of clouds. It was shown that even the challenging cloud detection over snow and ice can be improved, especially for SPOT VGT. Seasonal and regional distinction was demonstrated to be a valuable step towards a comprehensive validation of pixel classification results. A reasonable agreement with the corresponding MODIS results improves confidence in the Idepix classification. However, it is noted that it is extremely difficult to evaluate the identification of cloud or snow pixels based on a limited number of case studies. From experience, good pixel classification results are strongly dependent on the threshold tuning. Therefore, further improvements could be achieved if more fine tuning of thresholds would be performed. This in turn requires more data than has been used up to now for validation. For a more systematic evaluation of the cloud detection, a



higher level product assessment is definitely needed. Significant progress has been achieved using a very simple algorithm to combine AATSR and MERIS to detect sea-ice and its qualitative as well as quantitative assessment is shown here.

The validation of AOT and SDR/BBDR provided indirect insights into the performance of the pixel classification. Misclassified pixels lead to artefacts in these higher level products (bright spots, borders around coastline) or unrealistic high/low values. In particular, the aerosol retrieval is sensitive to insufficiently screened sub-pixel clouds, by increasing the aerosol optical thickness. This was obvious through the inter-comparison of AOT with other instruments and ground based measurements.

An assessment of AOD time series globally with AERONET for the whole of 2005 indicated that VGT and MERIS AOD retrievals were generally statistically significant except for barren and shrub IGBP land cover classes and they were generally higher than corresponding values from AERONET. The uncertainty estimates were also not within the actual error bars as defined by the comparison with AERONET.

The main findings of the BBDR validation exercise are for SDR retrieval that the GlobAlbedo MERIS SDR agrees well with the SCAPE-M processor. There is a good correspondence of MERIS FR SDRs with coincident CHRIS/PROBA SDRs over homogeneous areas. For the Narrow-to-Broadband conversion, it appears there are no instrument-dependent biases in the GlobAlbedo N2B conversion and a very good correspondence with MODIS' Liang N2B approach. For BBDR consistency, there are no apparent biases between MERIS and VGT BBDRs. A positive bias was detected in AATSR-nadir with respect to MERIS and VGT. With one exception, BBDR uncertainties from MERIS were within the corresponding values from VGT.

GlobAlbedo products have been assessed for 11 so-called "validation tiles", incorporating 44 tower sites of which 20 were European Fluxnet sites, 8 were US SURFRAD sites, 1 was a BSRN site and 12 were US AmeriFLUX sites with data only for 2005. These tower and GlobAlbedo products were also compared with, where visible, the METEOSAT First Generation disk products as well as global products from MODIS, MISR and Geoland2. Preliminary conclusions are that for "no-snow" and many "snow" products, the GlobAlbedo-derived Blue-Sky albedo values are in better agreement, than the MODIS Collection 5 priors and the Collection 5 8-daily results, with the tower albedometer measurements of the ground area around the towers. For global analyses, GlobAlbedo albedos are in better agreement with MODIS than MISR. The reason for this is currently not known. The estimated uncertainty of each albedo appears to be reasonable at present but is positively correlated for GlobAlbedo with the albedo value. Land cover analysis of albedos indicates that there is little difference between different vegetation types using broadband albedos for the tiles studied. Triple collocation appears to be a potentially useful technique for analysing systematic errors due to issues within the albedos such as residual clouds, snow-cloud contamination and sample numbers. This analysis method will be further explored in future.



CONTENTS

1	Executive Summary	5
2	Introduction.....	9
3	Purpose and Scope	9
4	Applicable and Reference documents.....	9
4.1.1	Applicable documents	9
4.1.2	Reference Documents.....	9
5	Definitions and Abbreviations.....	13
5.1	Definitions	13
5.2	Abbreviations	13
6	Products assessed.....	14
6.1	Impact of AATSR nadir and AATSR forward on BRDF retrievals	14
7	Radiometric inter-calibration product	16
7.1	Methods used.....	16
7.2	Analysis	17
7.3	Validation summary.....	17
8	Cloud detection product	18
8.1	Methods used.....	18
8.2	Analysis	19
8.2.1	Visual inspection for different seasons and regions	19
8.2.1.1	Mid-Latitudes, Summer.....	19
8.2.1.2	Mid-Latitudes, Spring.....	26
8.2.1.3	Mid-Latitudes, Winter.....	28
8.2.1.4	Arctic, Summer	31
8.2.1.5	Arctic, Spring	34
8.2.1.6	Tropics, Summer	37
8.2.1.7	Antarctica: Clouds over ice	40
8.2.2	Cloud classification: Introduction of a "cloud buffer" and comparison with MODIS prior outliers.....	41
8.2.3	Cloud/Snow distinction: Comparison with MODIS data	43
8.3	Cloud/snow mask improvements.....	45
8.3.1	MERIS	45



8.3.2	VGT	47
8.4	Validation summary	50
9	Atmospheric correction product.....	51
9.1	Methods used.....	51
9.2	Analysis	52
9.3	Validation summary	62
10	SDR product.....	63
10.1	Methods used	63
10.2	Validation of the SDR intermediate product.....	63
10.3	Validation of the N2B conversion approach	64
10.4	Analysis	64
10.5	Validation summary	70
11	BB Albedo product.....	71
11.1	Qualitative Assessments of GlobAlbedo products (“Known Issues”)	71
11.2	Tower intercomparisons with GlobAlbedo and other EO-derived Blue Sky Albedos.....	72
11.3	Methods used.....	81
11.4	Analysis	86
11.4.1	Intercomparison of tower albedos with spaceborne albedos	86
11.4.2	GlobAlbedo uncertainties compared with differences with tower values.....	96
11.4.3	GlobAlbedo values as a function of land cover	97
11.4.4	Intercomparison of global albedo results with MISR and MODIS	100
11.4.5	Triple Collocation to uncover systematic errors	102
11.5	Validation summary	104
12	General format.....	104
12.1	Ease of data use.....	104
12.2	Problems encountered	105
13	Summary	105
14	Recommendations	105



2 Introduction

This document describes the steps taken and the results obtained to validate the GlobAlbedo intermediate and final output set of all **Products**. The reader is referred to RD9 for a description of what was planned to be performed in this phase of the project. Ground-based measurements, such as the NASA AERONET sun photometry measurements and the entire FLUXNET and SURFRAD (RD20) ground albedometer measurements are used together to quantify the accuracy of the intermediate and output products. For certain intermediate products where “ground truth” data are not available, visual qualitative analysis has been performed. Global analysis is performed with level-3 products from MISR, MODIS, GEOLAND, METEOSAT and for the tower sites for as much of the entire time series as possible at specific tower sites with MODIS priors.

3 Purpose and Scope

In Phase 2 of the GlobAlbedo project, the final Products (described in RD1) have been processed using the algorithms outlined in the ATBDs (RD4-8). In this report, these Final Products are validated over areas where ground-based sun photometer and tower-based albedometer measurements are available. In addition, where no such correlative data exist, a visual qualitative analysis is performed. The triple collocation employed the product set for GlobAlbedo, MODIS and MISR but only on a monthly time-step for the 12 years available.

4 Applicable and Reference documents

4.1.1 Applicable documents

ID	Title	Issue	Date
[AD 1]	EOEP-DUEP-EOPS-SW-09-0001 SoW Statement of Work for DUE-GlobAlbedo Project	1.0	6/4/09
[AD 2]	GlobAlbedo AO/1-6060/09/I-OL Proposal, University College London	1.0	02/06/09

4.1.2 Reference Documents

RD1 GlobAlbedo_FPS_v1 (2013) GlobAlbedo Final Product Set. Author: Jan-Peter Muller, G. Lopez.

RD2 GlobAlbedo_TS_D02_v1_2 (2010) GlobAlbedo Technical Specifications. Authors: J-P Muller, P. Lewis, P. North, C. 48pp

RD3 Wolfe, R., Roy, D., Vermote, E. (1998) MODIS land data storage, gridding, and compositing methodology: Level 2 grid. IEEE Trans. Geoscience and Remote Sensing, 36 (4), 1324-1338



RD4 GlobAlbedo_ATBD_V4.0 (2013). GlobAlbedo: Algorithm Theoretical Basis Document. Authors: P. Lewis, C. Brockmann, O. Danne, J. Fischer, D. Fisher, L. Guanter, A. Heckel, S. Kharbouche, O. Krueger, G. López, J-P. Muller, P. North, D. Potts, R. Preusker

RD5 GlobAlbedo-BBDR-ATBD-V4.0 (2013). GlobAlbedo: Algorithm Theoretical Basis Document – SDR/BBDR retrieval. Authors: L. Guanter, R. Preusker, J. Fischer, G. López, P. Lewis, A. Heckel, P. North, D. Potts, J-P. Muller

RD6 GlobAlbedo-Albedo-ATBD-V4.0 (2013). GlobAlbedo: Algorithm Theoretical Basis Document - Albedo Retrieval. Authors: P. Lewis, G. López, L. Guanter.

RD7 GlobAlbedo-PixelID-ATBD-V3.0 (2013). GlobAlbedo: Algorithm Theoretical Basis Document - Pixel Classification. Authors: C. Brockmann, O. Krueger, O. Danne

RD8 GlobAlbedo-Aer-ATBD-V3.0 (2013). GlobAlbedo: Algorithm Theoretical Basis Document - Aerosol Retrieval. Authors: A. Heckel, P. North, L. Guanter, R. Preusker, J. Fischer, G. López, P. Lewis.

RD9 GlobAlbedo_PVP_V3.0 (2011). GlobAlbedo Product Validation Plan. Authors: J-P. Muller, C. Brockmann, L. Guanter, P. North, N. Shane, G. López

RD10 Holben, B., et al. (2001): An emerging ground-based aerosol climatology: Aerosol optical depth from AERONET, *J. Geophys. Res.*, 106(D11), 12067-12097

RD11 Vidot, J., Santer, R., and Aznay, O. (2008): Evaluation of the MERIS aerosol product over land with AERONET, *Atmos. Chem. Phys.*, 8, 7603-7617

RD12 Levy, R. C., Remer, L. A., Kleidman, R. G., Mattoo, S., Ichoku, C., Kahn, R., and Eck, T. F. (2010): Global evaluation of the Collection 5 MODIS dark-target aerosol products over land, *Atmos. Chem. Phys. Discuss.*, 10, 14815-14873, doi:10.5194/acpd-10-14815-2010

RD13 BEAM MERIS-AATSR-Synergy processor ATBD, http://www.brockmann-consult.de/beam-wiki/download/attachments/51970061/synergy-land_aerosol-atbd.pdf?version=1&modificationDate=1276173583061



RD14 P.R.J. North, C. Brockmann, J. Fischer, L. Gomez-Chova, W. Grey, A. Heckel, J. Moreno, P. Preusker, and P. Regner, (2008) MERIS/AATSR synergy algorithms for cloud screening, aerosol retrieval and atmospheric correction. In Proc. 2nd MERIS/AATSR User Workshop, ESRIN, Frascati, 22- 26 September 2008. (CD-ROM), ESA SP-666, ESA Publications Division, European Space Agency, Noordwijk, The Netherlands.

RD15 L. Guanter, L. Gómez-Chova, J. Moreno, (2008) Coupled retrieval of aerosol optical thickness, columnar water vapor and surface reflectance maps from ENVISAT/MERIS data over land, *Remote Sensing of Environment*, 112, 2898–2913

RD16 L. Guanter, A. Ruiz-Verdú, D. Odermatt, C. Giardino, S. Simis, V. Estellés, T. Heege, J. A. Domínguez-Gómez, and J. Moreno, (2010) Atmospheric correction of ENVISAT/MERIS data over inland waters: Validation for European lakes, *Remote Sensing of Environment*, 114, 467-480.

RD17 S. Liang, (2010) Narrowband to broadband conversions of land surface albedo. I algorithms. *Remote Sensing of Environment*, 76, 213–238.

RD18 C. Cao, S. Uprety, J. Xiong, A. Wu, P. Jing, D. Smith, G. Chander, N. Fox, S. Ungar, (2011) Establishing the Antarctic Dome C Community Reference Standard Site towards Consistent Measurements from Earth Observation Satellites, *Can. J. Remote Sens.* in press.

RD19 M.O. Roman, C.B. Schaaf, C.E. Woodcock, A.H. Strahler, X. Yang, R.H. Braswell, P.S. Curtis, K.J. Davis, D. Dragoni, M.L. Goulden, L. Gu, D.Y. Hollinger, T.E. Kolb, T.P. Meyers, J.W. Munger, J.L. Privette, A.D. Richardson, T.B. Wilson, S.C. Wofsy, The MODIS (Collection V005) BRDF/albedo product (2009): Assessment of spatial representativeness over forested landscapes, *Remote Sens. Environ.* 113, 2476-2498.

RD20 J. Liu, C. Schaaf, A. Strahler, Z. Jiao, Y. Shuai, Q. Zhang, M. Roman, J. Augustine, E. Dutton, Validation of Moderate Resolution Imaging Spectroradiometer (MODIS) albedo retrieval algorithm (2009) Dependence of albedo on solar zenith angle, *J. Geophys. Res.* 114,11.

RD21 G. Schaepman-Strub, M.E. Schaepman, T.H. Painter, S. Dangel, J. Martonchik, (2006) Reflectance quantities in optical remote sensing—definitions and case studies, *Remote Sens. Environ.* 103, 27-42.

RD22 J.G. Salomon, C.B. Schaaf, A.H. Strahler, F. Gao, Y. Jin, (2006) Validation of the MODIS Bidirectional Reflectance Distribution Function and Albedo Retrievals Using



Combined Observations From the Aqua and Terra Platforms, IEEE Trans. Geosci. Remote Sensing 44, 1555-1565.

RD23 F. Gao, C. Schaaf, A. Strahler, A. Roesch, W. Lucht, R. Dickinson, (2005), MODIS bidirectional reflectance distribution function and albedo Climate Modeling Grid products and the variability of albedo for major global vegetation types, J Geophys Res-Atmos 110 D01104.

RD24 Y.F. Jin, C.B. Schaaf, C.E. Woodcock, F. Gao, X.W. Li, A.H. Strahler, W. Lucht, S.L. Liang, (2003), Consistency of MODIS surface bidirectional reflectance distribution function and albedo retrievals: 2. Validation, J. Geophys. Res.-Atmos. 108, art. no.-4159.

RD25 S.L. Liang, H.L. Fang, M.Z. Chen, C.J. Shuey, C. Walthall, C. Daughtry, J. Morisette, C. Schaaf, A. Strahler, (2002), Validating MODIS land surface reflectance and albedo products: methods and preliminary results, Remote Sens. Environ. 83, 149-162.

RD26 A. Stoffelen, (1998) Toward the true near-surface wind speed: Error modeling and calibration using triple collocation, Journal of Geophysical Research 103, 7755-7766.

RD27 K. Scipal, T. Holmes, R. de Jeu, V. Naeimi, W. Wagner, (2008), A possible solution for the problem of estimating the error structure of global soil moisture data sets, Geophys. Res. Lett. 35, art. no. L24403.

RD28 S. Caires, A. Sterl, (2003), Validation of ocean wind and wave data using triple collocation, Journal of Geophysical Research 108, 3098-3114.

RD29 P. Janssen, S. Abdalla, H. Hersbach, J.-R. Bidlot, (2007) Error estimation of buoy, satellite, and model wave height data, J. Atmos. Ocean. Technol. 24, 1665-1677

RD30 Muller, J.-P., R. Preusker, J. Fischer, M. Zuhlke, C. Brockmann, and P. Regner, (2007), ALBEDOMAP: MERIS land surface albedo retrieval using data fusion with MODIS BRDF and its validation using contemporaneous EO and in situ data products. Proc. IGARSS Int. Geoscience and Remote Sensing Symp., Barcelona, Spain, Institute of Electrical and Electronics Engineers, 2404-2407

RD31 Cescatti et al. Intercomparison of MODIS albedo retrievals and in situ measurements across the global FLUXNET network. Remote sensing of environment (2012) vol. 121 pp. 323-334. DOI: 10.1016/j.rse.2012.02.019



Title: GlobAlbedo Final Validation Report

Doc. No. GlobAlbedo_FVR_V1.2

RD31 GlobAlbedo Consortium (2012): UCL Proposal in Response to ESRIN CCN SoW for DUE GlobAlbedo Evolution [ESRIN Contract 4200022390/09/I-OL].

RD32 Fisher, D., & Muller, J. P. (2013). Global warping coefficients for improving ATSR co-registration. *Remote Sensing Letters*, 4(2), 151-160.

5 Definitions and Abbreviations

5.1 Definitions

5.2 Abbreviations

AATSR	Advanced Along Track Scanning Radiometer
ATBD	Algorithm Theoretical Basis Document
BBA	Blue-sky Broad Albedo
BBDR	Broad Band directional reflectance
BHR	Bi-Hemispherical diffuse Reflectance
BRDF	Bidirectional Reflectance Distribution Function
DHR	Directional Hemispherical Reflectance
FR	Full resolution
MERIS	Medium Resolution Imaging Spectrometer
MSSL	Mullard Space Science Laboratory
NDVI	Normalized differences vegetation index
NIR	Near-Infrared (0.7-3 μ m)
SDR	Surface Directional Reflectance
SW	Short Wave (0.3-3 μ m)
TOA	Top-of-atmosphere
VIS	Visible wavelengths (0.3-0.7 μ m)
VGT	SPOT's Vegetation instrument



6 Products assessed

The products assessed are taken from throughout the processing chain from the calibrated reflectance through the cloud and snow masking (and sea-ice detection) through the atmospheric correction through the narrow-to-broadband directional reflectance (BBDR) to the final BRDF to the predicted blue-sky albedo over a tower albedometer site through to the final global DHR and BHR products are assessed with the final Products for all years, wherever correlative data is available. RD5 describes the overall methods.

6.1 Impact of AATSR nadir and AATSR forward on BRDF retrievals

In order to measure the impact of the inclusion of AATSR data on the BRDF model inversion, three different processing chains were implemented:

- a) Only MERIS and VGT were used,
- b) Only AATSR nadir-view, MERIS and VGT
- c) All samples from AATSR, forward and nadir view, MERIS and VGT.

The tests were applied for tile h25v06 located in the Himalayas region, the extent coordinates of the tile are:

ULC_X: 80°49'44.54"E

ULC_Y: 30° 0'0.00"N

URC_X: 92°22'33.76"E

URC_Y: 30° 0'0.00"N

LLC_X: 74°29'32.80"E

LLC_Y: 20° 0'0.00"N

LRC_X: 85° 8'3.20"E

LRC_Y: 20° 0'0.00"N

Number of samples

The first impact of including AATSR is on the temporal weighted number of samples available for the BRDF model inversion. Figure 1 shows the spatial distribution of the samples for the 16-day time period going from April 7 to 22, 2005 for all cases, case c) shows the greatest number of samples.

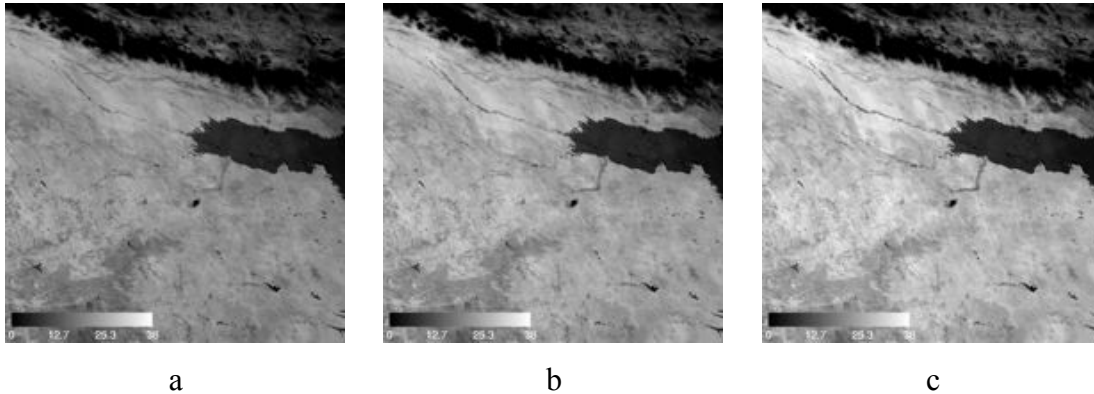


Figure 1. Temporal weighted number of samples used for the BRDF model inversion during April 7-22, 2005. See text for a description of the 3 different cases

In order to extract the samples contributed by AATSR a subtraction of the samples used in, case a) minus the ones used in cases b) and c), was computed, Figure 2 shows the spatial distribution of the AATSR samples.

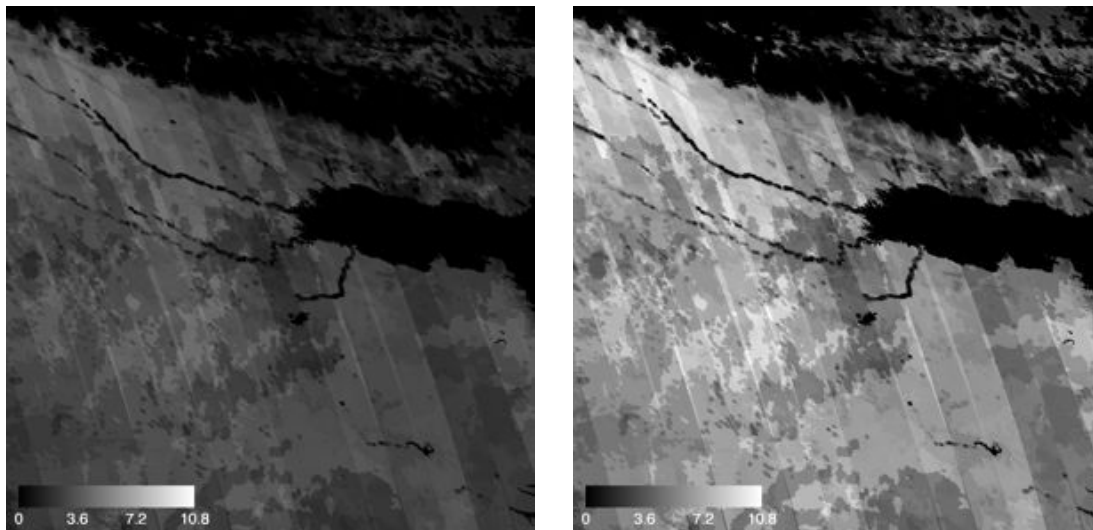


Figure 2. AATSR weighted number of samples used for the BRDF model inversion, on the left for case b), on the right case c).

Misregistration

The most visible impact was due to the misregistration errors.

Goodness of fit

An estimate of the model parameters derived from the three different cases were used to calculate the goodness of fit χ_a^2 , χ_b^2 and χ_c^2 . This measure describes how well it fits a set of observations, with **values closer to zero indicating that the model fits better to the observation set.**

$$\chi^2 = F_t^T \left[\sum_{i=0}^{i=N} K_i^T C_{O,i}^{-1} K_i \right] F_t + F_t^T \left[\sum_{i=0}^{i=N} K_i^T C_{O,i}^{-1} R_i \right] - 2 \left[\sum_{i=0}^{i=N} R_i^T C_{O,i}^{-1} R_i \right]$$

where, for a set of N observations, F are the derived BRDF model parameters for each broadband, K are the modified kernel terms for each of the three kernels, for each of the three broadbands, C_o the uncertainty associated to the observations and R the observations for each broadband.

The best goodness of fit was found for case a) when using **only MERIS and VGT** data for the BRDF model inversion, Figure 3 shows on the left χ_a^2 scaled 0.001-1000.0 and on the centre and right the difference between the χ_b^2 , χ_c^2 with respect to χ_a^2 , in both cases, b) and c) the goodness of fit was greater than case a), This demonstrates that the set of observations a) fit the model better **without the inclusion of AATSR** data. Therefore, even though AATSR contributes in terms of more observations, these samples do not provide valuable information to enhance the model inversion.

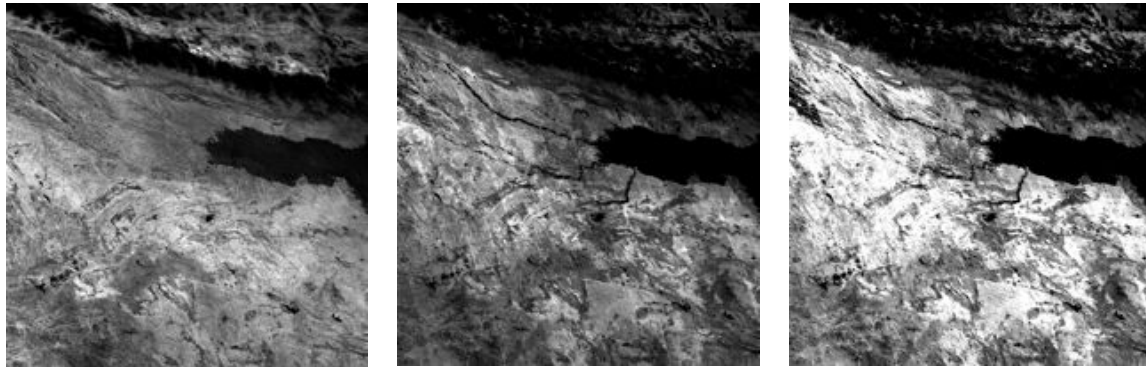


Figure 3. On the left χ_a^2 , the image is scaled 0.001-1000.0, on the centre $\chi_b^2 - \chi_a^2$, on the right $\chi_c^2 - \chi_a^2$, the last two images are scaled 0.001-140

7 Radiometric inter-calibration product

These are described in Appendix 2 of RD5. See also the discussion on SDR in section 9 of this report including an assessment of SDR using CHRIS-PROBA.

7.1 Methods used

These are described in Appendix 2 of RD5 and SDR in section 9 of this report. In summary, time series of measurements from AATSR, MERIS and VGT were acquired over a stable site during November and December 2008-January 2009. These data were then radiometrically de-calibrated into spectral reflectance. These spectral reflectances were then corrected for Ozone absorption to an equivalent Top-of-Atmosphere reflectance



with the same Ozone content. A cloud mask was applied (as VGT data was not acquired at the same time as the other 2 sensors so only land surface pixels could be compared).

7.2 Analysis

These are described in Appendix 2 of RD5 and SDR in section 9 of this report. In summary, the pixel reflectances were compared against each other after the pre-processing described in the previous section. Sensor inter-calibration coefficients were then derived which are summarised below.

7.3 Validation summary

The table shown as Figure 25 in Appendix 2 of RD5 is again shown here for completeness. The radiometric calibration coefficients are similar to the ones which have been generated by RAL for previous years using different numbers of pixels. They are within each other's error bars and so are considered to be consistent here. See also SDR in section 9 of this report for a discussion of the SDR products when compared against CHRIS-PROBA.

<i>AATSR vs MERIS</i>	AATSR Report PO-RP-RAL-AT-0599 intercomparison results (page 32 and 33)					
RAL (2002-2008)	Ratio AATSR/MERIS	StdDev	Offset	Slope	Number of data points	
550/560nm band	1.0374	0.0152	0.6956	1.0176	Unspecified	
660/665nm band	1.0288	0.0108	0.4993	1.0152	Unspecified	
870/865nm band	1.0369	0.0079	0.6179	1.0198	Unspecified	
	Best fit coefficients of bandwidth and ARF corrected, normalised TOA reflectance AFTER ozone correction					
<i>AATSR vs MERIS</i>	Ratio AATSR/MERIS	StdDev	Offset	Slope	R-squared	Number of data points
550/560nm band	1.025273127	0.0072287	-0.169	1.2189	0.7585	15
660/665nm band	1.009335959	0.0099814	0.0726	0.93	0.4636	15
870/865nm band	1.026507198	0.0072884	-0.023	1.0523	0.8741	15



<i>MERIS vs VGT</i>						
	Mean ratio VGT/MERIS	StdDev	Offset	Slope	R-squared	Number of data points
442 vs 450 nm band	1.012482984	0.0397508	1.395	-0.4961	0.5801	8
665 vs 645 nm band	0.95342094	0.0067775	-0.0835	1.0447	0.471	8
865 vs 835 nm band	0.970944006	0.0083773	0.3891	0.5376	0.4385	8
<i>AATSR vs VGT</i>						
	Mean ratio VGT/AATSR	StdDev	Offset	Slope	R-squared	Number of data points
660 vs 645 nm band	0.947402892	0.0077898	0.3805	0.5341	0.7431	8
870 vs 840 nm band	0.945720049	0.0085332	0.4086	0.5025	0.4745	8
1600 vs 1665 nm band	1.134511487	0.0790827	0.0226	0.977	0.9189	8

Figure 4. Sensor intercalibration coefficients for AATSR, MERIS and VEGETATION for December 2008-January 2009 over DOME-C. Number of points refers to the mean value over a maximum of 225 pixels if all are cloud-free.

8 Cloud detection product

8.1 Methods used

For cloud detection within GlobAlbedo the method of Pixel identification is applied. The term “Pixel identification” refers to a classification of a measurement made by a space borne radiometer, for the purpose of identifying properties of the measurement which are influencing further algorithmic processing steps. Most importantly is the classification of a measurement as being made over cloud, a clear sky land surface or a clear sky ocean surface. The term “pixel” is often used for such a measurement in order to express it being part of a spatially oriented collection of many measurements, which all are geo- located and which form, as a whole, an image of the earth below the satellite.

The validation of pixel identification information is not easy because it is not a physical quantity but a context related, qualitative information. It also is not a self-consistent information but has to be considered in connection with the further processing: if a pixel, which extends over a finite area of 1km x 1km and which is a mixture of different surface types, is considered as land, water or cloud, depends on the ability of the subsequent processing to treat it as either of these classes.

The main tool to validate the performance of the pixel classification is therefore done indirectly by investigating the higher level products. Systematic errors, e.g. increased surface reflectances next to clouds, or bright spots in L3 albedo maps, are a possible effect of wrongly classified cloud pixels.



8.2 Analysis

The validation of the pixel identification flag can be performed in two different ways: 1) visual inspection; and 2) assessment of its effects on higher level products. Method 1 is subjective because it is performed by an (experienced) scientist but has been proven in the past to give most insight into performance for critical cases, and to help understanding the reasons for failure. Method 2) is most relevant for the purpose of GlobAlbedo, and when looking to time series and averages can reveal problems, which are not detectable with single image samples.

Following step 1 initially, a certain number of scenes from each sensor are selected. The data cover pure clear sky, totally cloudy as well as more “ambiguous” pixels (haze, multi-layer clouds, clouds over snow, bright sand). The products also cover representative observational conditions, i.e. season, location, viewing and observation angles.

The following section (7.2.1) presents examples from visual inspections covering data from all three sensors for different seasons and regions. The same orbits are selected for MERIS and AATSR for this purpose and the closest possible in time corresponding VGT data (different swaths and overpass times) is selected. A further validation approach is the comparison of Idepix results with MODIS cloud and snow classification. Examples are presented in sections 7.2.2 and 7.2.3.

8.2.1 Visual inspection for different seasons and regions

Examples from the visual inspections presented in the following subsections include:

- MERIS, AATSR and VGT: Inspection of a number of cases based on a coarse seasonal/regional classification:
 - Arctic, Antarctica: Spring and summer (daylight conditions)
 - Mid-latitudes: All seasons
 - Tropics: Summer (small seasonal variations, assuming they are negligible for pixel classification)
- VGT: special case of clouds over ice (Dome-C comparison)

8.2.1.1 Mid-Latitudes, Summer

The first comparisons were made for mid latitude summer conditions. All scenes show improvement after further adjustment of the thresholds used for cloud detection. Also, the Idepix cloud classification shows an improvement with regard to 'standard' cloud flags distributed with the products. This is especially true for AATSR and VGT.

The Idepix pixel identification algorithm was improved in several iterative steps. For the AATSR nadir view, Figure 5 shows a comparison of cloud detection results with the RGB picture for a mid latitude summer scene. Cloud detection results are shown for a first threshold tuning and after a further threshold adjustment. Also, snow covered pixels are detected. The results after the first threshold tuning were generally regarded as too conservative (too many clouds undetected). The centre image shows the improvement after a further threshold adjustment. Especially for shallow cumulus cloud fields, the results look much more reasonable when compared to the RGB.



For the same scene, Figure 6 shows a comparison of Idepix cloud classification with the standard AATSR L1b 'cln_cloudy' flag. It is obvious that the Idepix classification is significantly better; most of the false alarms of the 'cln_cloudy' flag. The same is true for the forward view (Figure 7).

Figure 8 shows the same comparison as Figure 5 (same day and region), but for a MERIS scene. Similar to AATSR, more clouds are detected after further threshold tuning, and the result looks more reasonable compared to the RGB.

Figure 9 shows the same way of comparison as Figure 6 and Figure 7, but also for the MERIS scene of Figure 8. The differences between the MERIS L1b 'bright' flag and Idepix cloud classification are not that obvious, but at least for this clouds Idepix seems to derive slightly better results.

Figure 10 shows the same type of comparison as Figure 5 and Figure 8 (same day and region), but for a SPOT VGT scene. Similar to AATSR, more clouds are detected after a further threshold tuning, and the result looks more reasonable compared to the RGB.

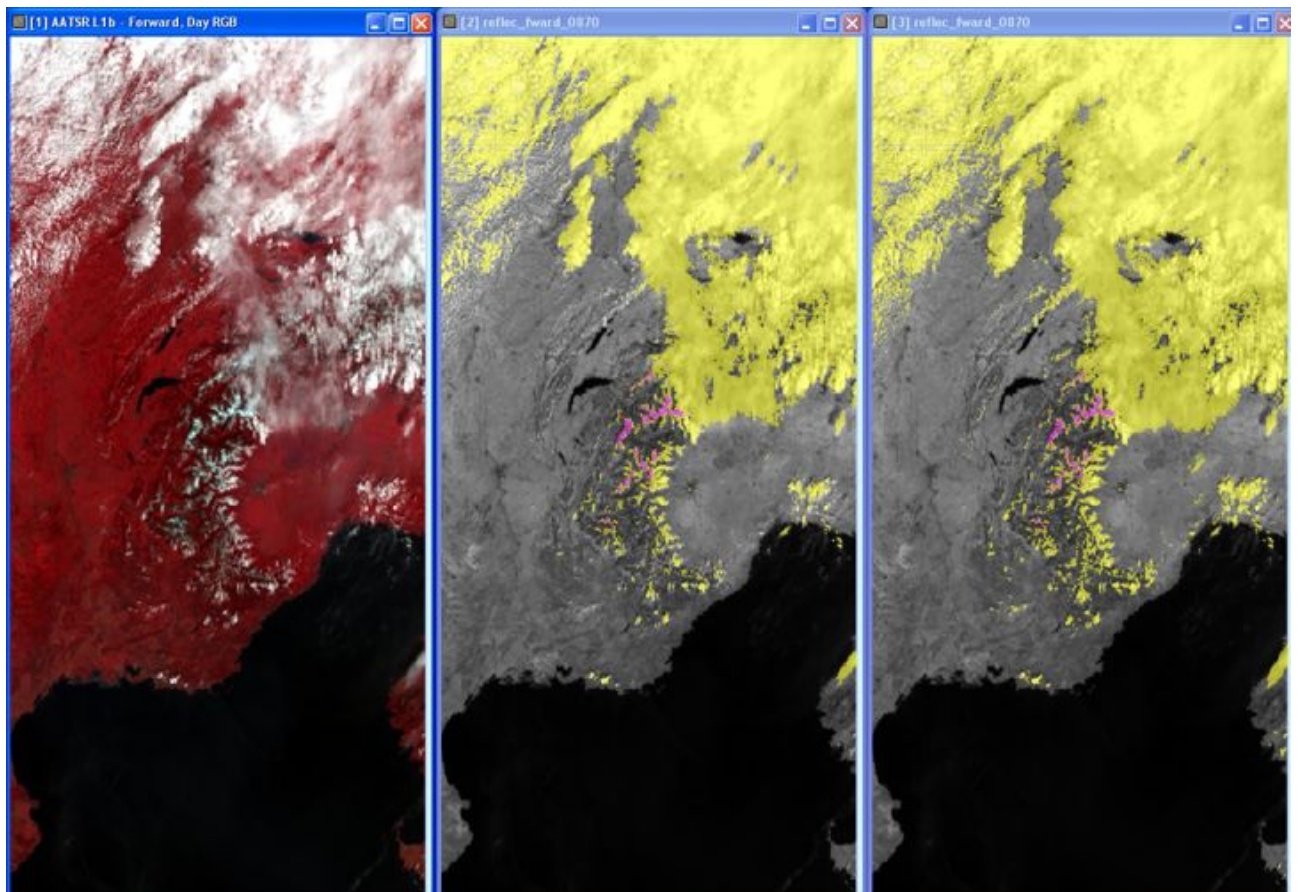


Figure 5: Comparison of cloud detection results (middle and right, in yellow) with the AATSR (forward view) RGB picture for mid latitude summer. Cloud detection results are shown for a first thresho (middle) and after a further threshold adjustment (right). Snow covered pixels are indicated in purple.

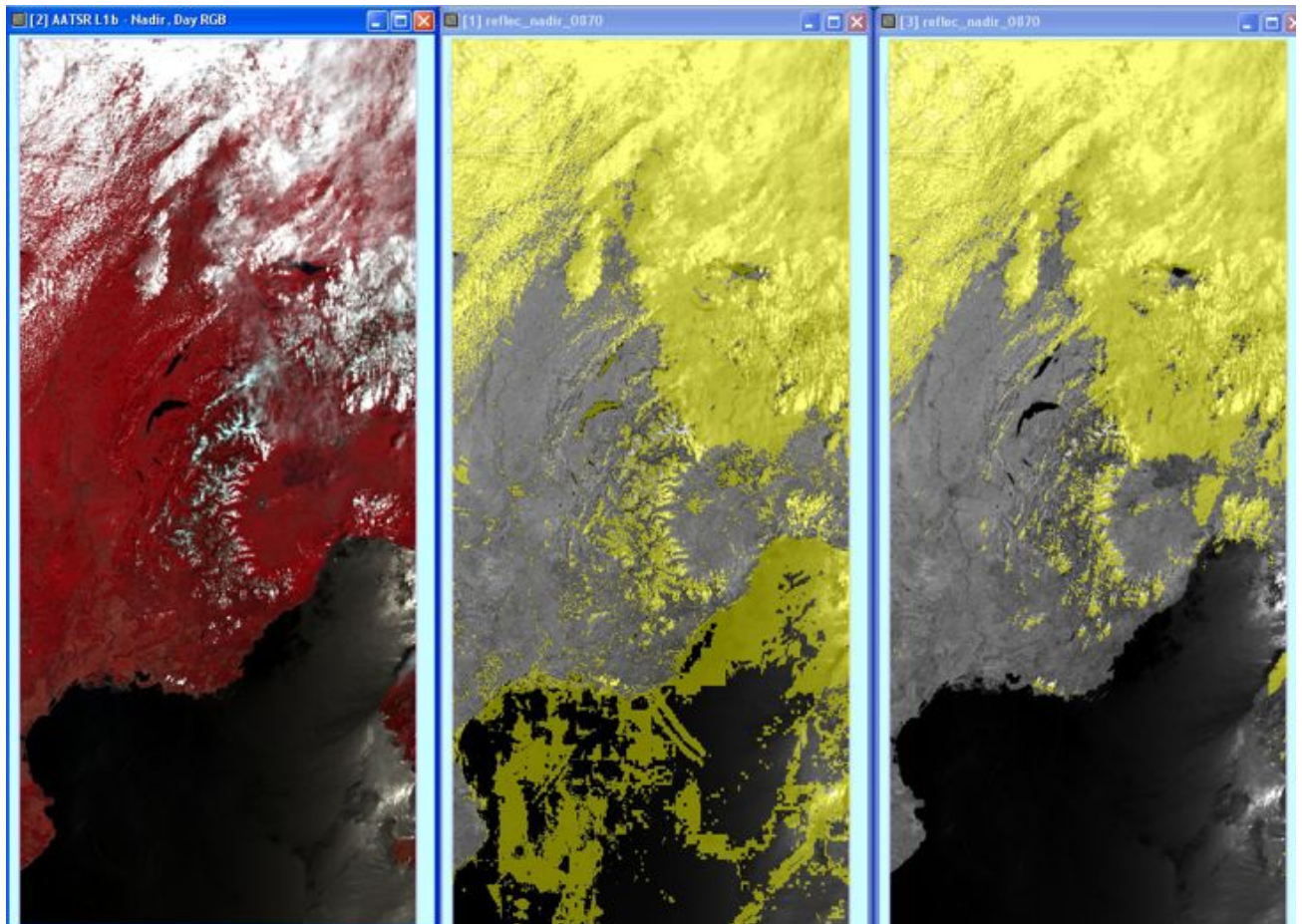


Figure 6: Comparison of cloud detection results (middle and right, in yellow) with the AATSR (nadir view) RGB picture for mid latitude summer (same scene as previous figure). Cloud detection results are shown for AATSR 'cln_cloudy' flag (middle) and Idepix after further threshold adjustment (right, same as in figure above).

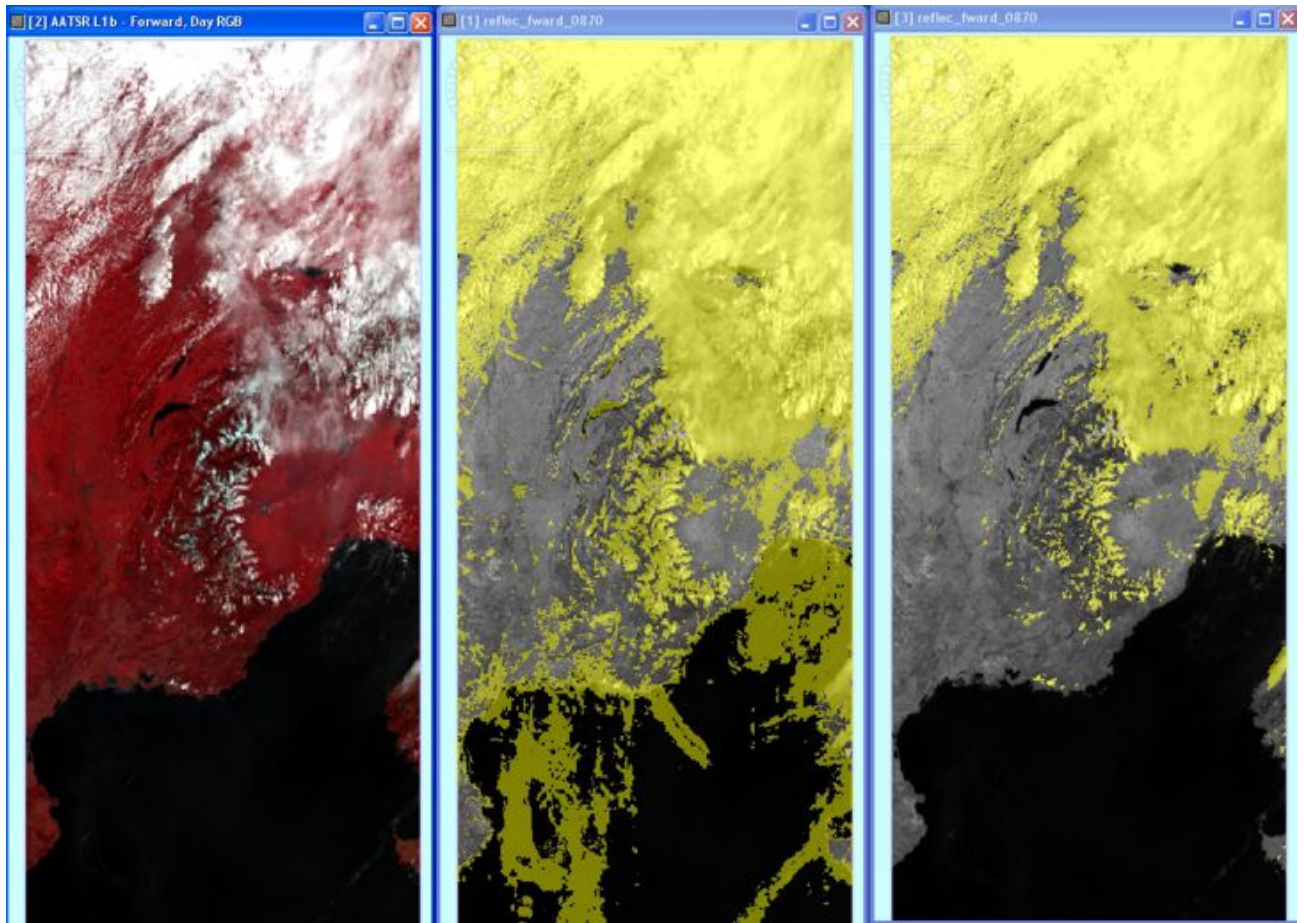


Figure 7: Comparison of cloud detection results (middle and right, in yellow) with the AATSR (forward view) RGB picture for mid latitude summer (same scene as previous figure). Cloud detection results are shown for AATSR 'clf_cloudy' flag (middle) and Idepix after further threshold adjustment (right).

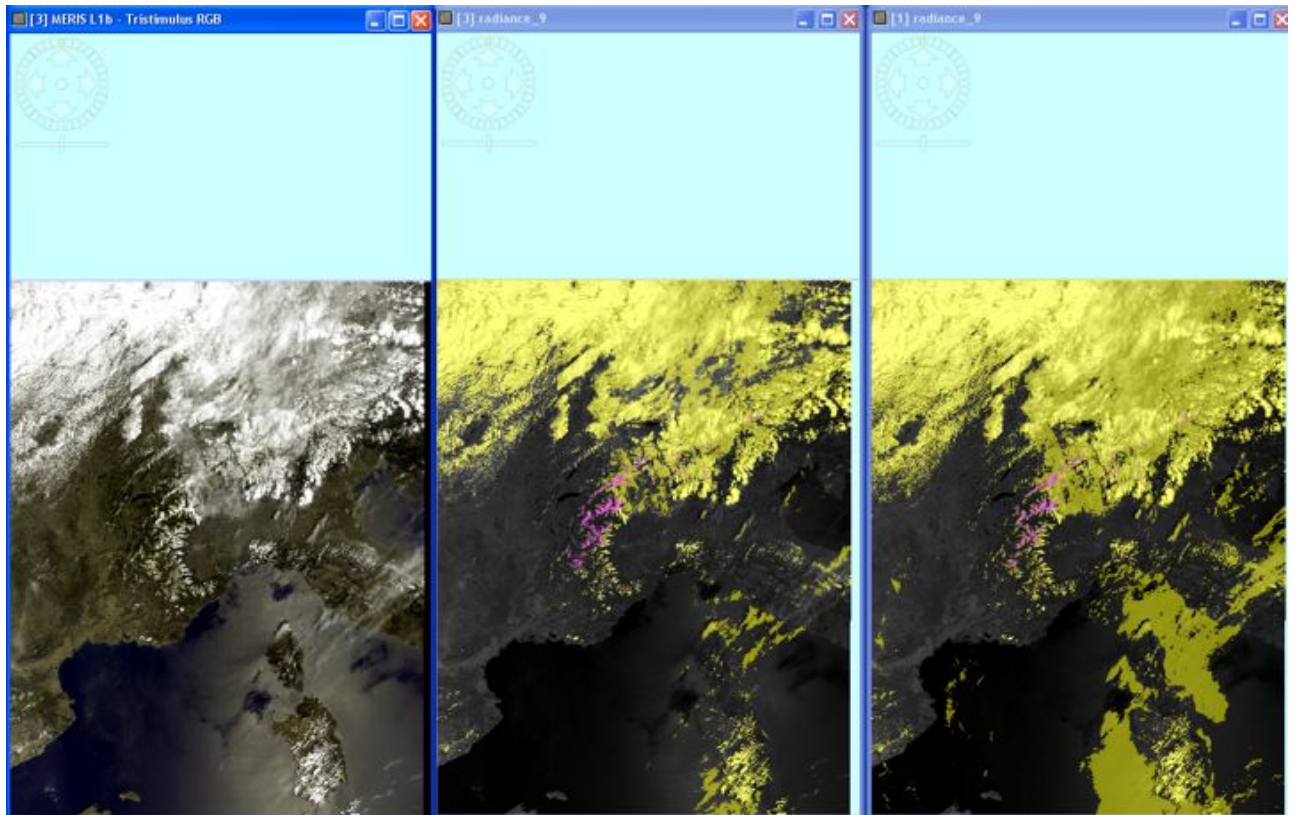


Figure 8: Comparison of cloud detection results (middle and right, in yellow) with the MERIS RGB picture for mid latitude summer (same day and region as for AATSR above). Cloud detection results are shown for a first Idepix threshold tuning (middle) and after a further threshold adjustment (right). Snow covered pixels are indicated in purple.

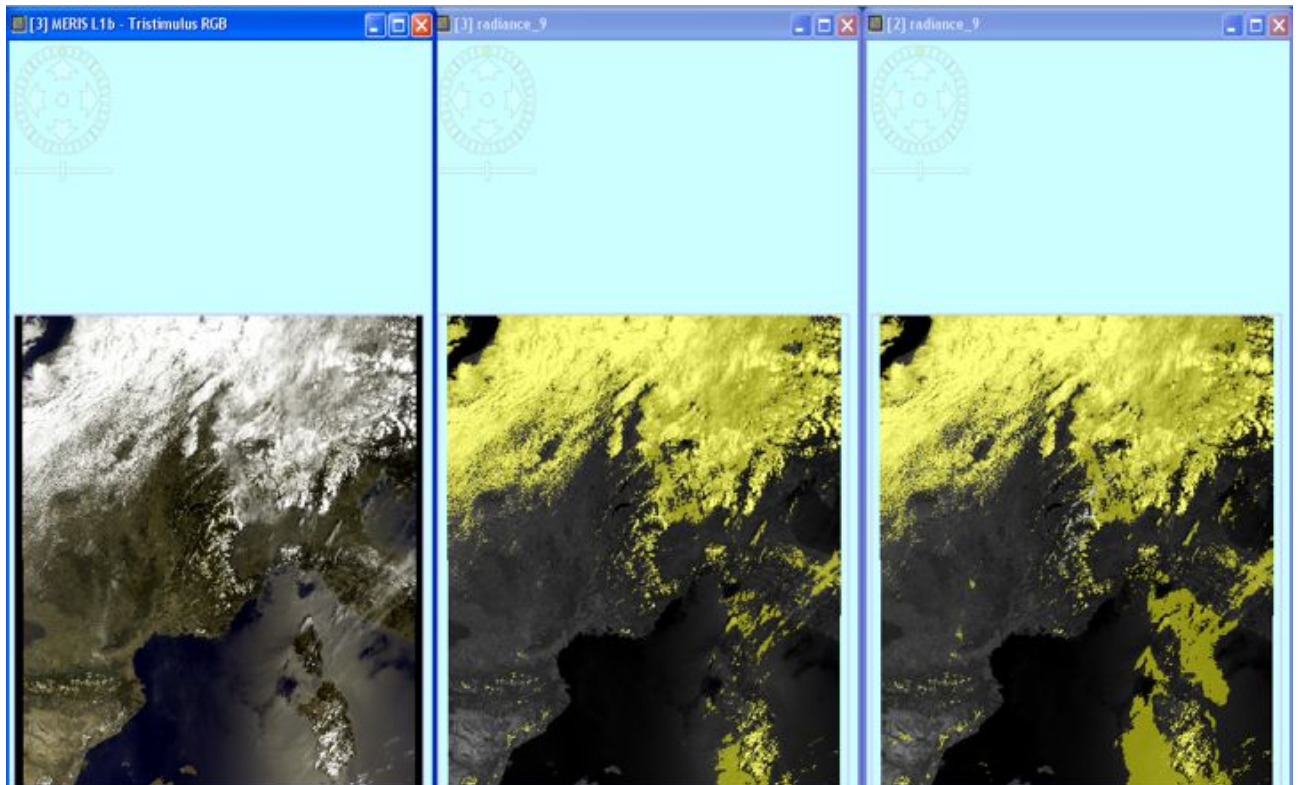


Figure 9: Comparison of cloud detection results (middle and right, in yellow) with the MERIS RGB picture for mid latitude summer (same scene as above). Cloud detection results are shown for MERIS L1b 'bright' flag (middle) and Idepix after further threshold adjustment (right).

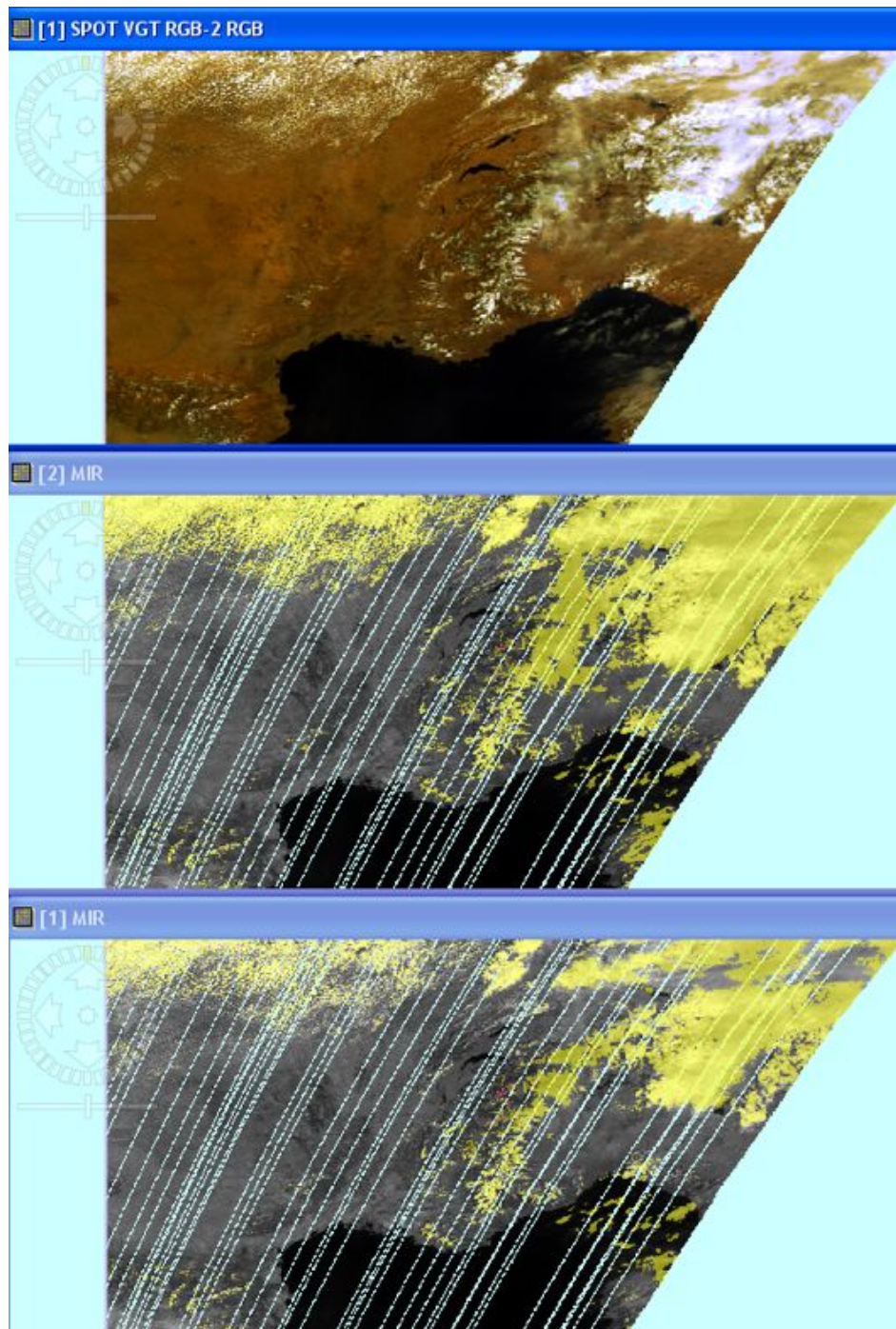


Figure 10: Comparison of cloud detection results (middle and lower, in yellow) with the VGT RGB picture (upper) for mid-latitude summer (same day and region as for MERIS and AATSR examples above). Cloud detection results are shown after a first threshold tuning (lower) and after further threshold adjustment (middle). Snow covered pixels are indicated in purple. Stripes in the figures originate from the underlying VGT level 1b reflectance data in MIR band.



8.2.1.2 Mid-Latitudes, Spring

The following examples show Idepix cloud/snow classification results for 'Mid Latitudes'/'Spring' in comparison with the underlying RGB images.

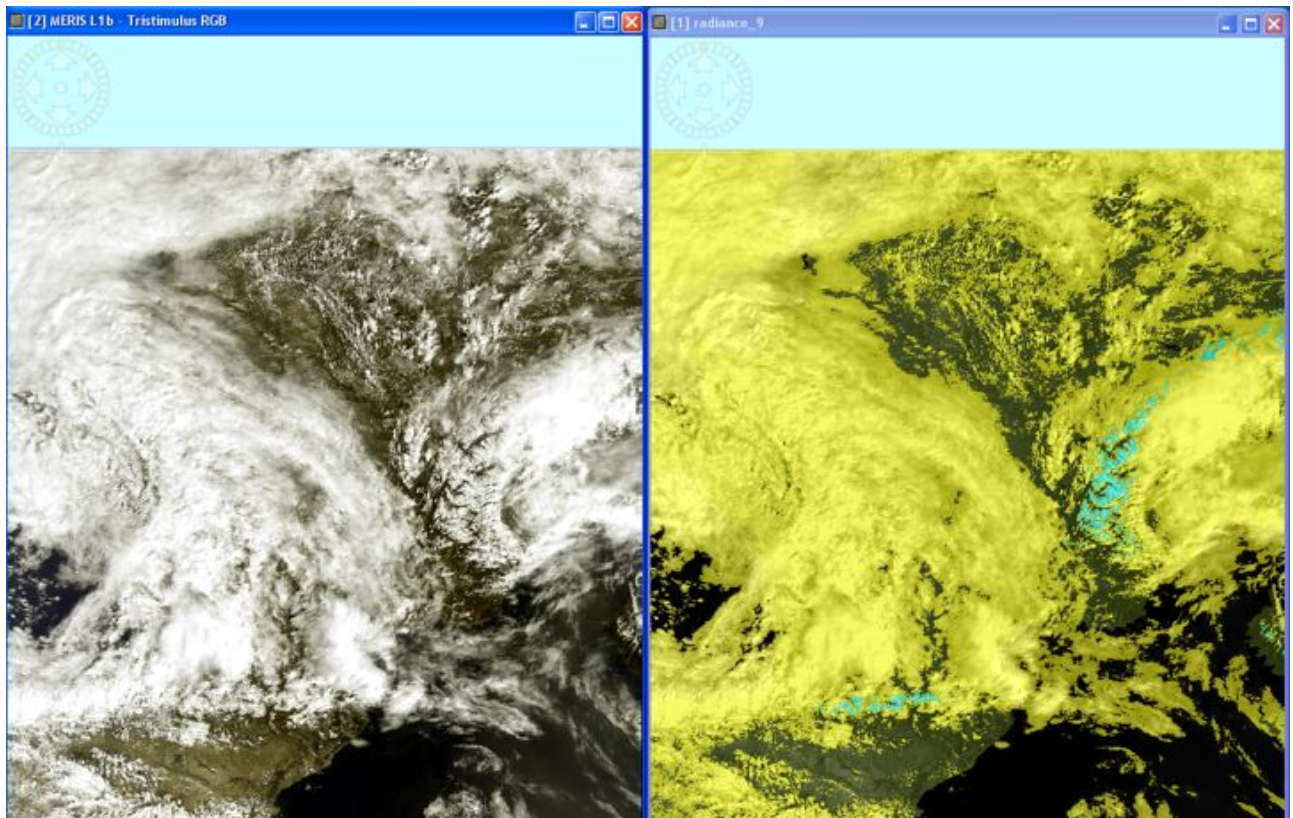


Figure 11: Comparison of cloud detection results from latest Idepix version (right, in yellow) with the MERIS RGB picture for mid latitude spring over France (March 29th, 2005). Snow covered pixels are indicated in blue.

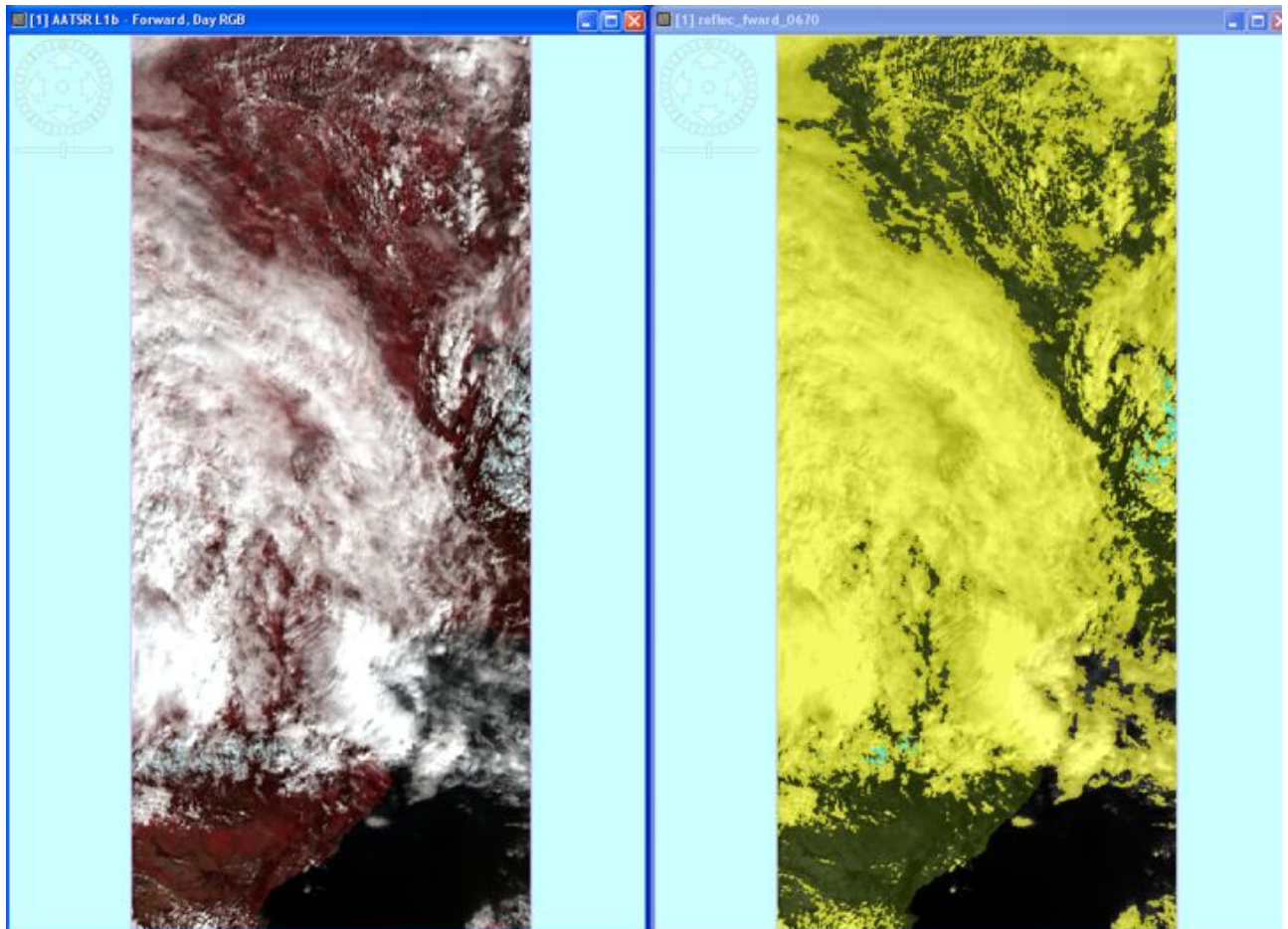


Figure 12: Comparison of cloud detection results from latest Idepix version (right, in yellow) with the AATSR (forward view) RGB picture for mid latitude spring over France (March 29th, 2005). Snow covered pixels are indicated in blue.

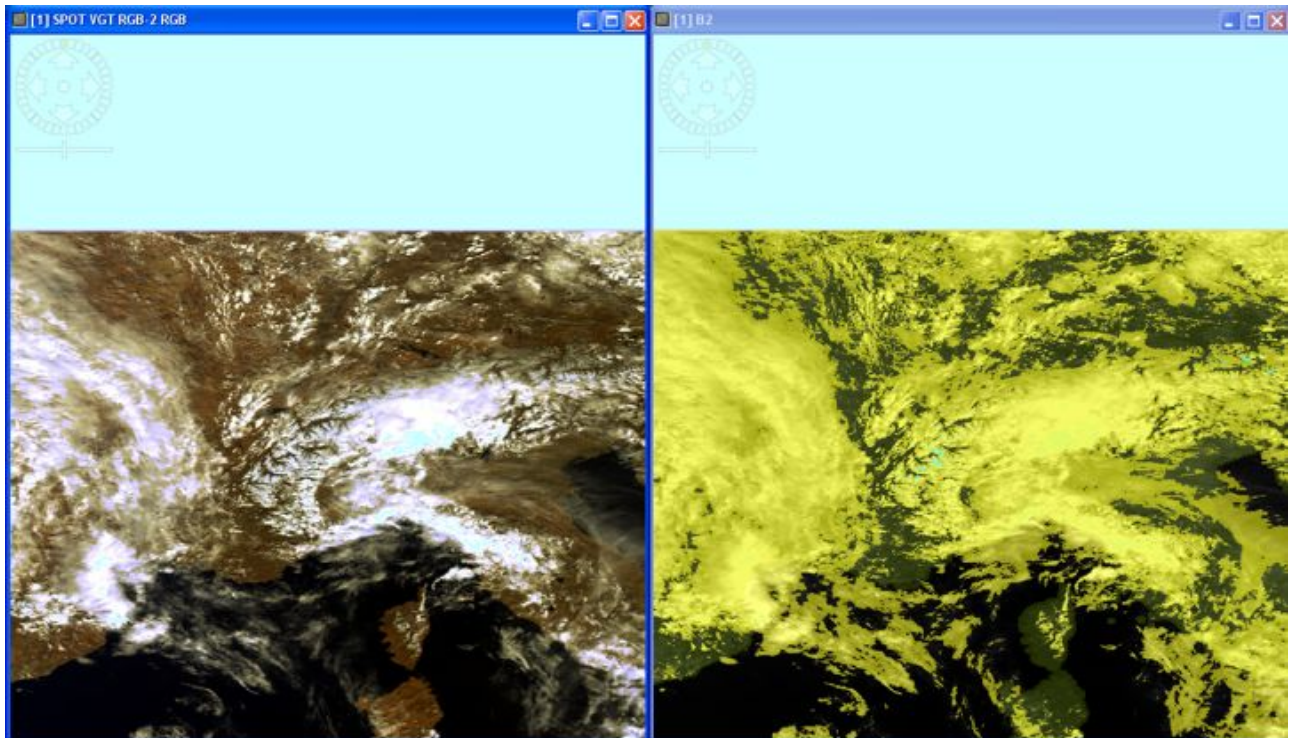


Figure 13: Comparison of cloud detection results from latest Idepix version (right, in yellow) with the SPOT VGT RGB picture for mid latitude spring over Southern France and Northern Italy (March 29th, 2005). Snow covered pixels are indicated in purple.

8.2.1.3 Mid-Latitudes, Winter

The following examples show Idepix cloud/snow classification results for 'Mid Latitudes'/'Winter' in comparison with the underlying RGB images.

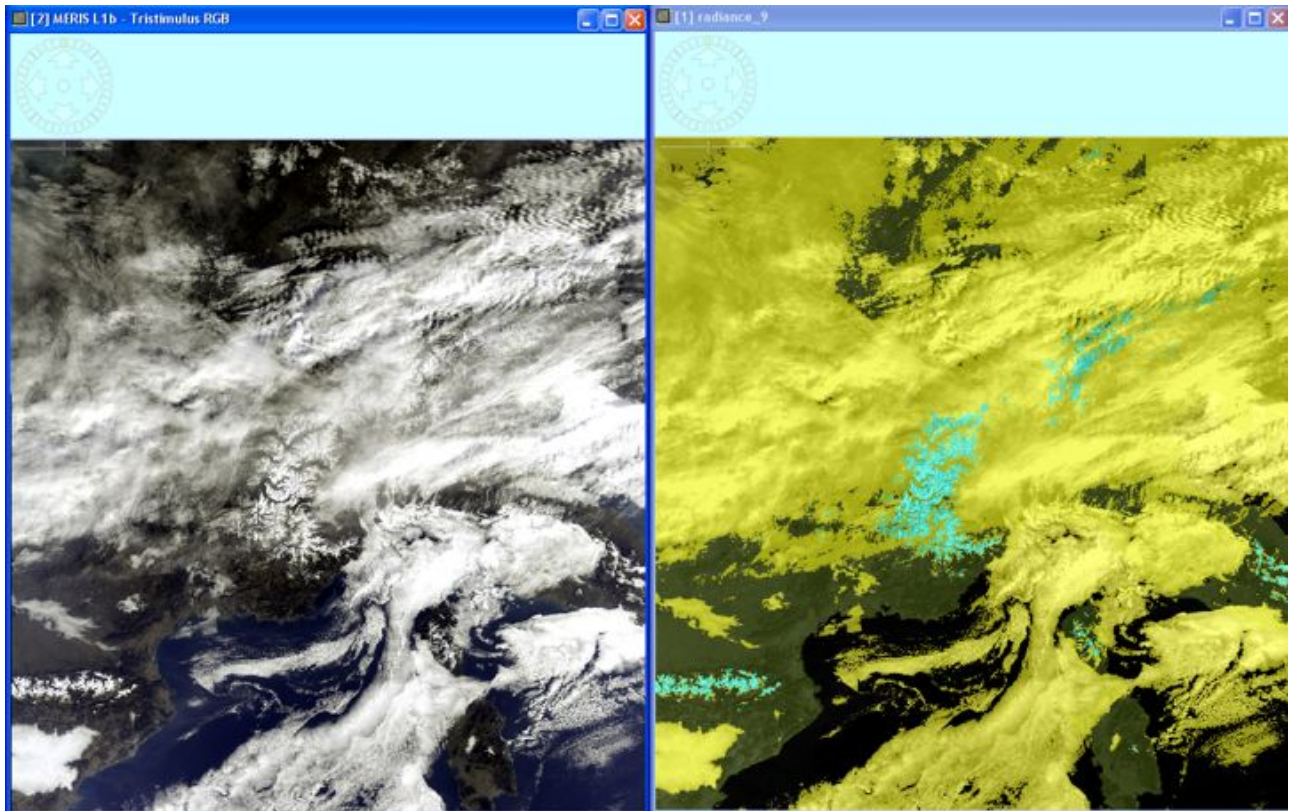


Figure 14: Comparison of cloud detection results from latest Idepix version (right, in yellow) with the MERIS RGB picture for mid latitude winter over France (January 9th, 2005). Snow covered pixels are indicated in blue.

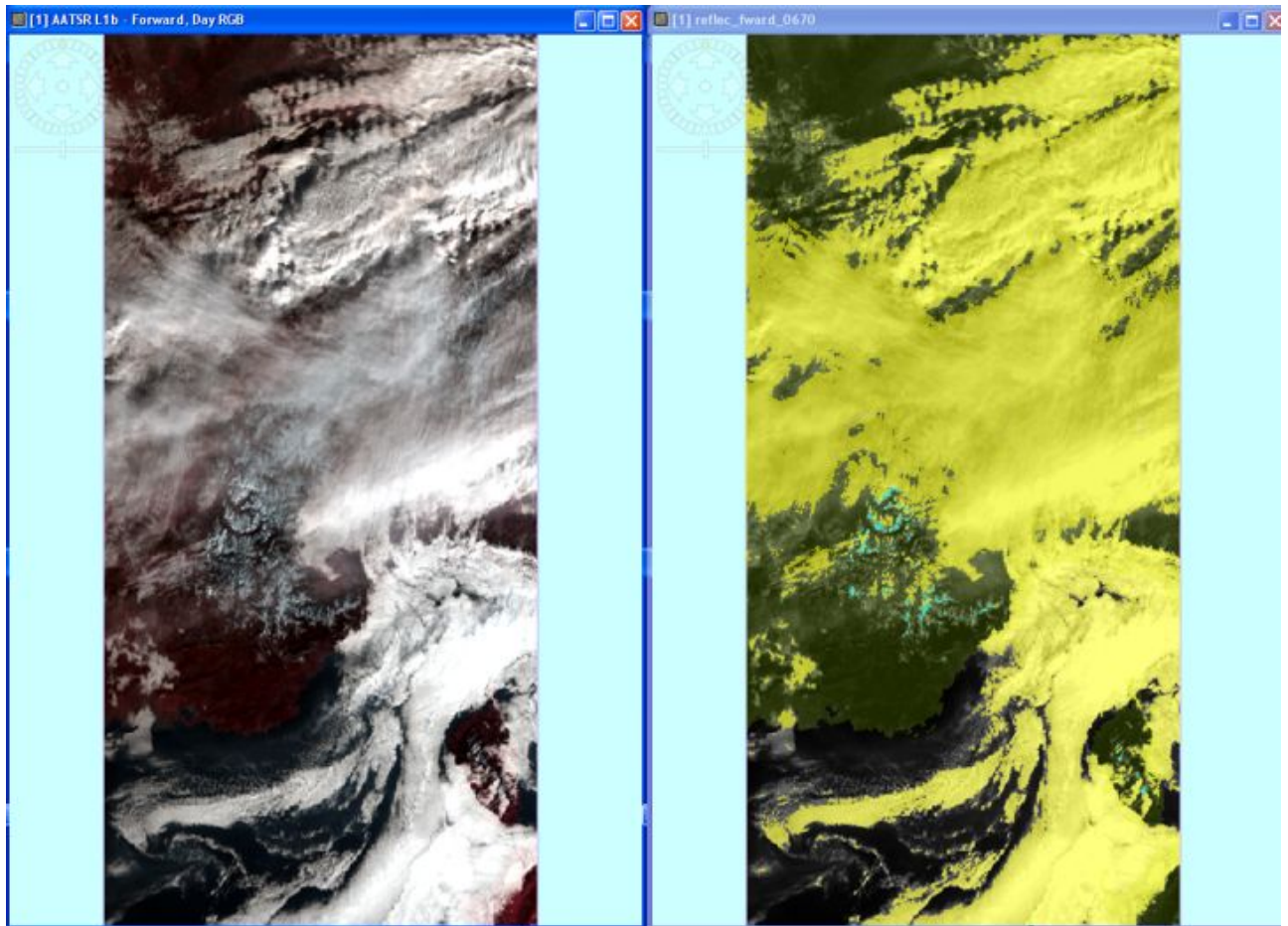


Figure 15: Comparison of cloud detection results from latest Idepix version (right, in yellow) with the AATSR (forward view) RGB picture for mid latitude winter over France (January 9th, 2005). Snow covered pixels are indicated in blue.

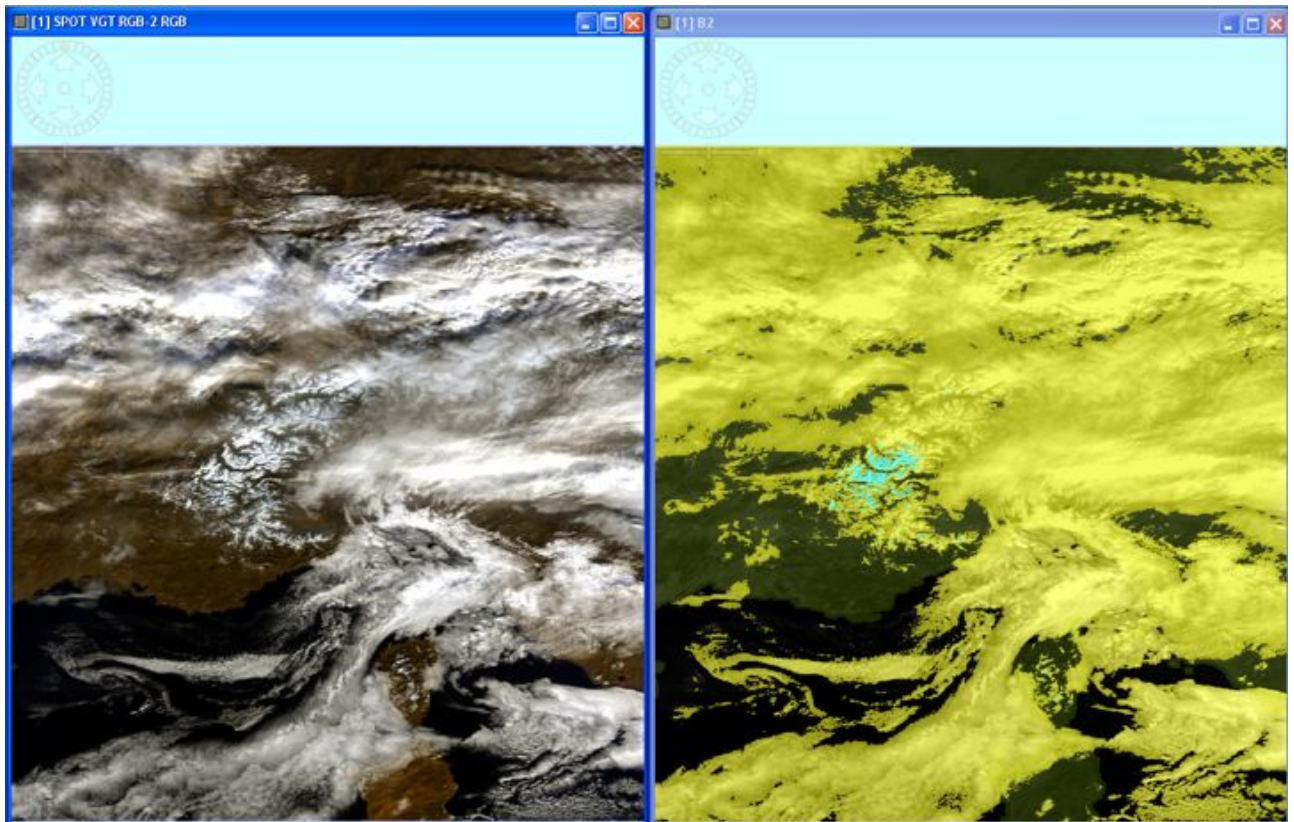


Figure 16: Comparison of cloud detection results from latest Idepix version (right, in yellow) with the SPOT VGT RGB picture for mid latitude winter over Southern France and Northern Italy (January 9th, 2005). Snow covered pixels are indicated in purple.

8.2.1.4 Arctic, Summer

The following examples show Idepix cloud/snow classification results for 'Arctic'/'Summer' in comparison with the underlying RGB images.

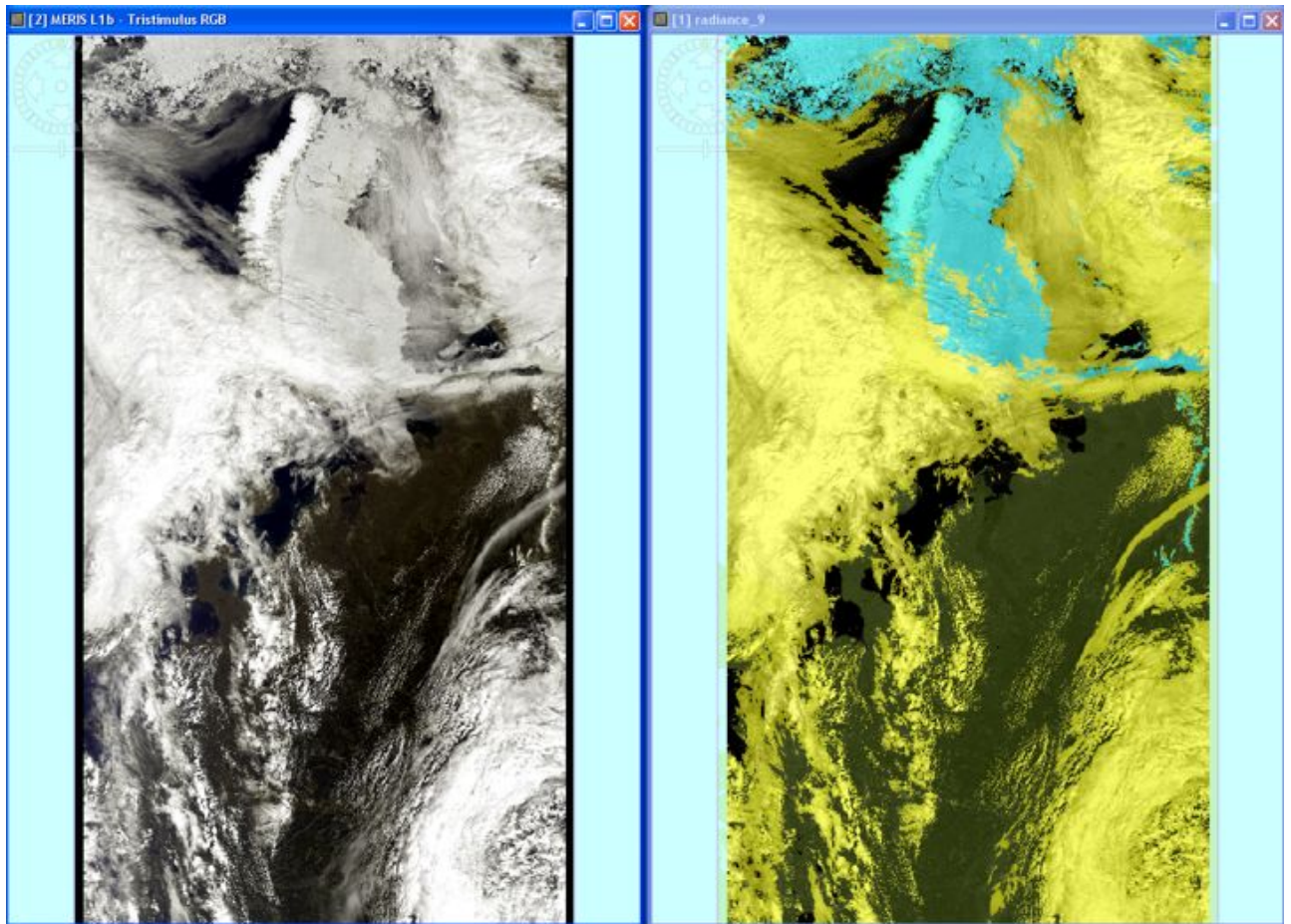


Figure 17: Comparison of cloud detection results from latest Idepix version (right, in yellow) with the MERIS RGB picture for Arctic summer over a part of Siberia (June 24th, 2005). Snow covered pixels are indicated in blue.

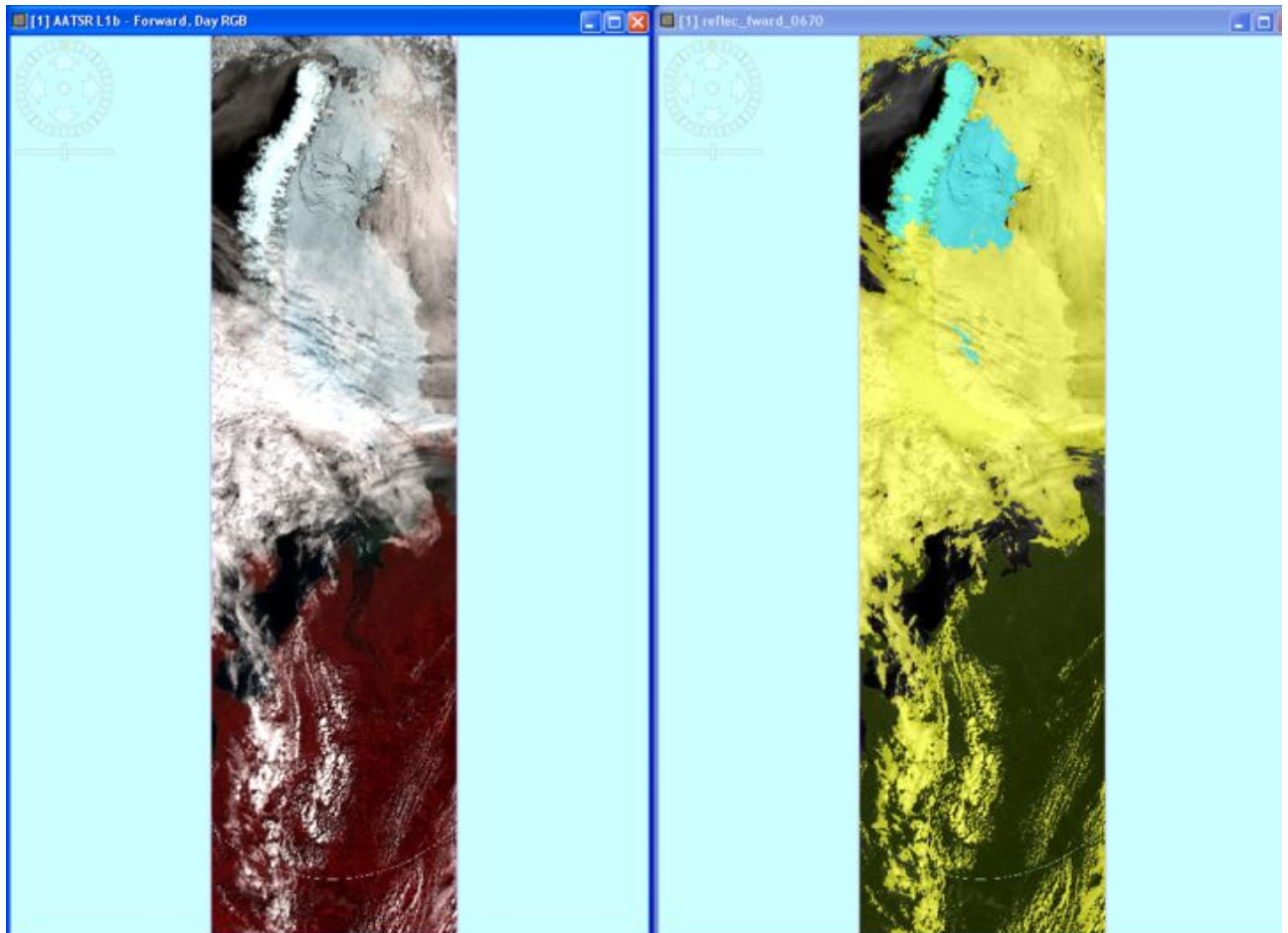


Figure 18: Comparison of cloud detection results from latest Idepix version (right, in yellow) with the AATSR (forward view) RGB picture for Arctic summer over a part of Siberia (June 24th, 2005). Snow covered pixels are indicated in blue.

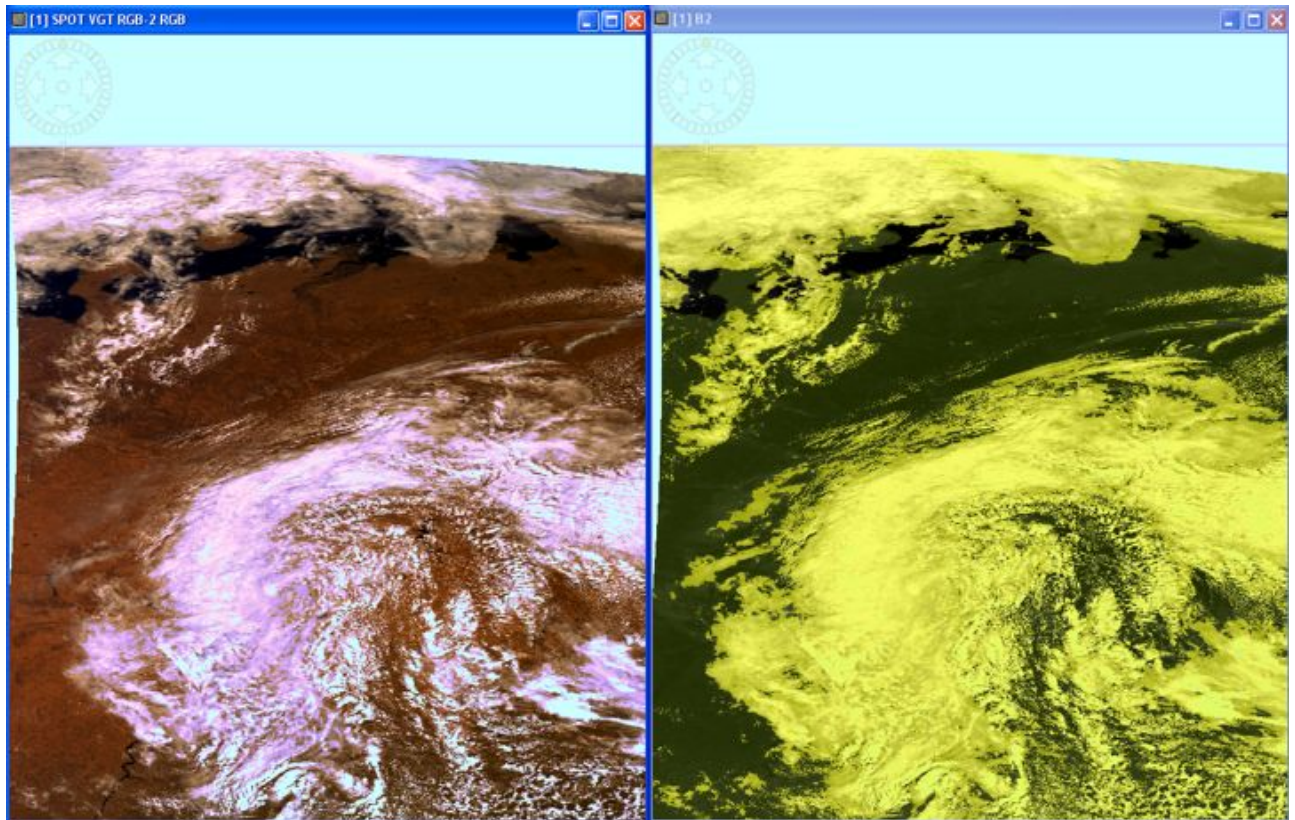


Figure 19: Comparison of cloud detection results from latest Idepix version (right, in yellow) with the SPOT VGT RGB picture for Arctic summer over a part of Siberia (June 24th, 2005).

8.2.1.5 Arctic, Spring

The following examples show Idepix cloud/snow classification results for 'Arctic'/'Spring' in comparison with the underlying RGB images.

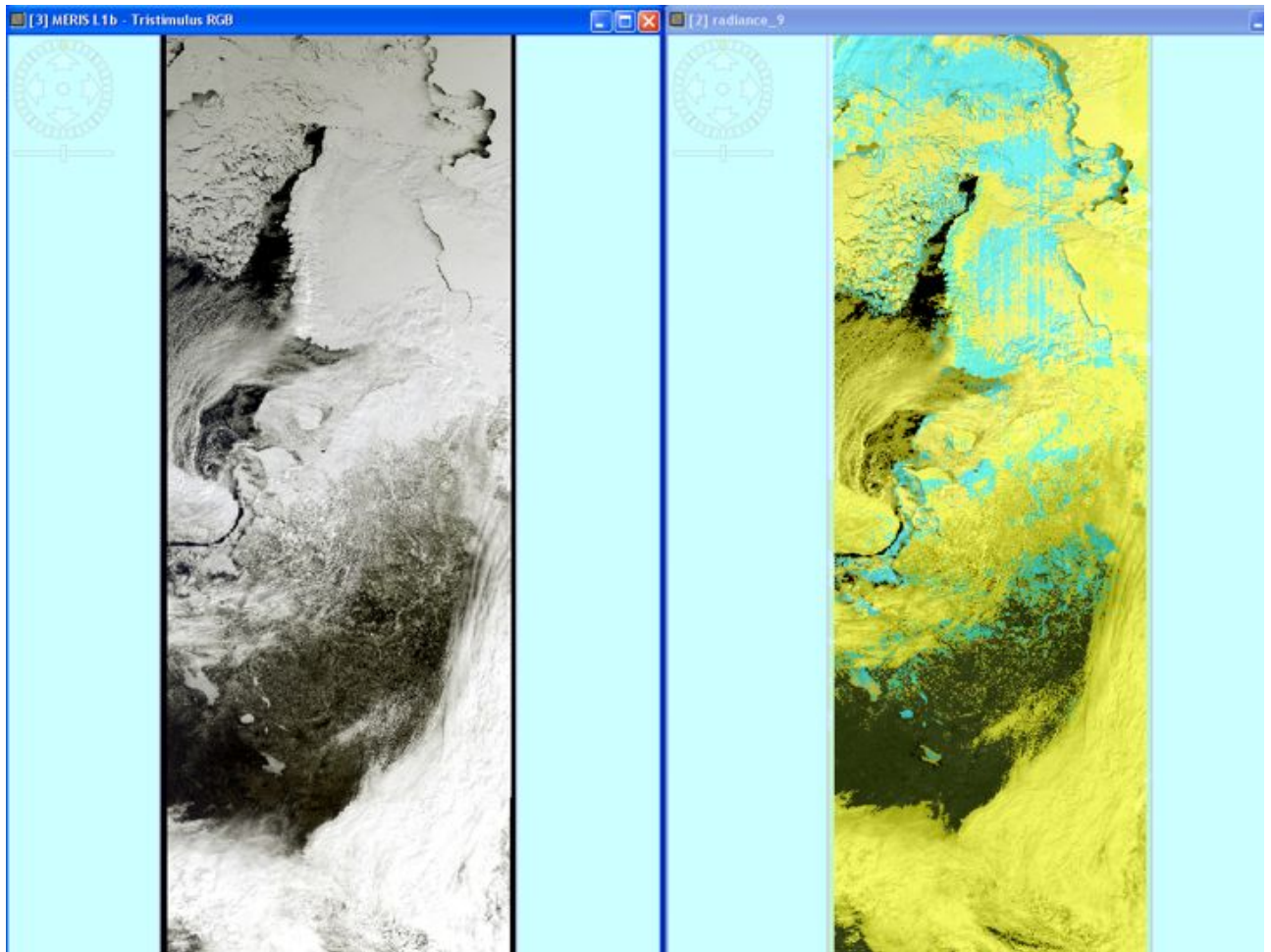


Figure 20: Comparison of cloud detection results from latest Idepix version (right, in yellow) with the MERIS RGB picture for Arctic spring over a part of Siberia (April 18th, 2005). Snow covered pixels are indicated in blue.

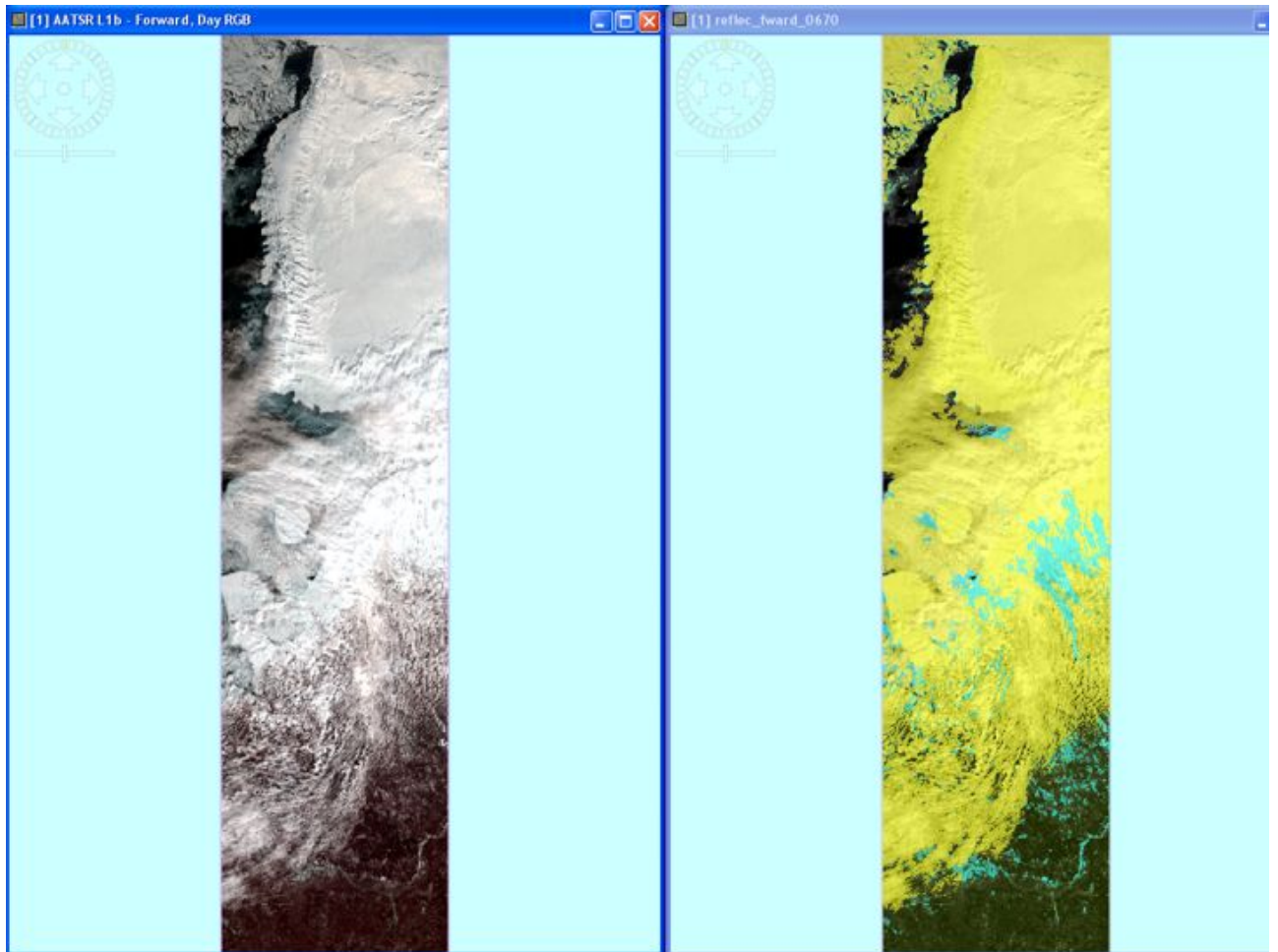


Figure 21: Comparison of cloud detection results from the latest Idepix version (right, in yellow) with the AATSR (forward view) RGB picture for Arctic spring over a part of Siberia (April 18th, 2005). Snow covered pixels are indicated in blue.

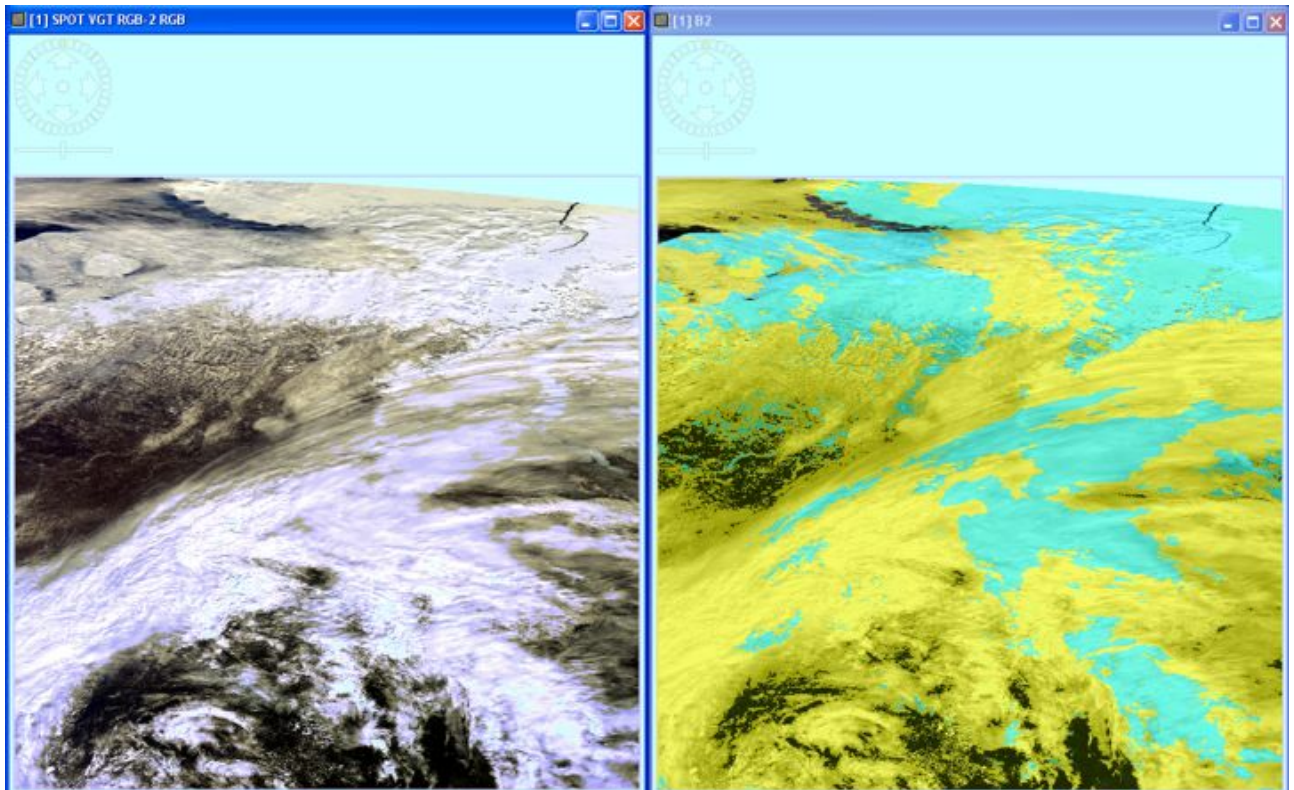


Figure 22: Comparison of cloud detection results from the latest Idepix version (right, in yellow) with the SPOT VGT RGB picture for Arctic spring over a part of Siberia (April 18th, 2005).

8.2.1.6 Tropics, Summer

The following examples show Idepix cloud/snow classification results for 'Tropics'/'Summer' in comparison with the underlying RGB images.

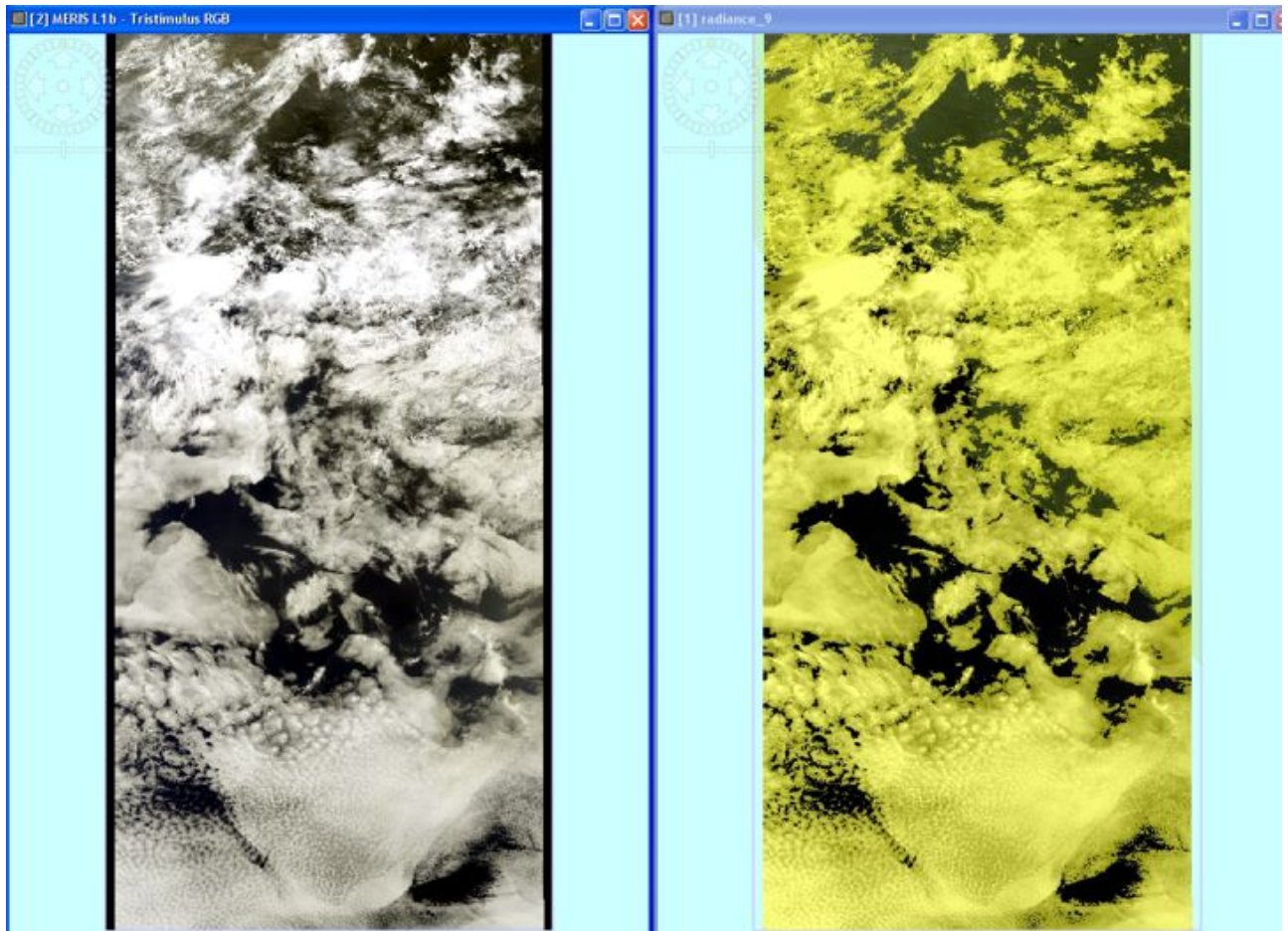


Figure 23: Comparison of cloud detection results from the latest Idepix version (right, in yellow) with the MERIS RGB picture for Tropical summer over west Africa near the equator (June 22th, 2005).

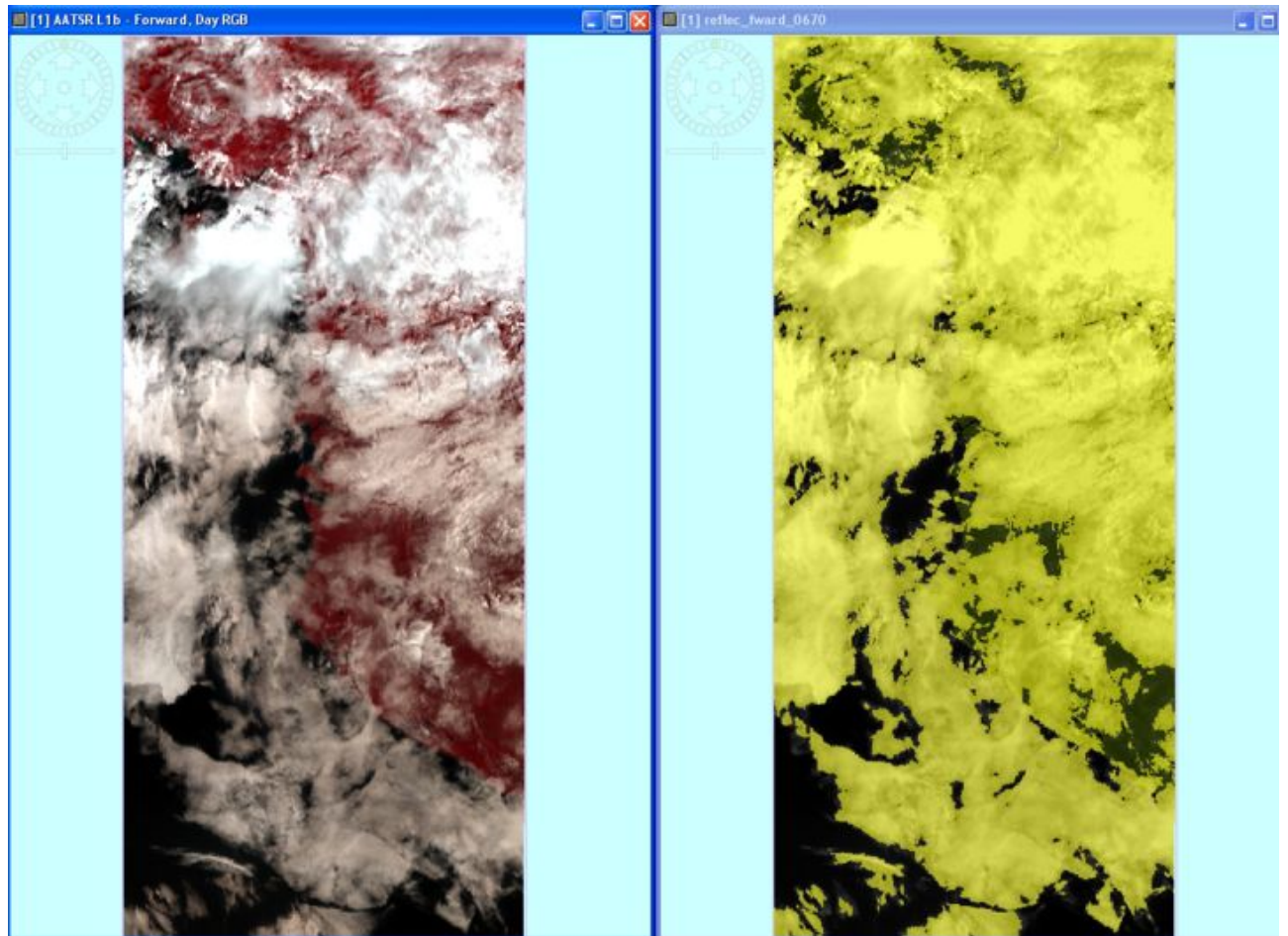


Figure 24: Comparison of cloud detection results from the latest Idepix version (right, in yellow) with the AATSR (forward view) RGB picture for Tropical summer over west Africa near the equator (June 22th, 2005).

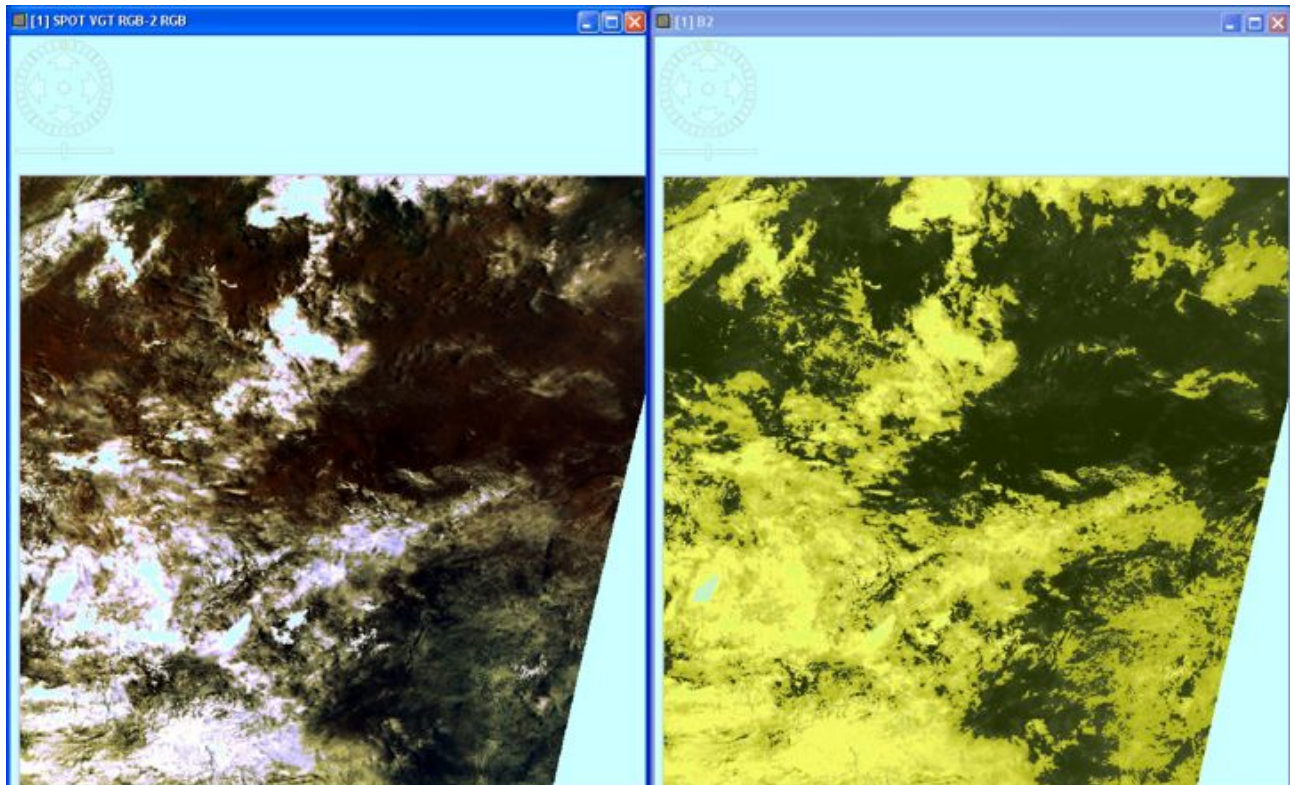


Figure 25: Comparison of cloud detection results from latest Idepix version (right, in yellow) with the SPOT VGT RGB picture for Tropical summer over west Africa near the equator (June 22th, 2005).

8.2.1.7 Antarctica: Clouds over ice

Figure 29 shows the same type of comparison as Figure 6, Figure 7 and Figure 9, but for a SPOT VGT example taken from a DOME-C dataset. It can be seen that Idepix after further threshold tuning obviously gives a very reasonable result which is significantly better than the VGT 'cloud certain' flagging, and also compared to the Idepix result from the first threshold tuning. However, it must be noted that cloud detection over ice is extremely difficult, and other examples which have been investigated do not show the improvement as clearly as this case.

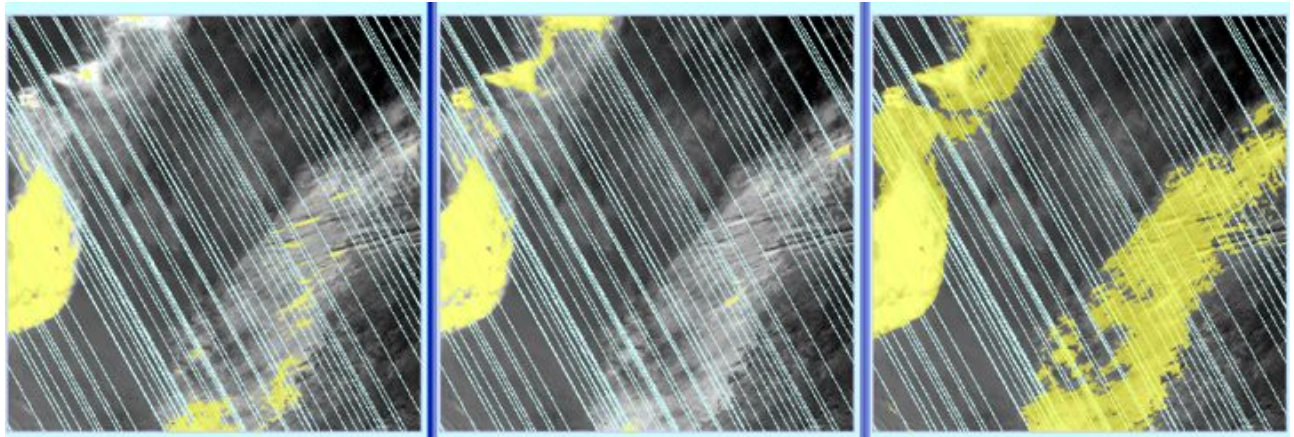


Figure 26: Cloud detection from operational VGT product (left, 'cloud certain' flag) and from Idepix after first threshold tuning (middle) and after a further threshold adjustment (right). The scene has been taken from a DOME-C dataset and illustrates the difficult case of cloud detection over ice.

8.2.2 Cloud classification: Introduction of a "cloud buffer" and comparison with MODIS prior outliers

As an alternative validation approach besides simple visual inspection, the Idepix cloud classification results have been compared with 'outliers' (i.e. flagged as clouds) taken by comparing the SDR or BBDR reflectance from the corresponding MODIS prior products. Examples of these inter-comparisons are shown in Figure 27 and Figure 31. The examples also illustrate the application of a 'cloud buffer', which is a further tuning option in Idepix and simply flags a certain region around a cloudy pixel as a buffer. This additional flag helps to further minimize the number of pixels which appear to be cloudy, but which were flagged as cloudy. This is often useful in edge regions of larger cloud fields where the clouds become very thin.

Figure 27 and 31 show an example for tile h18v04 for MERIS and VGT. For both, MODIS prior outliers are in red, Idepix cloud mask in yellow. For both examples, the upper right image shows the MODIS prior outliers together with the cloud mask of the first Idepix version, indicating that Idepix lost too many clouds. The lower left image shows the cloud masks with the recent Idepix, already detecting many more clouds. The lower right image shows the same, but with the cloud buffer as mentioned above (buffer width = 2 pixels), which leads to a result quite close to the MODIS priors. However, we can also see that the priors do not necessarily deliver the "cloud truth", i.e., for MERIS, a lot of comparably bright pixels which are obviously cloud-free (South France, North-east Spain) are flagged as outliers.

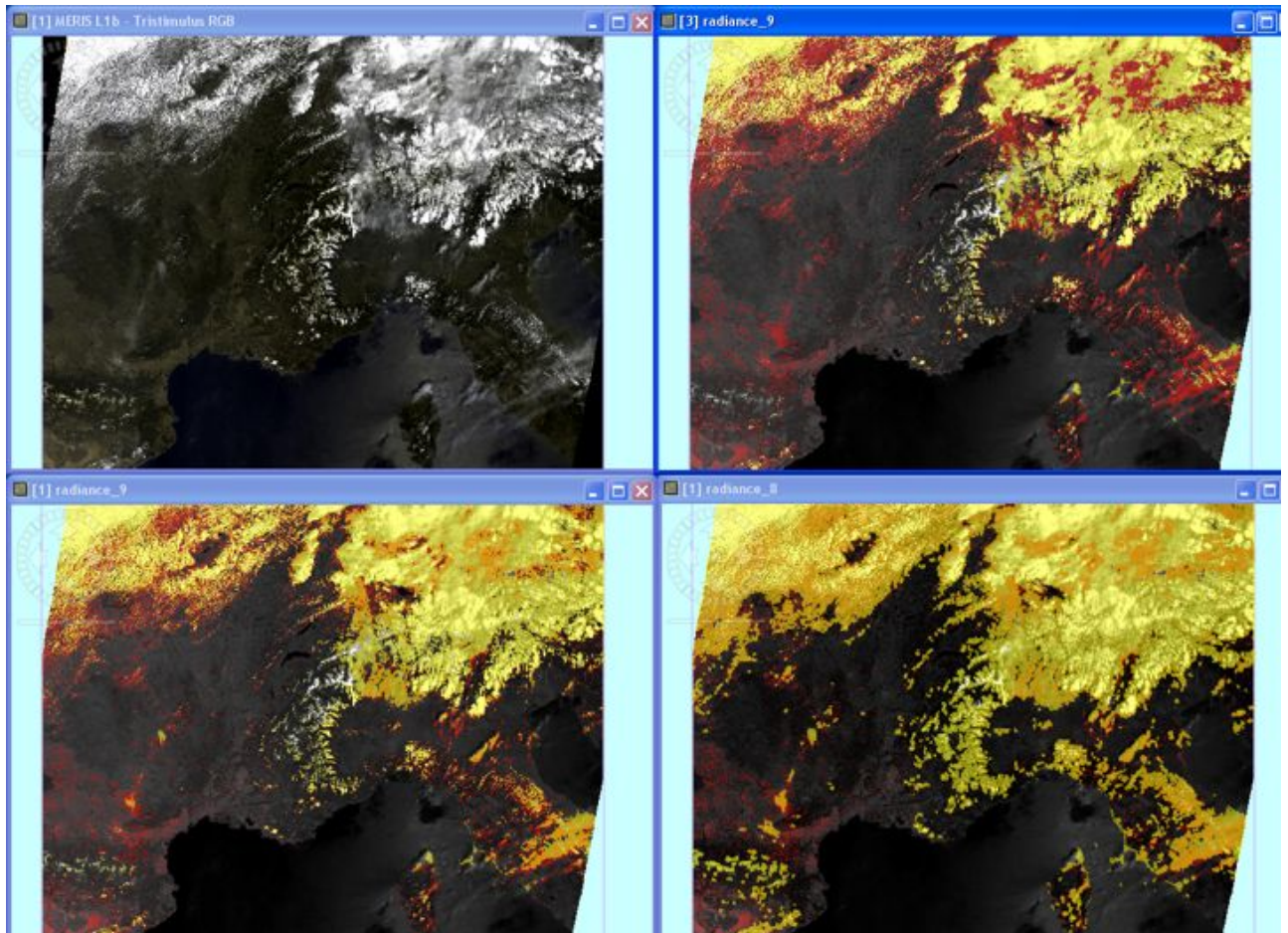


Figure 27: Comparison of Idepix cloud detection results over land (MERIS) with MODIS prior outliers over Southern France and Northern Italy (MODIS tile h18v04, June 17th, 2005). Upper left: MERIS RGB, upper right: Idepix (first version), lower left: latest Idepix version, lower right: latest Idepix version using a two-pixel cloud buffer. MODIS prior outliers are in red, Idepix cloud mask in yellow.

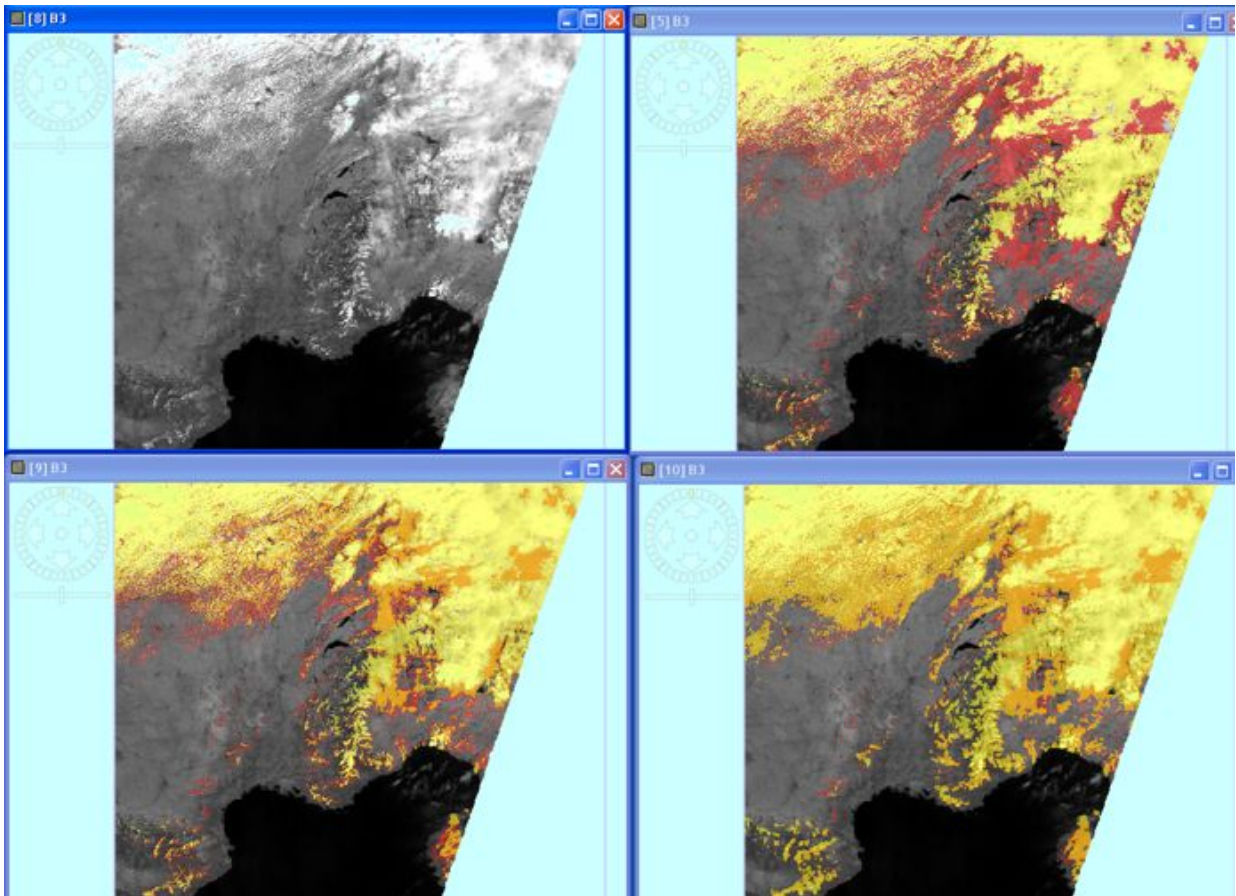


Figure 28: Same as previous figure, but for SPOT VGT.

8.2.3 Cloud/Snow distinction: Comparison with MODIS data

In a similar way as described in the previous section, the Idepix cloud/snow classification has been compared with MODIS data available from the MOD10A1 daily snow products, which contain a cloud as well as a snow flag. The examples in Figure 29 and 33 show a scene for MODIS tile h22v02 (part of central Siberia, May 11th, 2005), snow and clouds over more or less flat land).

The results show in general good agreement. However, from a visual inspection of the RGBs it is obvious that all sensors (including MODIS) have some problems to distinguish snow from neighbored cloudy pixels. Also, all sensors seem to miss a few pixels which a human observer would likely classify as either cloud or snow. Overall, for both MERIS and VGT the Idepix classification leads to a bit more cloudy pixels than MODIS and to a bit less snow covered pixels than MODIS. This should be ok for the "Globalbedo point of view" where doubtful pixels are better flagged out than being processed and introducing undesired effects (as it was the case with the first Idepix version which generally classified too few clouds, as shown above).

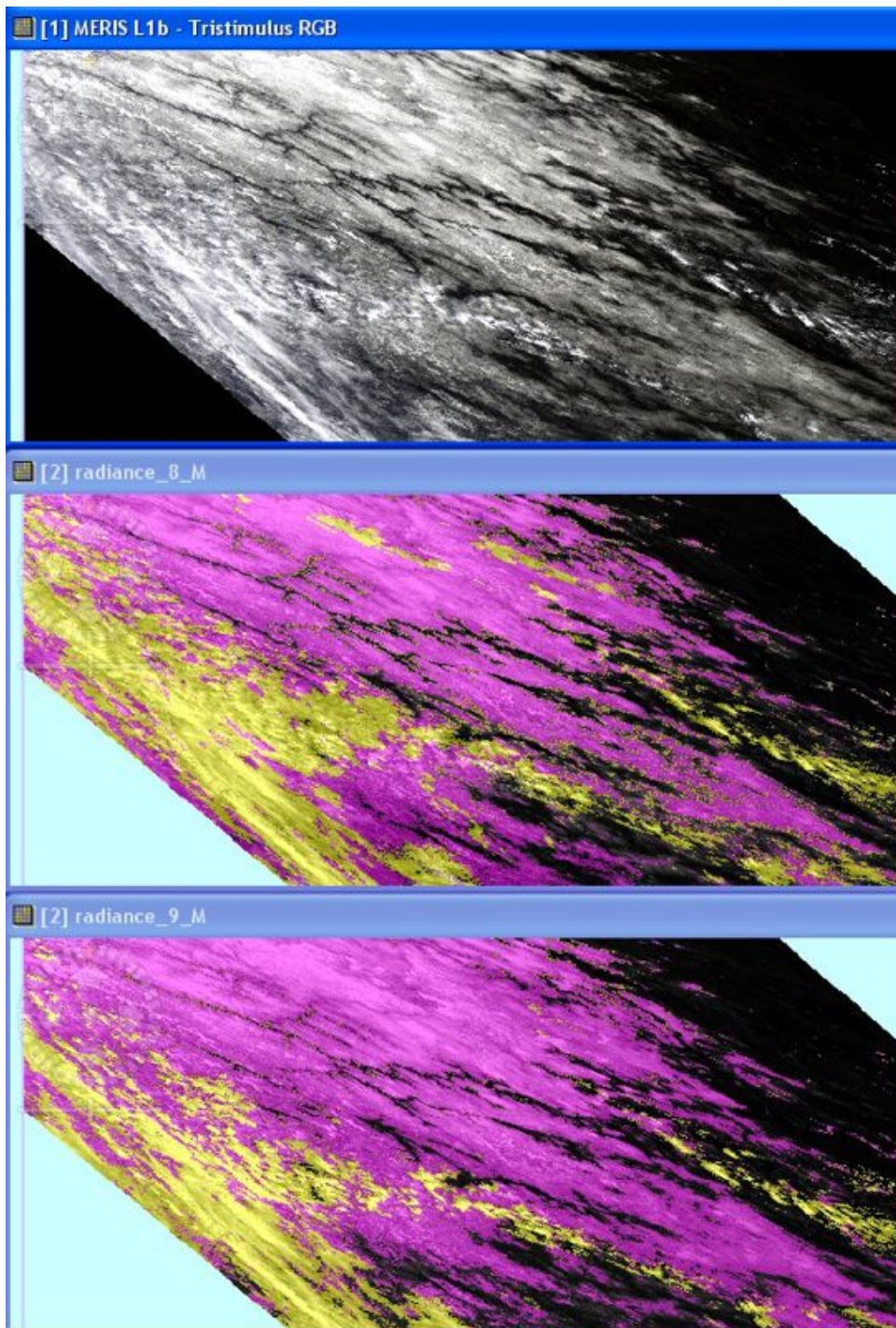


Figure 29: Comparison of Idepix cloud and snow detection results (MERIS) with MODIS cloud/snow flags from MOD10A1 snow product, for MODIS tile h22v02 (part of central Siberia, May 11th, 2005). Top image: RGB, centre image: Idepix, bottom image: MODIS. Cloud=yellow, snow=purple.

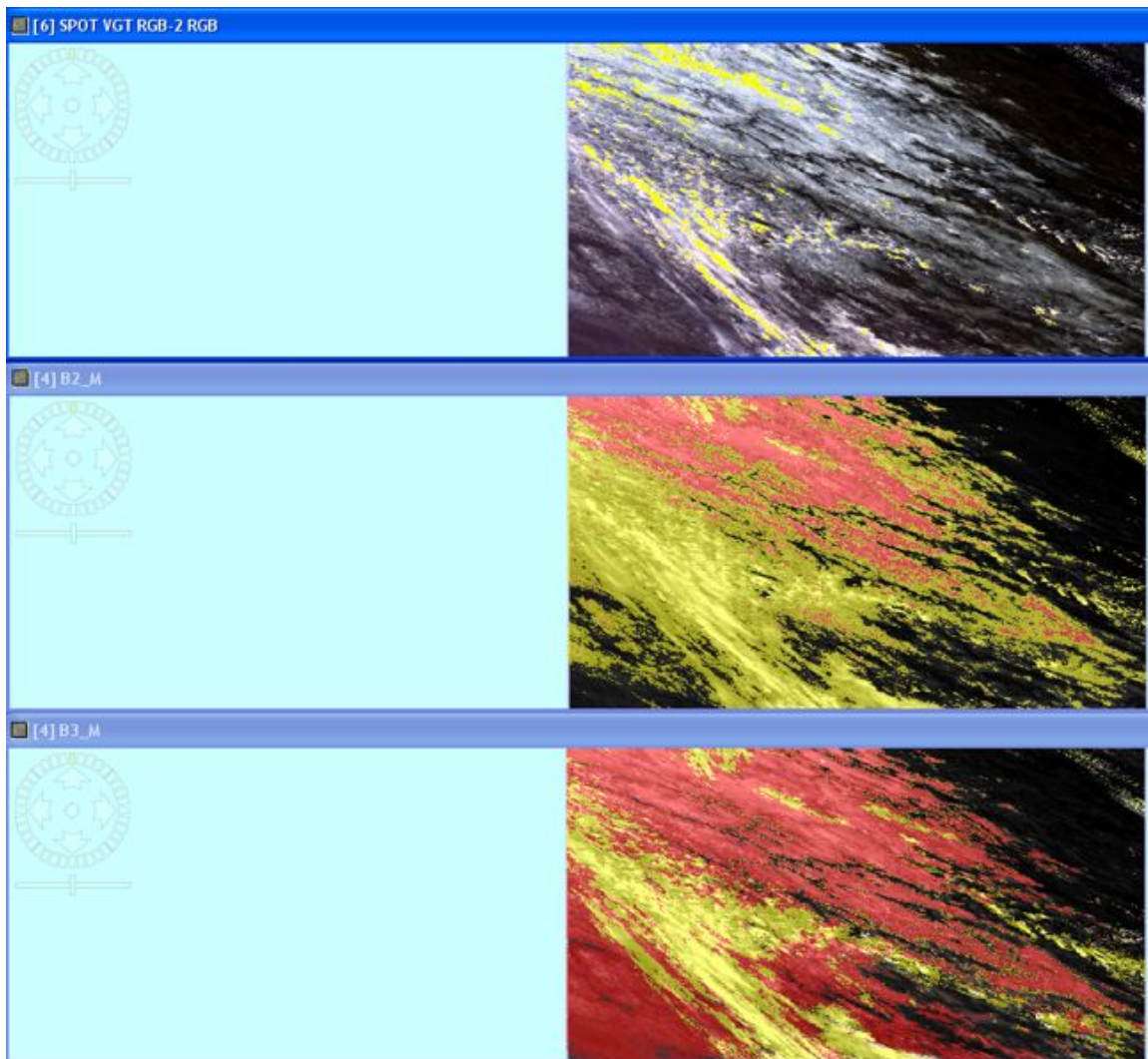


Figure 30: Comparison of Idepix cloud and snow detection results (SPOT VGT) with MODIS cloud/snow flags from MOD10A1 snow product, for MODIS tile h22v02 (part of central Siberia, May 11th, 2005). Top image: RGB, centre image: Idepix, bottom image: MODIS. Cloud=yellow, snow=red.

8.3 Cloud/snow mask improvements

The extension and further improvement of IDEPIX is still an ongoing BC activity. The GlobAlbedo processing software can benefit from latest improvements at any time since IDEPIX is used as plugin which can be easily updated. This section illustrates improvements in the results of the IDEPIX version used for the GlobAlbedo QR, compared to the IDEPIX version which the results reported in the PPVR (D-10) were obtained from.

8.3.1 MERIS

From threshold adjustments in the IDEPIX classification for MERIS, the following improvements could be achieved:

- reduction of cloud artefacts in desert regions
- reduction of cloud artefacts at coastlines
- reduction of cloud artefacts from sunglint over water (not relevant for GlobAlbedo)

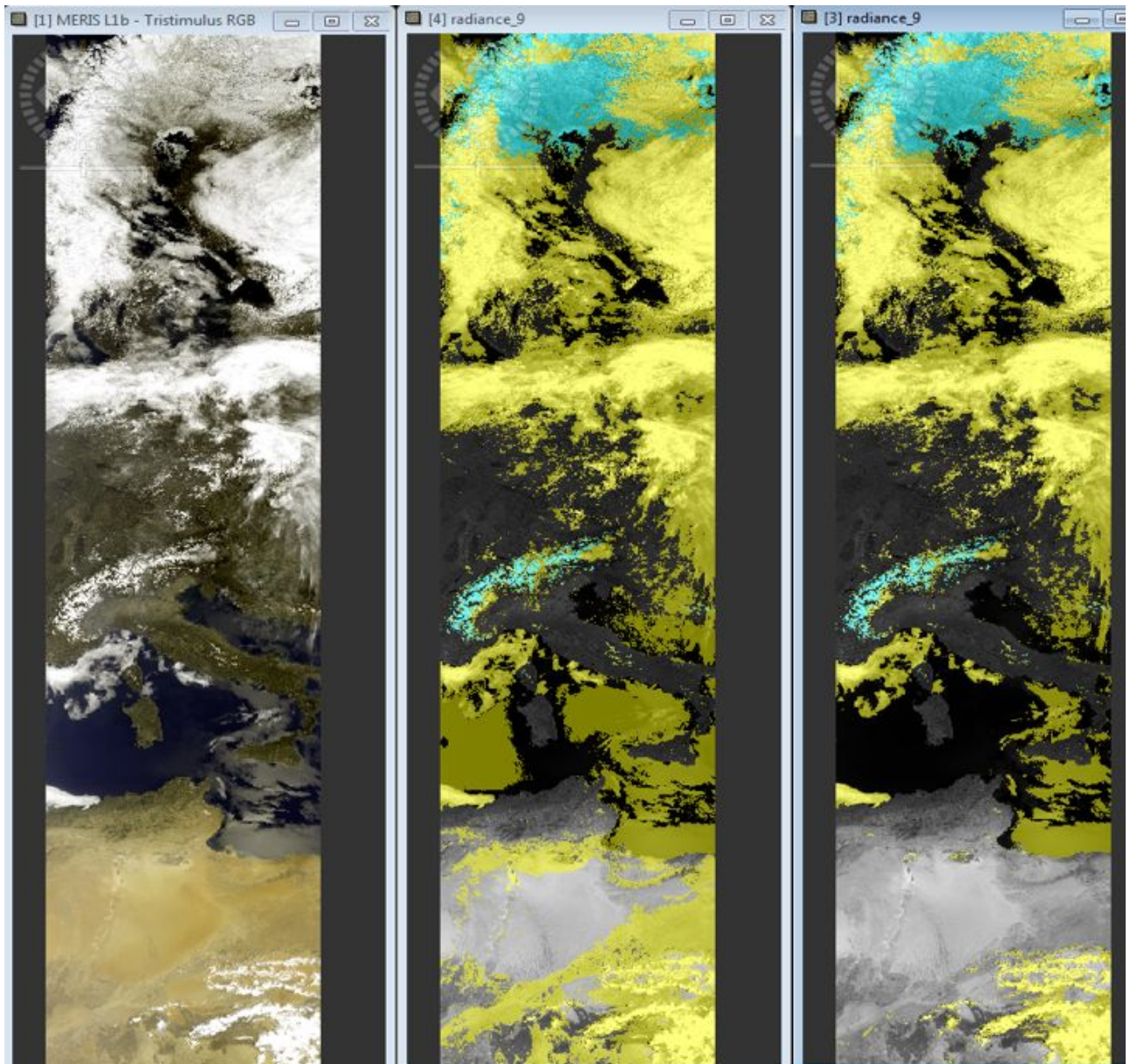


Figure 31: Comparison of MERIS cloud/snow detection results from ‘PPVR Idepix version’ (center) with ‘QR Idepix version’ (right) for May 1st, 2005. The MERIS RGB picture is on the left. Cloud pixels are indicated in yellow, snow covered pixels in blue.

Figure 31 shows a subset of a MERIS swath from May 1st, 2005, covering regions from Northern Europe down to the North African deserts. It can be seen that the cloud artefacts

obviously present in the result of the ‘PPVR Idepix version’ are significantly reduced (almost eliminated) in the QR Idepix version’. On the other hand, we see only slight changes (if any) over the European land surfaces, the good results could be kept. This example also illustrates the reduction of sunglint pixels misclassified as clouds over the Mediterranean Sea. Although water pixels are not relevant for GlobAlbedo, this is an important improvement for the application of Idepix in other projects.

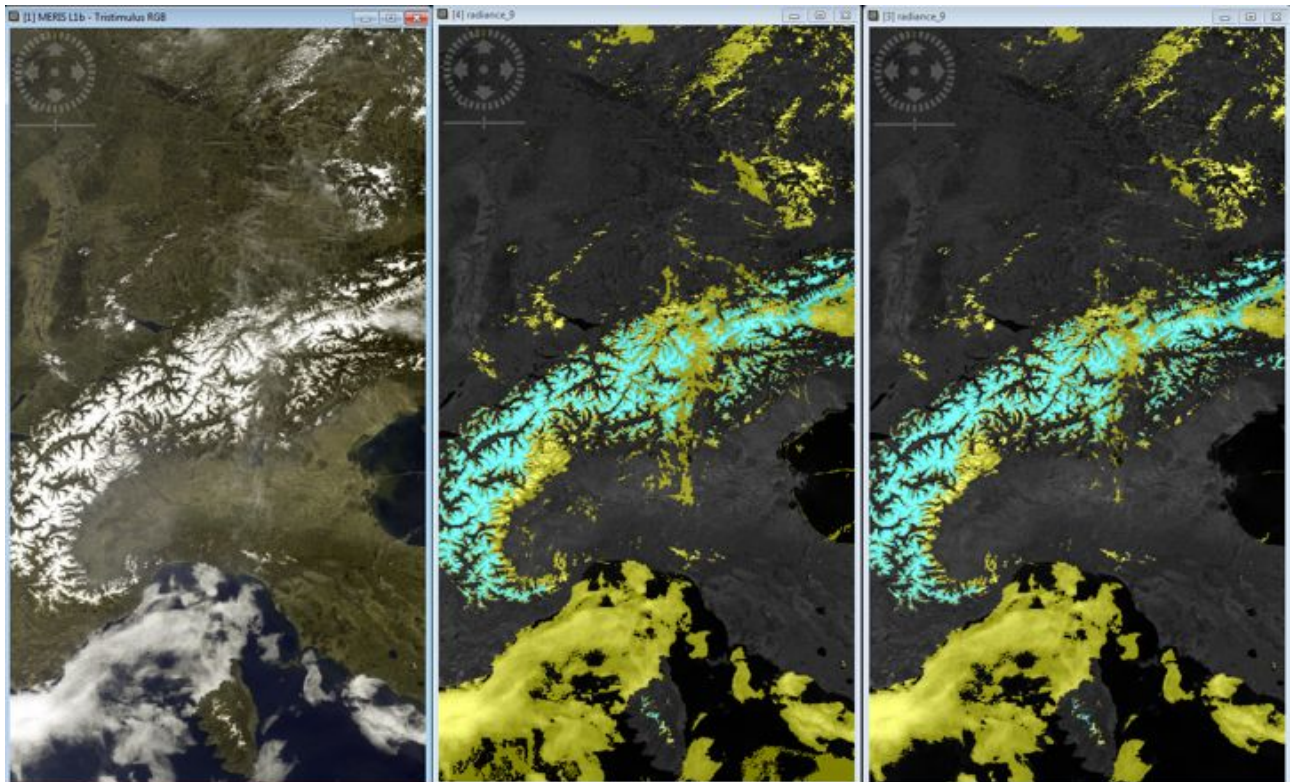


Figure 32: Same as previous figure, but zoomed into the region around the Alps.

Figure 32 shows the same scene, but zoomed into the region around the Alps. As said above, changes in the classification between the two Idepix versions are small. Overall, the snow detection over the Alps looks quite good. Some pixels appearing as snow from the RGB are classified as clouds, but the distinction between clouds and snow is very hard even from the RGB

8.3.2 VGT

From threshold adjustments in the IDEPIX classification for VGT, the following improvements could be achieved:

- reduction of cloud artifacts in the vicinity of snow

The results of previous IDEPIX versions indicated that the fraction of clouds in the vicinity of snow was obviously overestimated for VGT. With further threshold adjustments, this

effect could be significantly reduced (although not completely eliminated), as shown in the following figures.

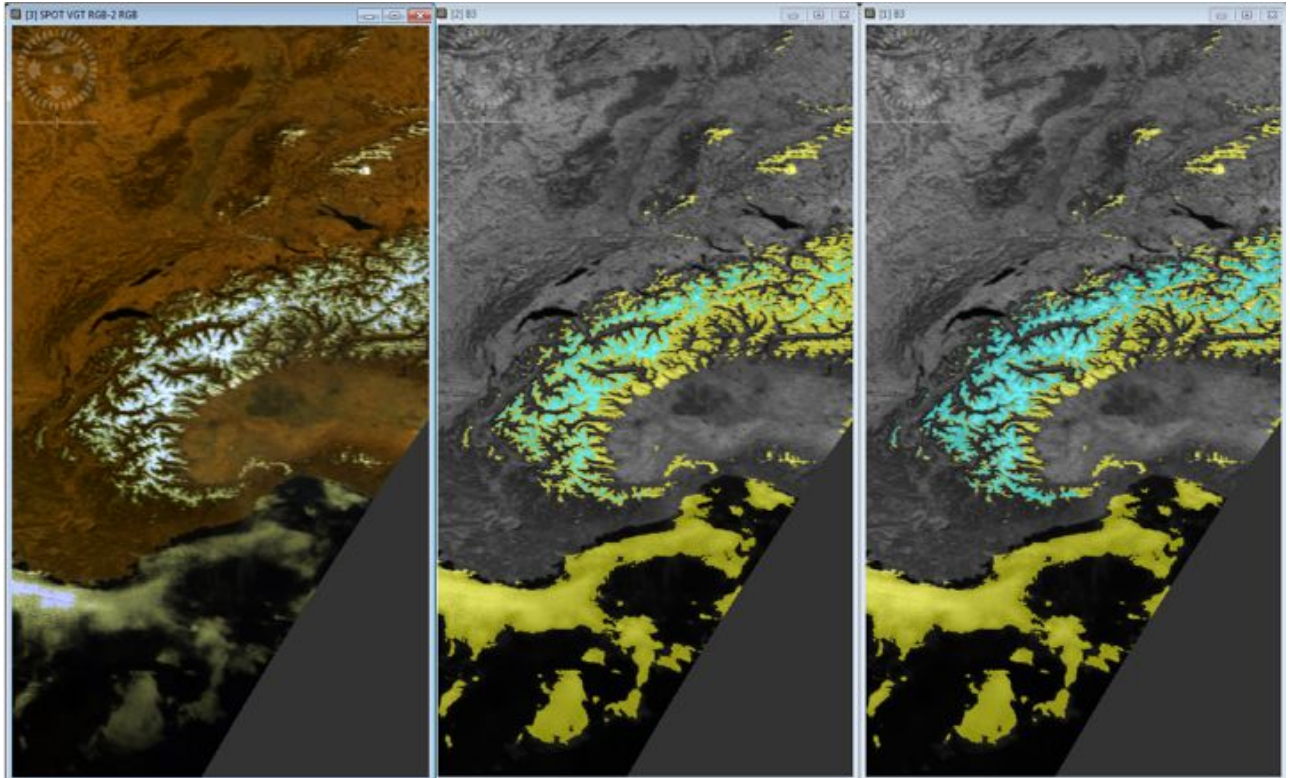


Figure 33: Same day and similar region as in previous figure, but for a VGT scene.

Figure 33 shows a VGT scene for a similar region and the same day as in previous figure. At observation time the Alps region appears to be almost cloud-free. It is clearly visible that the appearance of snow was underestimated in the 'PPVR Idepix version', and pixels were misclassified as clouds instead. In the 'QR Idepix version', this effect is significantly reduced. The cloud classification for the few 'real' cloud patches in this scene looks almost perfectly over both land and water.

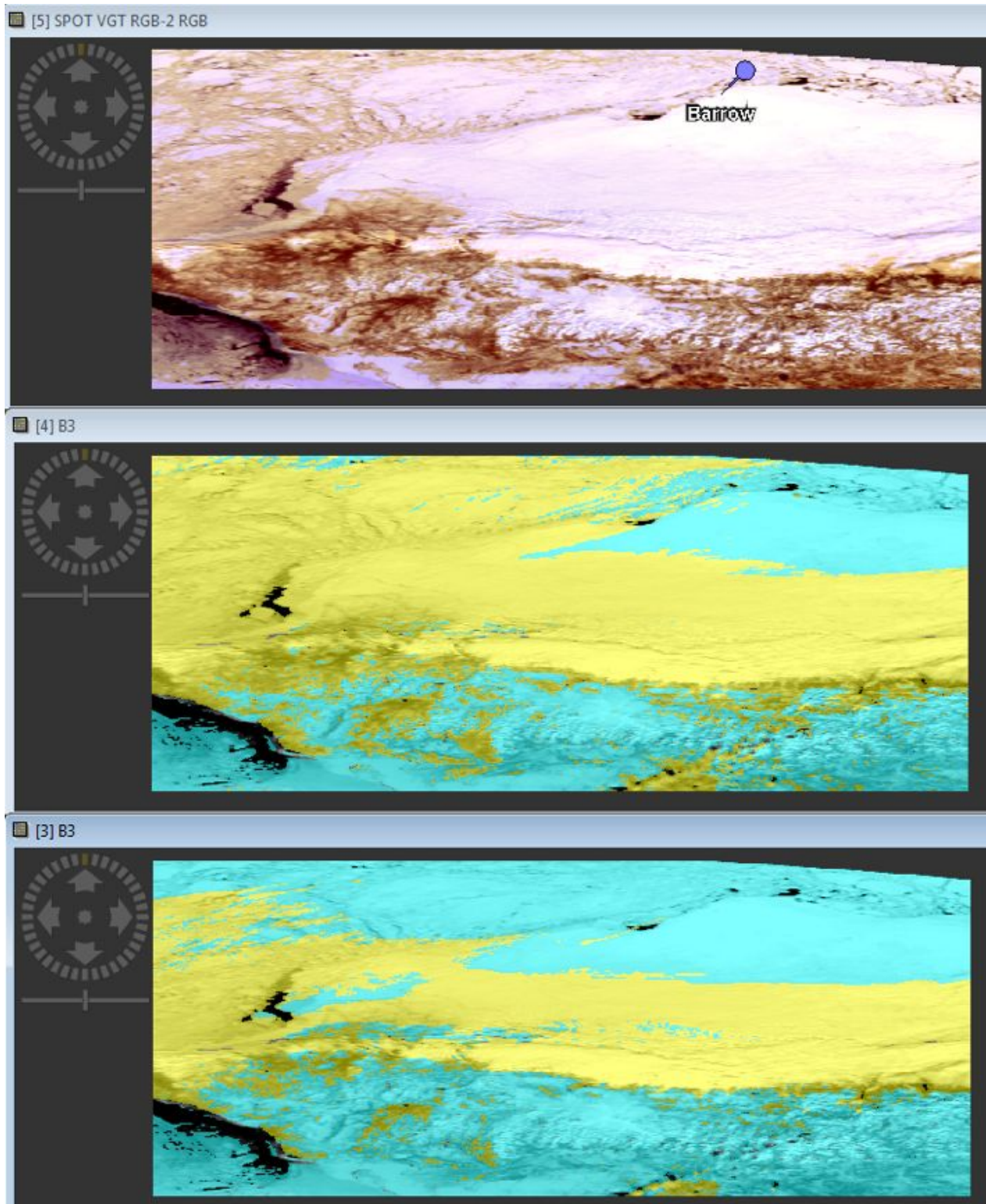


Figure 34: Comparison of VGT cloud/snow detection results from 'PPVR Idepix version' (center) with 'QR Idepix version' (bottom) for May 1st, 2005 in the region around Barrow (Alaska). The VGT RGB picture is on top. Cloud pixels are indicated in yellow, snow covered pixels in blue.

Figure 34 shows another example for the classification of clouds over large snow/ice areas in polar regions. This VGT scene is from May 1st, 2005 in the region around Barrow (Alaska). Even from the RGB it is quite difficult to identify the cloud fields and their boundaries. However, as in the previous example, the 'QR Idepix version' now classifies more pixels as snow than the 'QR Idepix version', and the result looks more reasonable.

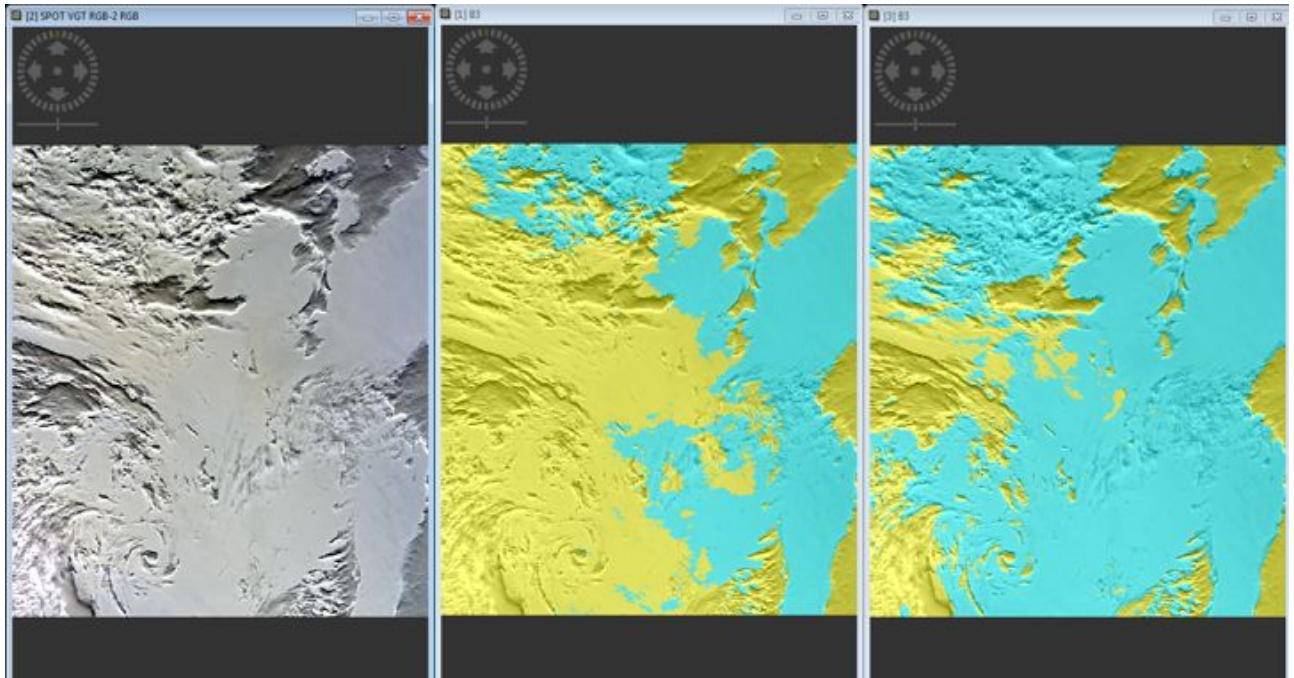


Figure 35: Comparison of VGT cloud/snow detection results from 'PPVR Idepix version' (center) with 'QR Idepix version' (right) for January 6th, 2009, in the DOME-C region (Antarctica). The VGT RGB picture is on the left. Cloud pixels are indicated in yellow, snow covered pixels in blue.

Figure 35 shows another VGT example from January 6th, 2009, in the DOME-C region (Antarctica). Here, the cloud identification from the RGB is a bit easier than for the Barrows scene because the sun illumination of the southern edges of the cloud fields gives a good contrast. Again, the 'QR Idepix version' result looks more reasonable, although it is still not perfect and there are obviously remaining misclassifications of snow/ice as clouds, and also vice versa.

8.4 Validation summary

The examples presented give a first insight of the performance of the pixel classification within GlobAlbedo. The cloud detection using the Pixel identification method (IDEPIX) provides realistic results for various atmospheric conditions and allows for adequate classification of clouds. It can be shown that even the cloud detection over snow and ice can be improved (as shown for SPOT VGT). The presented seasonal and regional distinction is a valuable step towards a comprehensive validation of pixel classification results. Also, the reasonable agreement with corresponding MODIS results improves confidence in the Idepix classification. However, it should be noted that it is extremely hard to evaluate the identification of cloud or snow pixels based on a still limited number of



case studies. An additional finding is that good results are strongly dependent on the threshold tuning for the Pixel identification. Therefore, further improvements could be achieved if more fine tuning of thresholds would be performed. This in turn would still need more data than used up to now for validation.

For a capacious evaluation of the cloud detection a higher level product assessment is definitely needed. The validation of AOT and SDR/BBDR will give indirectly insight into the performance of the pixel classification. Misclassified pixels lead to artefacts in these higher products (bright spots, borders around coastline) or unrealistic high/low values. In particular the aerosol is sensitive to not sufficiently screened sub-pixel clouds, by increasing the aerosol optical thickness. This will become obvious by the inter-comparison of AOT with other instruments and ground based measurements.

9 Atmospheric correction product

An important intermediate step of the pre-processing is the atmospheric correction of the measured top of atmosphere (TOA) reflectances. Apart from cloud detection which is part of the pixel classification step (see section 7) the amount aerosol in the atmosphere, i.e. the retrieval of aerosol optical depth (AOD) needs to be estimated. The AOD retrieval is performed individually for each sensor employing slightly different algorithms to account for the different instrument characteristics (for details see [RD4]).

This section describes the validation of the intermediate aerosol products derived from MERIS, AATSR and VGT as proposed in the product validation plan (PVP) [RD9].

Due to technical issues during the generation of the PPVR, the AATSR data could not be updated. However regarding the AOD retrieval itself, there have been no changes to the AATSR algorithm. It should further be noted that from the results for VGT and MERIS the validation improved significantly due to the use of the latest cloud screening algorithm.

9.1 Methods used

Following the PVP the validation of the AOD consists of two main parts: Firstly a quantitative analysis compares the retrieved AOD of the satellite instruments with ground based measurements made by sun photometer instruments of the AERONET network [RD10]. Secondly a qualitative analysis is performed comparing the spatial distribution of the AOD with those of other satellite products, i.e. MERIS level 2 [RD11], MODIS collection 5 [RD12] and Synergy AOD [RD13,14].

In order to obtain a sufficient number of match-ups between AERONET and the satellite, a temporal window of 45 minutes is applied to the AERONET data centred at the time of the satellite overpass. Multiple AERONET measurements within this time are averaged. A standard deviation is calculated which is used as a measure of AOD variability during that time. Due to the small number of AERONET samples in 45 minutes this standard deviation should be considered as indicator rather than a quantitative measure of variability.

The satellite data is filtered for valid aerosol retrievals. The AOD algorithm includes a spatial interpolation component to fill small spatial gaps. While this gap filling is used to estimate the AOD for the atmospheric inversion, it is not an actual measurement and thus



not included in the product validation. Furthermore the satellite AOD and AOD uncertainty are averaged over a box of 9x9km centred at the AERONET station.

9.2 Analysis

The validation of the AOD retrieval of the Globalbedo Final Product set for 2005 is mainly performed by comparisons of the retrieved AOD for the sensors VGT and MERIS against ground based sun photometer measurements performed by CIMEL instruments within the AERONET. From the AERONET data base all available data for 2005 was searched for spatial and temporal match ups with the satellite orbital (level-2) measurements. Figure 36 shows a map with the locations of all available AERONET stations for 2005 as reported on the AERONET website.

The following criteria were used to identify match ups:

- Satellite data of 17x17 pixels centred at the location of a AERONET station were averaged. No threshold was applied, so even a single valid retrieval within a 16km distance from the AERONET station would produce a positive match.
- AERONET data from a 2 hour time window centred at the actual overpass time of the satellite instrument is averaged. However we require that at least 3 valid AERONET measurements are available in this time window. Furthermore, matches are only valid if the maximum variation, i.e. the difference between minimum and maximum value, is below 0.1. The later criterion is used to filter conditions when the AOD rapidly changing.

Based on this selection a total number of 8,513 matches for VGT and 4211 matches for MERIS were identified for the year 2005.

To gain information on potential regional biases, the match-up data set was separated into six geographical regions, which are highlighted in Figure 36. The individual regional scatter plots showing retrieved AOD versus AERONET AOD are shown in Figure 37 for VGT and in Figure 38 for MERIS. The colour coding indicates the density of samples. The plots show a large amount of scatter despite a reasonable correlation. A qualitative analysis of the distribution of points indicates a considerable underestimation of AOD by the satellite retrievals. The retrieval approach of fitting a linear combination of predefined vegetation and bare soil surface spectra in its current implementation seems to struggle especially in those regions which have a high fraction of non vegetated surfaces.

In order to investigate the dependence of the AOD retrievals with respect to the underlying surface types, the comparison was repeated with the data set separated by IGBP land cover type instead of geographic regions. For this analysis the MODIS IGBP land cover map of 2005 was used to classify the location of the AERONET stations accordingly.

The respective scatter plots are shown in Figure 39 for VGT and Figure 40 for MERIS. In these plots it becomes clear that all terrain types containing a certain fraction of vegetation show reasonable correlations with AERONET. However in regions of low vegetation (barren or shrubs) the retrievals do seem to fail and provide generally too high results, not well correlated with AOD. As for the other land cover types the retrieval shows a



correlation between 0.6 and 0.8 for both VGT and MERIS. However the satellite retrievals are clearly underestimating the true AOD as can be seen for the linear regression slopes. The detailed analysis of regression slopes, offset and correlation coefficients is presented in Table 8-1 for VGT and Table 8-2 for MERIS. Focussing only on surface types such as forest, crop, crop mix, grass and savannah the average slope for VGT is 0.47 and for MERIS 0.57 with respective correlations of 0.77 for VGT and 0.67 for MERIS.

In order to evaluate the uncertainty in AOD associated by the satellite retrieval the uncertainties of AOD were compared to the true difference between retrieved AOD and AERONET AOD. The results of this comparison are shown in the plots of Figure 41 for VGT and Figure 42 for MERIS. In these plots the individual retrieval uncertainties are averaged in bins of the true error. The error bars in these plots represent the respective standard deviations in these bins. The plots show, that the true error in our AOD retrieval is presently not sufficiently described by the uncertainty estimation of the satellite retrievals. In general the uncertainty seems to be too low and is furthermore not in all cases correlated to the true error as can be seen from the low slopes in the figures. The original definition of the per pixel uncertainty estimation in the retrieval still allows for a scaling factor. Optimisation might potentially improve the slope in these figures. However as noted earlier, the true error (AOD difference to AERONET) is currently dominated by the systematic underestimation of AOD. These systematic errors are not fully understood and therefore difficult to be properly included in the uncertainty estimation for the retrieval.

Despite the apparent problems these AOD retrievals currently present an important improvement especially for the VGT instrument which provides only a very crude climatological estimate of a minimum aerosol amount following a simple latitudinally dependent parameterisation.

Aeronet by regions

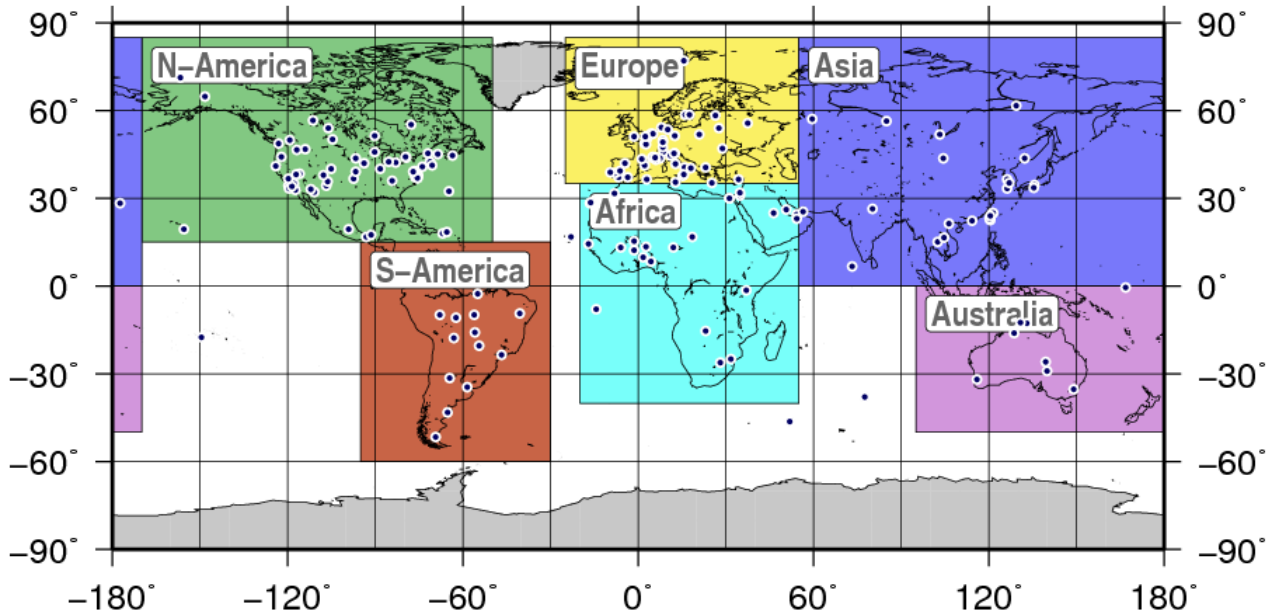


Figure 36: Map indicating the regions defined for the regional comparison plots as well as the locations of AERONET stations providing data for 2005 (black dots with white border)



VGT AOD Validation by region

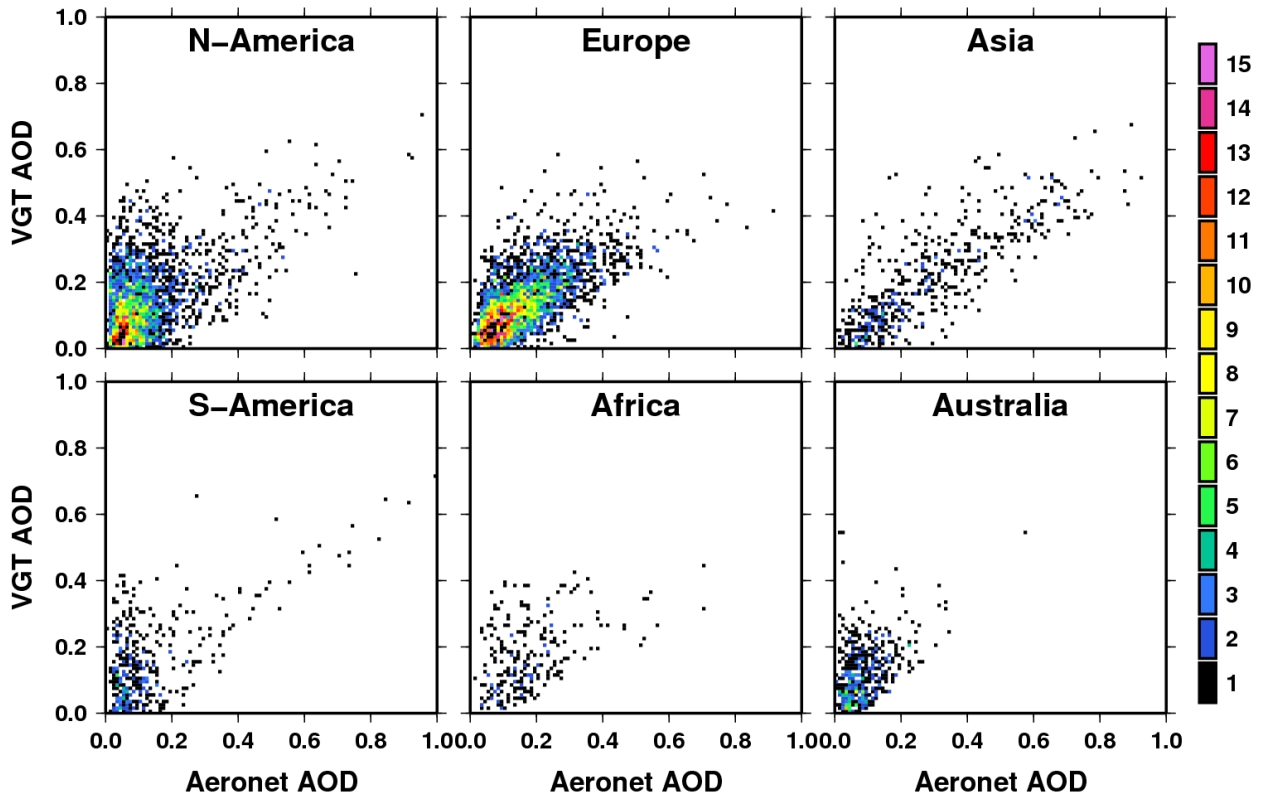


Figure 37: VGT AOD validation against co-located AERONET ground based AOD measurements separated by geographic region.



MERIS AOD Validation by region

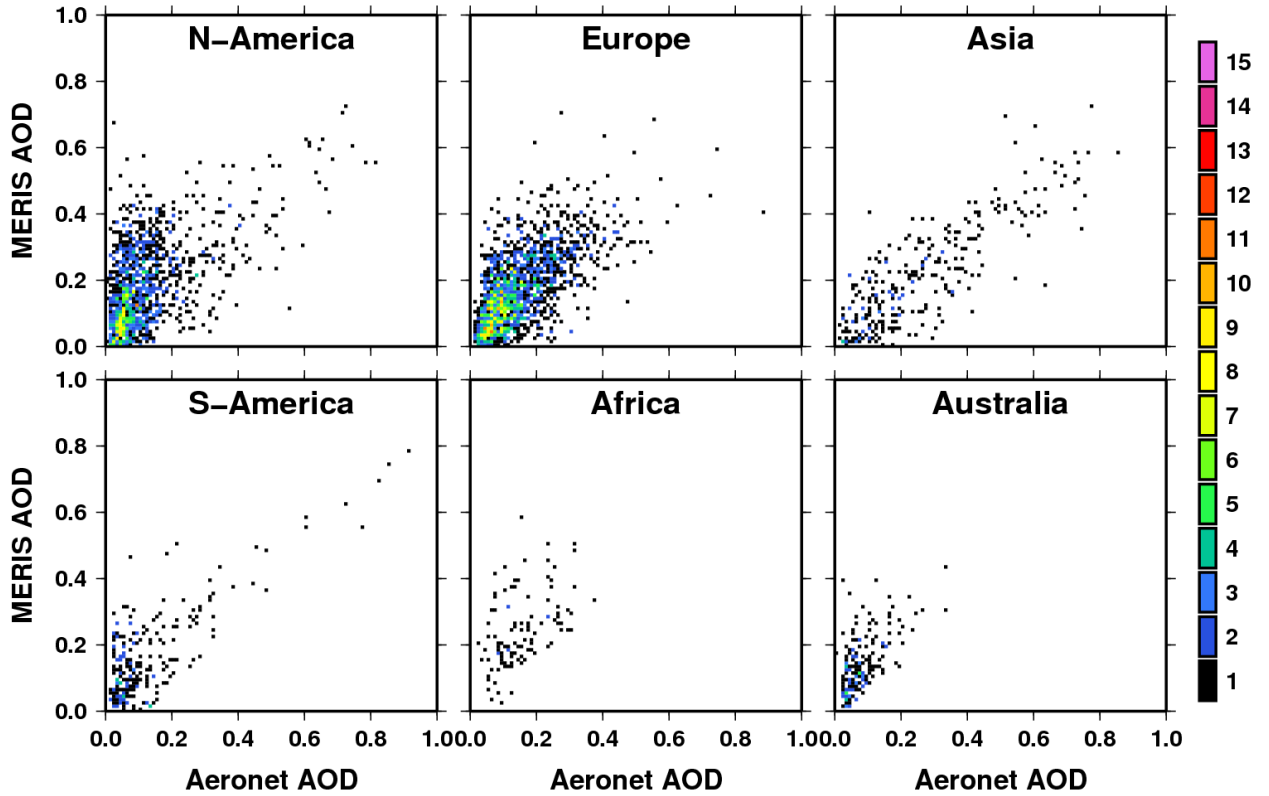


Figure 38: Regional MERIS AOD validation

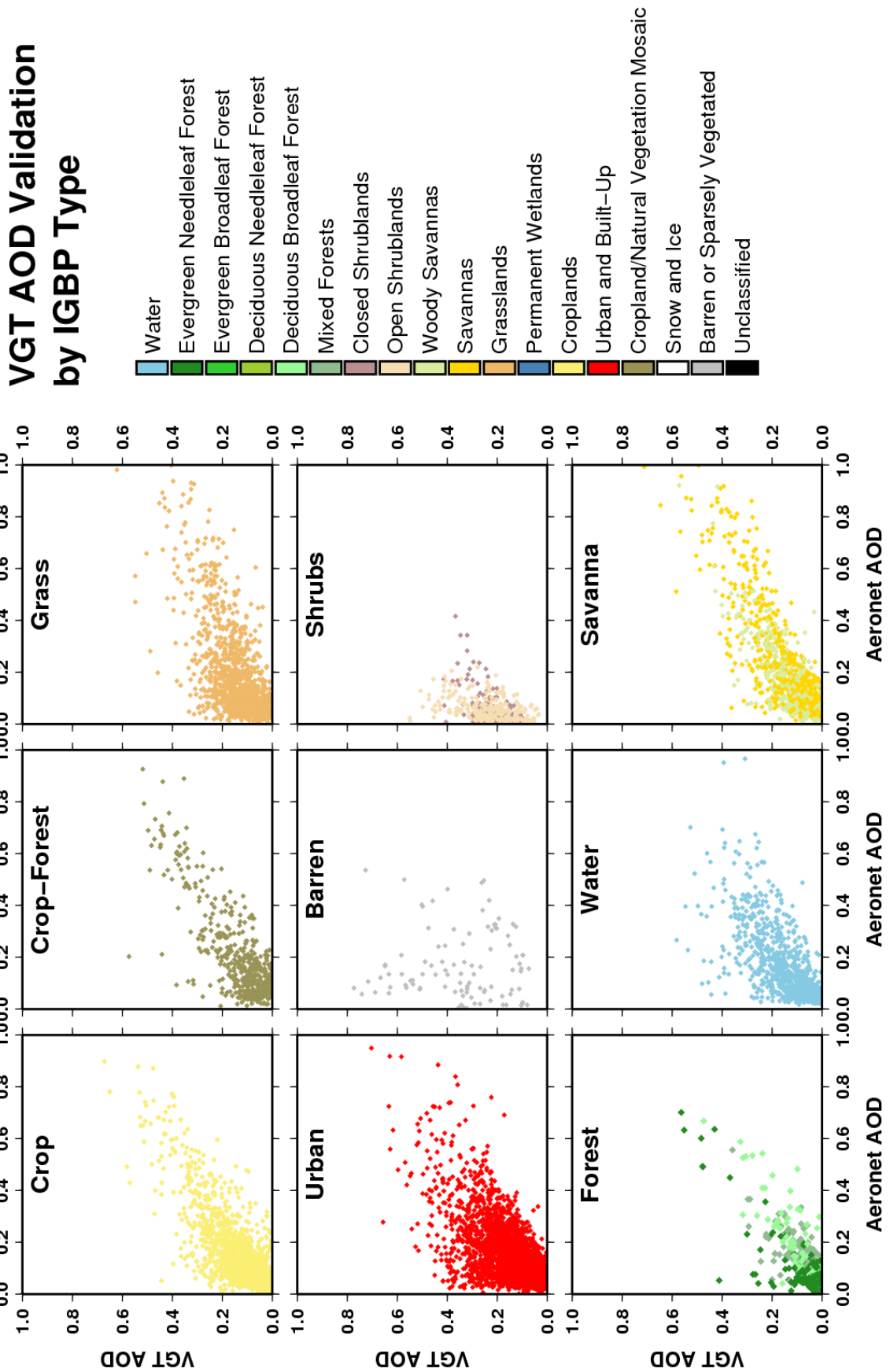


Figure 39: VGT AOD validation vs AERONET separated by IGBP land cover type



MERIS AOD Validation by IGBP Type

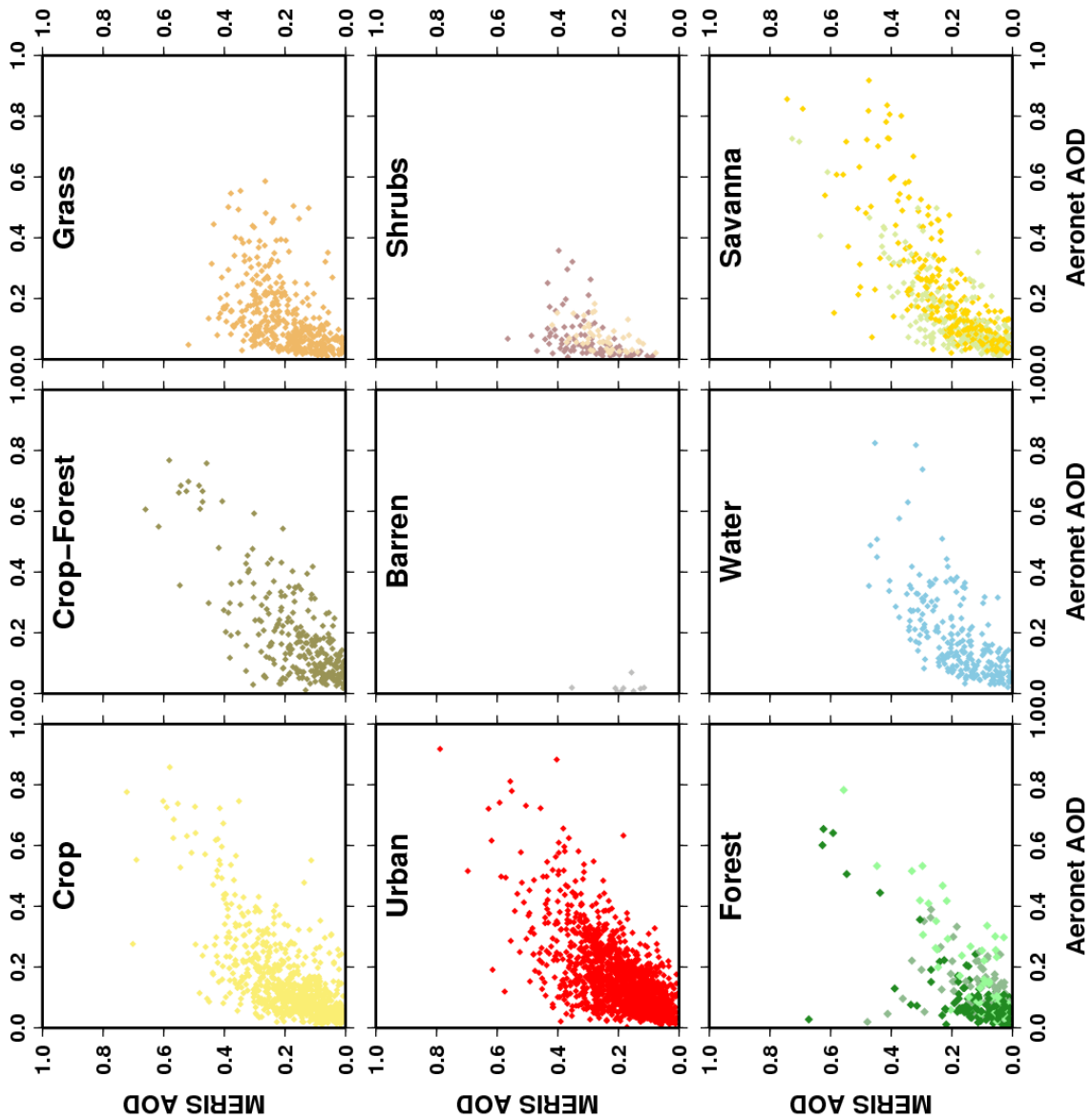
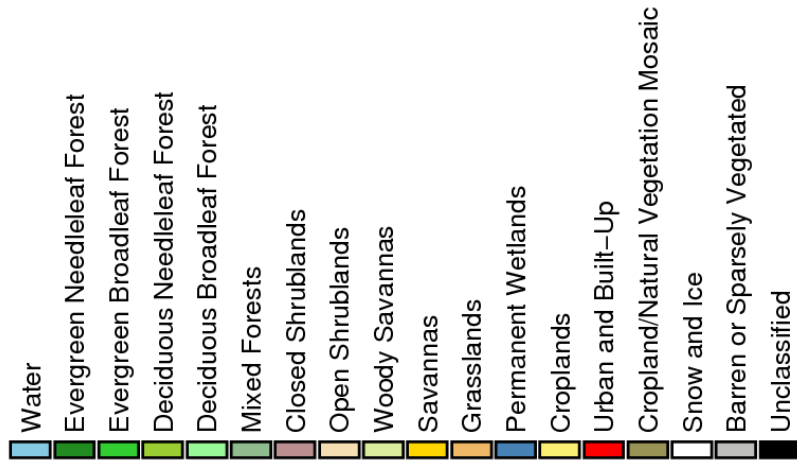


Figure 40: MERIS AOD validation vs AERONET separated by IGBP land cover type



Title: GlobAlbedo Final Validation Report

Doc. No. GlobAlbedo_FVR_V1.2

	Slope	Offset	Correlation
Forest	0.510 +- 0.019	0.020 +- 0.004	0.808 +- 0.031
Crop	0.573 +- 0.012	0.049 +- 0.003	0.776 +- 0.016
Crop / Forest Mix	0.526 +- 0.018	0.032 +- 0.005	0.803 +- 0.028
Grass	0.317 +- 0.011	0.084 +- 0.003	0.642 +- 0.023
Shrubs	0.698 +- 0.078	0.185 +- 0.006	0.410 +- 0.046
Savanna	0.447 +- 0.009	0.052 +- 0.003	0.842 +- 0.017
Barren	0.016 +- 0.140	0.342 +- 0.030	0.012 +- 0.102
Urban	0.544 +- 0.013	0.068 +- 0.003	0.626 +- 0.015
Water	0.502 +- 0.020	0.072 +- 0.005	0.663 +- 0.027

Table 8-1: VGT AOD validation statistics separated by land cover type



Title: GlobAlbedo Final Validation Report

Doc. No. GlobAlbedo_FVR_V1.2

	Slope	Offset	Correlation
Forest	0.616 +- 0.043	0.042 +- 0.007	0.649 +- 0.045
Crop	0.627 +- 0.024	0.092 +- 0.005	0.682 +- 0.026
Crop / Forest Mix	0.623 +- 0.032	0.047 +- 0.008	0.764 +- 0.039
Grass	0.433 +- 0.041	0.138 +- 0.007	0.468 +- 0.045
Shrubs	0.552 +- 0.114	0.249 +- 0.011	0.382 +- 0.079
Savanna	0.580 +- 0.018	0.091 +- 0.005	0.801 +- 0.025
Barren	-0.392 +- 1.366	0.196 +- 0.037	-0.108 +- 0.376
Urban	0.637 +- 0.019	0.089 +- 0.004	0.656 +- 0.019
Water	0.518 +- 0.039	0.084 +- 0.009	0.660 +- 0.050

Table 8-2: MERIS AOD validation statistics separated by land cover type



VGT AOD Uncertainty Validation

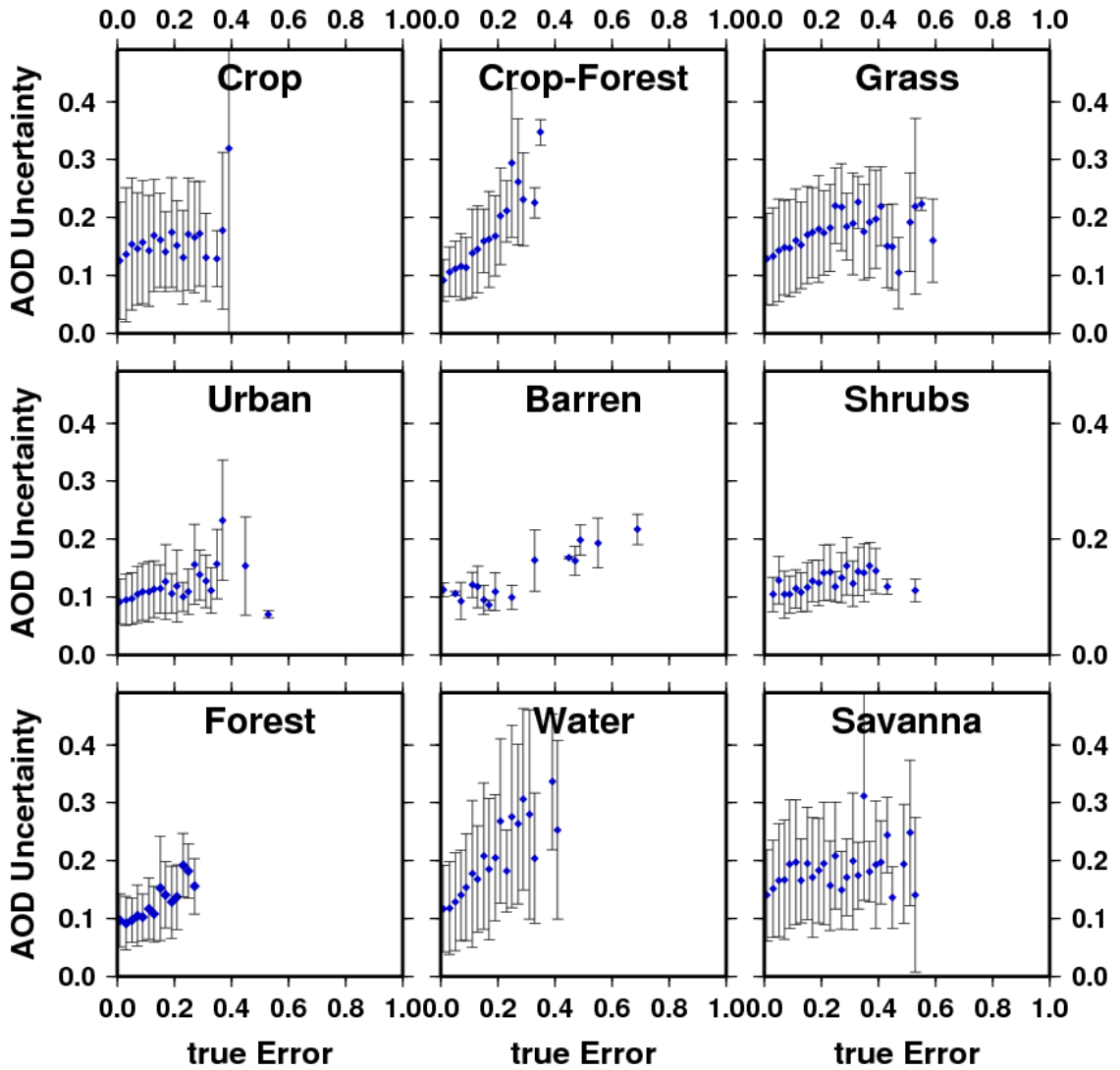


Figure 41: AOD uncertainty evaluation for VGT

MERIS AOD Uncertainty Validation

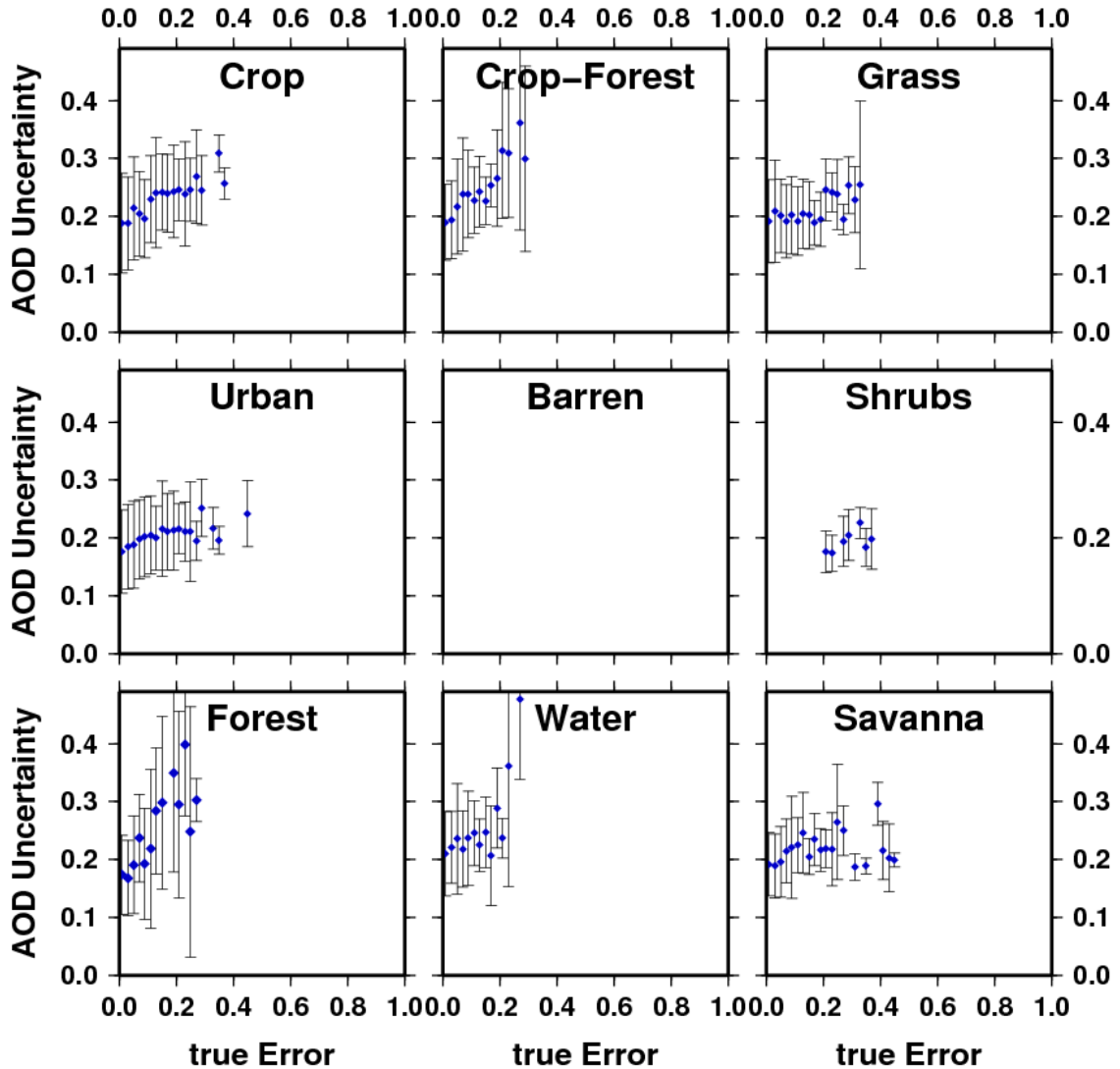


Figure 42: AOD uncertainty evaluation for MERIS

9.3 Validation summary

- Temporal evolution of AOD time series is comparable to AERONET under cloud free conditions
- In cloud free cases AOD of AATSR is slightly underestimating AERONET, AOD of VGT is significantly underestimating



- Time series at AERONET stations show large number of positive outliers due to cloud / cloud edge interferences. Better filtering will be required.
- Spatial distribution of AOD is consistent with MERIS L2 and MODIS L2 images as well as results from BEAM MERIS-AATSR-Synergy processor.

10 SDR product

10.1 Methods used

This part of the GlobAlbedo Final Product validation exercise is to evaluate the quality of the BBDR product which is produced from MERIS, (A)ATSR and VGT data by the GlobAlbedo BBDR processor [RD5] following in the GlobAlbedo processing chain the pixel identification and aerosol retrieval processors.

The BBDR product is calculated by the GlobAlbedo BBDR processor through the spectral integration of a previously derived SDR product. Since SDR is a more extended variable in optical remote sensing, the validation of the GlobAlbedo BBDR product is performed following a two-step procedure, which consists in (a) evaluating the quality of the SDR product and (b) confirming the narrow-to-broadband (N2B) conversion is consistent for the three GlobAlbedo instruments and with other N2B conversion approaches.

10.2 Validation of the SDR intermediate product

One of the main challenges in the validation of medium resolution remote sensing products such as those in GlobAlbedo, which are sampled at a nominal ground sampling distance (GSD) of 1 km, is to find reliable validation references to compare with. In addition, a proper spectral sampling is needed for comparison with external spectrally-resolved validation references.

On the other hand, it must be taken into account that the accuracy of the GlobAlbedo SDR product is not only given by the physical formulation and assumptions of the BBDR processor itself, but also by the pre-processing steps which generate inputs to the BBDR processor, which are radiometric inter-calibration, pixel identification and aerosol retrieval. The validation exercise presented in this section is focused on those aspects only associated to the BBDR processor, assuming that those other processing steps are evaluated by other means detailed elsewhere in this document.

Under these considerations, the assessment of the intermediate SDR product has been based on MERIS full-resolution (FR) data because of its higher spatial resolution (GSD of 300 m) and spectral sampling (15 channels between 412 and 900 nm). Since the BBDR processor is based on a general approach which does not make any distinction between the three instruments, the evaluation of the SDR product from MERIS FR data is assumed to be also representative of that from MERIS RR, AATSR and VGT data if initial pre-processing steps are not taken into account.

The consistency of the MERIS FR SDR retrievals performed with the GlobAlbedo BBDR processor has been evaluated by comparison with:

- 1) SDR data retrieved from MERIS FR data with the SCAPE-M atmospheric correction processor. The SCAPE-M processor [RD15] was designed for SDR retrieval from MERIS top-of-atmosphere data over land and inland waters. It has its own built-in



aerosol retrieval approach, and it is based on MODTRAN4 radiative transfer calculations coupling scattering and absorption. It relies therefore on a fundamental basis different from that of the GlobAlbedo BBDR processor, which relies on MOMO look-up tables with separate gaseous absorption calculations. Since SCAPE-M performance has been extensively validated against ground-based measurements and other processing approaches [RD15, RD16], it is considered as a validation source for the GlobAlbedo SDR retrieval on its own.

- 2) Comparing with higher resolution CHRIS/PROBA data acquired concurrently to MERIS data. CHRIS/PROBA Mode 1 data present a GSD of around 30m and 62 bands in the 400-1000 nm spectral range also covered by MERIS. The higher spatial resolution minimises co-registration errors in the comparison. The comparison with CHRIS/PROBA data is not only aimed at the evaluation of the processing approach itself, but also at the resulting SDR product including possible radiometric uncertainties.

10.3 Validation of the N2B conversion approach

The N2B conversion approach implemented in GlobAlbedo for the conversion from SDR to BBDR data [RD5] is based on that of Liang (2000) [RD17] for MODIS. It enables to preserve the linear processing approach of the GlobAlbedo processing chain.

The GlobAlbedo N2B conversion approach has been tested in two ways:

- 1) Inter-sensor consistency: potential biases of the N2B conversion for MERIS, AATSR and VGT spectral settings are investigated.

Consistency with Liang's MODIS N2B conversion: possible deviations from the Liang approach are evaluated. Liang's approach is taken as a reference because it is a consolidated approach and because of the use of MODIS albedo as a prior for albedo retrieval in GlobAlbedo.

10.4 Analysis

The comparison of the GlobAlbedo MERIS SDR product with the equivalent one generated with the SCAPE-M processor has been performed over land and inland water pixels for several acquisitions dates and sites. The reason to include inland water surfaces in this analysis is the fact that water surfaces are considered a much better test for atmospheric correction than land surfaces due to their low reflectance and their characteristic spectral shape. Being water reflectance very low, small errors in the atmospheric characterisation would become apparent in the retrieved reflectance because most of the signal measured by the sensor in the space comes from atmospheric scattering.

An example of GlobAlbedo and SCAPE-M SDR retrievals is displayed in Figure 43. A green vegetation reflectance spectrum (top left), a bare soil spectrum (top right) and two water spectra (bottom) derived with the GlobAlbedo BBDR processor are compared to SCAPE-M retrievals from the same pixel. Error bars represent the surface heterogeneity through the standard deviation within a 3x3 pixel window. Despite the differences between the two processors discussed above, a good agreement in both spectral shape and reflectance levels is found in the four cases. The main discrepancies are found in the

shortest blue wavelengths in the vegetation and water spectra which present a very low reflectance in those wavelengths. Differences in absolute reflectance are around 2%, and can in principle be explained by small differences in the aerosol optical depth input to the SDR retrieval by each processor. An almost perfect match is found for the brighter bare soil pattern.

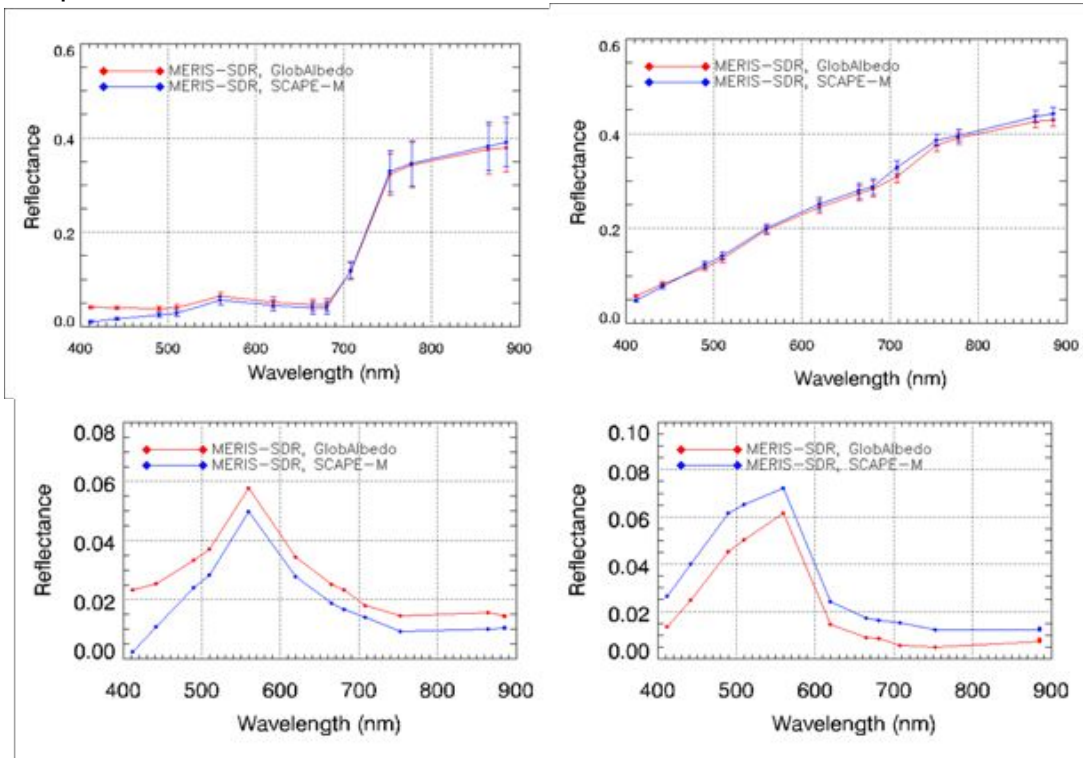


Figure 43: Comparison of spectral directional reflectance (SDR) from MERIS data over land (top) and inland water (bottom) surfaces derived with the SCAPE-M processor and the GlobAlbedo BBDR processor.

The comparison of MERIS FR SDR retrievals with CHRIS/PROBA data has made use of the SEN3EXP field campaign data base. SEN3EXP was held at different sites in summer 2009. Quasi-concurrent MERIS and CHRIS acquisitions were performed on 19/6/2009 over the Barrax study site (La Mancha, Spain, 39.1°N, -2.1°E). Reflectance data were extracted from pixels in the most homogeneous areas of the CHRIS swath. MERIS FR data were processed with the GlobAlbedo BBDR processor, while CHRIS data were atmospherically corrected with the set of pre-processing tools in the BEAM-CBOX software. The original data were acquired by the two sensors within 30min and from quasi-nadir view zenith angles.

The comparison for three different surfaces (green vegetation, bare soil and a mixed vegetation-soil surface) is plotted in Figure 44. Pixels were extracted manually from both MERIS and CHRIS images in order to ensure that the same area of around 1km x 1km was sampled for the two data sets. The results show a good correspondence of the retrieved spectra despite the very different spatial resolution, instrument characteristics and processing approaches. The main differences are observed in the near-infrared wavelengths, whereas a very good agreement is achieved in the visible channels. The

different spatial resolution and radiometric calibration differences are the most likely explanations for the mis-match in the near-infrared. It must be taken into account that CHRIS is an experimental instrument without onboard calibration means, and for this reason this comparison experiment is only considered as a consistency test rather than as an absolute validation evidence.

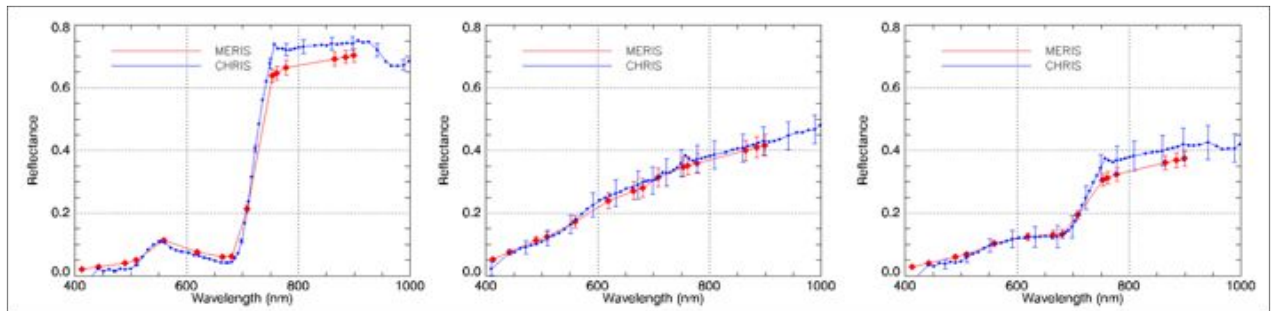


Figure 44: Comparison of spectral directional reflectance (SDR) from MERIS and CHRIS/PROBA data over land. Input data were acquired concurrently during the ESA SEN2FLEX 2005 field campaign

Once the quality of the GlobAlbedo SDR product over land has been checked with MERIS data, and assuming that the performance of the BBDR processor is the same for the three instruments in GlobAlbedo, the performance of the N2B conversion is investigated.

Instrument-related biases in the N2B have not been observed after comparing the BBDRs produced for the three instruments with the synthetic data set used in the calculation of the N2B conversion coefficients [RD5]. The intercomparison of the visible and near-infrared BBDRs derived from the same input reflectance spectra is presented in Figure 45. It can be stated that no systematic error in the conversion is to be expected in statistical terms, and that only small N2B conversion errors would be found in certain cases. In particular, almost identical results are retrieved for MERIS and VGT in the visible range and for VGT and AATSR in the near-infrared due to the relatively similar spectral sampling of each of those instruments in each of the spectral ranges, i.e. MERIS and VGT have a blue band for the conversion in the visible, and VGT and AATSR have a band around 1600nm used in the conversion in the near-infrared. For the same reason, larger deviations (with a random sign) may be found between MERIS/VGT and AATSR in the visible (around 5% relative root mean square error) and VGT/AATSR and MERIS in the near-infrared (around 3% relative root mean square error).

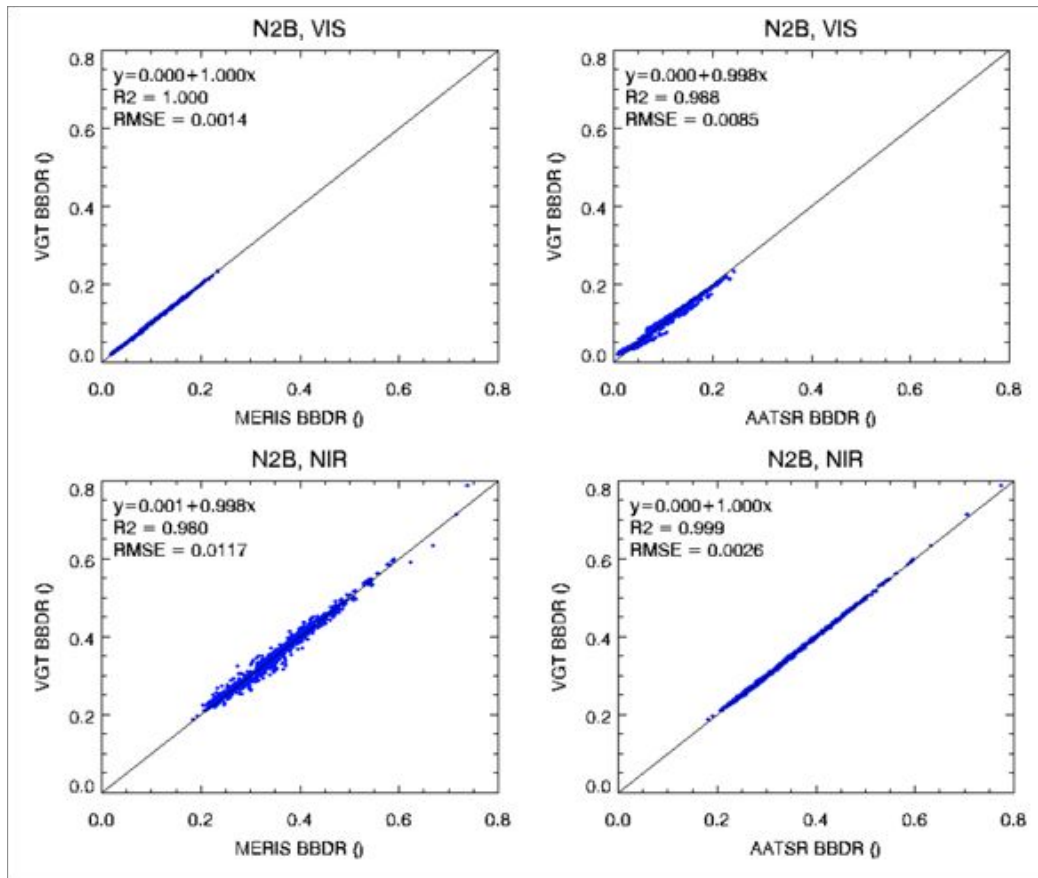


Figure 45: Inter-instrument comparison of the GlobAlbedo N2B conversion in the visible (VIS) and near-infrared (NIR) broadband windows.

The performance of the GlobAlbedo set of conversion coefficients was already compared to that of Liang (2000) in [RD5]. However, that comparison was biased by the fact that the same data base of reflectance spectra and atmospheric parameters used for the derivation of the GlobAlbedo coefficients was used for the assessment of both GlobAlbedo and Liang coefficients. A similar exercise has been repeated here using real image data which are independent of the training data base. A VGT SDR image has been converted to BBDR with either the GlobAlbedo and the Liang N2B coefficients. The results are depicted in Figure 46 under the same colour scale. Small differences are observed in the near-infrared range over some vegetated areas, whereas no apparent difference is found in the visible and shortwave BBDRs in the same areas.

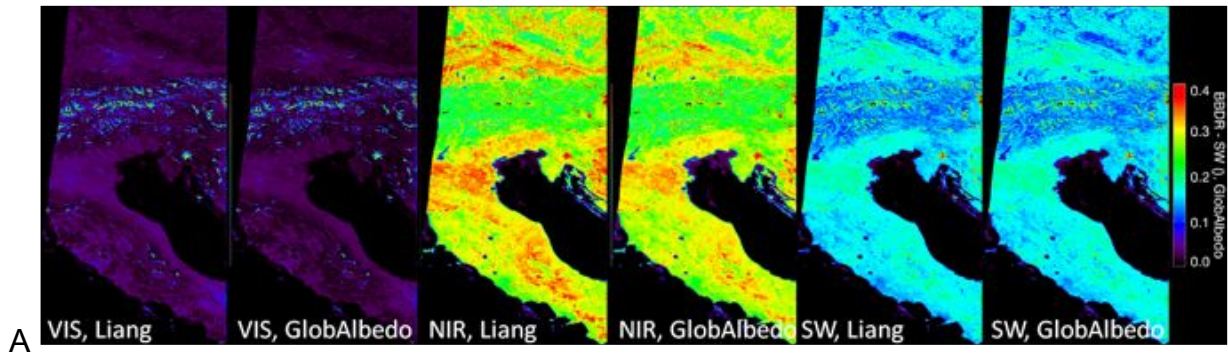


Figure 46: Visible (VIS), near-infrared (NIR) and shortwave (SW) BBDRs derived from VGT data using GlobAlbedo and Liang (2000) N2B conversion approaches.

The final exercise in this analysis of the GlobAlbedo BBDR product has been to look for inter-sensor systematic BBDR errors resulting from the complete processing chain, which include radiometric calibration, pixel identification, aerosol retrieval, SDR retrieval and N2B conversion. To investigate this, all the MERIS, AATSR-nadir and VGT BBDRs from the central pixel of the MODIS h10v04 tile between October 2004 and March 2006 have been plotted together.

Visible and near-infrared MERIS and VGT BBDRs for this timeframe are displayed in Figure 47. Only data acquired with view zenith angle differences of less than 10° are plotted in order to minimise BBDR differences due to directional reflectance effects. The results in Figure 9-5 are considered to be sufficient to discard evident inter-sensor BBDR systematic errors between MERIS and VGT in the entire GlobAlbedo processing chain.

The comparison between MERIS and AATSR-nadir is plotted in Figure 48. In this case, it can be observed that both visible and near-infrared BBDRs from AATSR-nadir are systematically higher than from MERIS. Since MERIS and AATSR-nadir have the same observation angle, and we assume that SDR retrieval and N2B conversion are not introducing any instrument-dependent error, those differences may be explained by systematic errors in aerosol retrieval and by radiometric calibration errors remaining after the instrument inter-calibration exercise. The latter option could be the most likely one due to the fact that the difference is larger in the near-infrared than in the visible range, where aerosol correction has the largest impact. Further analysis with more data is necessary in order to understand and correct this error in the BBDR processor.

The poor accuracy of the georeferencing of AATSR nadir and the very poor co-registration of AATSR nadir to forward (not shown here) also means that the effective resolution of AATSR is some 3-5 times worse than the nominal 1km pixel resolution. This also contributes to the poorer agreement of the BBDR between AATSR and MERIS, especially at NIR wavelengths.

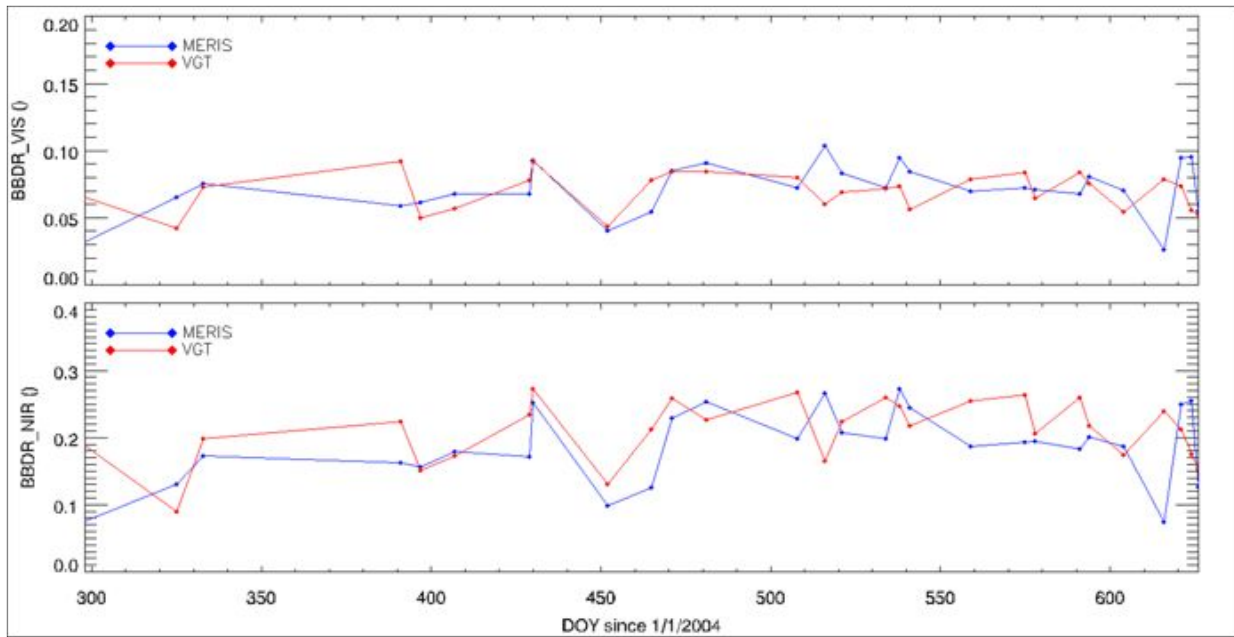


Figure 47. Temporal series of visible (VIS) and near-infrared (NIR) BBDRs derived from MERIS and VGT over the MODIS h10v04 tile.

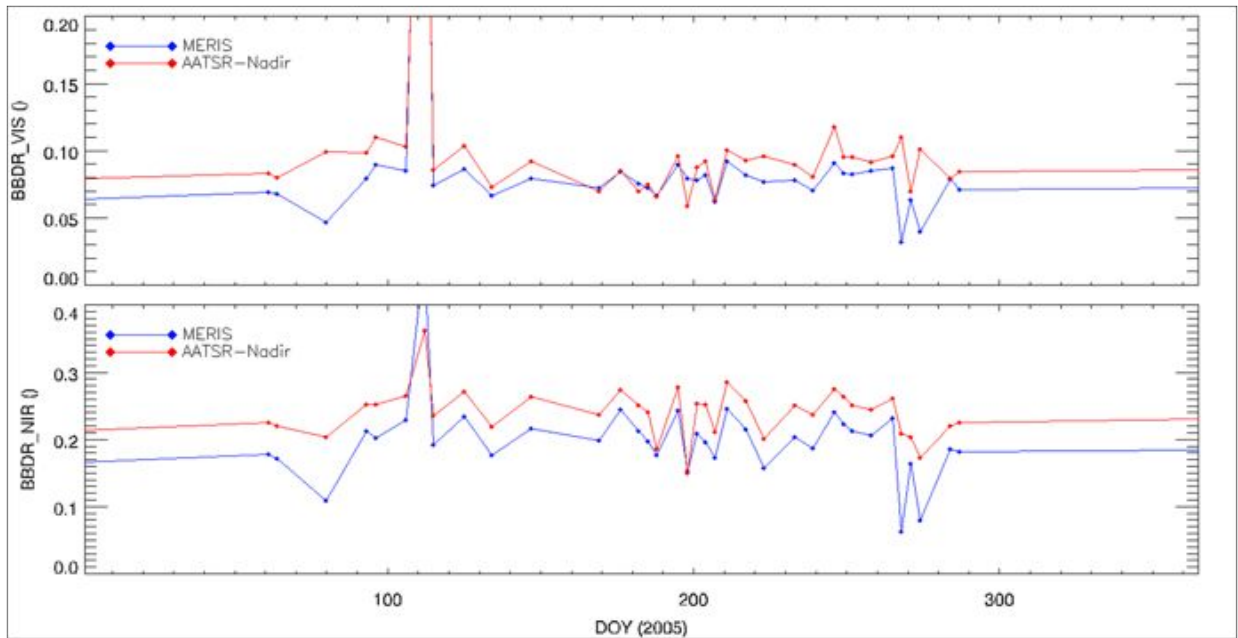


Figure 48. Temporal series of visible (VIS) and near-infrared (NIR) BBDRs derived from MERIS and AATSR-nadir data over the MODIS h10v04 tile.



10.5 Validation summary

The main findings of this BBDR validation exercise are

- SDR retrieval:
 - GlobAlbedo MERIS SDR agrees well with the SCAPE-M processor.
 - Good correspondence of MERIS FR SDRs with concurrent CHRIS/PROBA SDRs over homogeneous areas.
- Narrow-to-Broadband conversion:
 - No instrument-dependent biases in the GlobAlbedo N2B conversion.
 - Very good correspondence with MODIS' Liang N2B approach.
- BBDR consistency:
 - No apparent biases between MERIS and VGT BBDRs.
 - Positive bias detected in AATSR-nadir with respect to MERIS & VGT.



11 BB Albedo product

11.1 Qualitative Assessments of GlobAlbedo products (“Known Issues”)

A visual qualitative analysis was conducted of all the global mosaiced products from 1998-2011 at a resolution of 0.05° to assess what artifacts were present and what the root cause might be of these artifacts.

There are 3 sources for the observed artifacts:

- Problems with the use of the MODIS prior at polar latitudes to fill-in gaps due to low sun angles
- Problems with snow detection.
- Missing MERIS orbits and the cutoff of VEGETATION at latitudes $>65^\circ\text{N}$ and $<56^\circ\text{S}$

The artifacts appear in the dataset in the following forms:

- The tile h18v03 does not accurately follow seasonal albedo cycles due to problems with snow detection. This effect is presented in region of interest box 1 in Figure 49. The only year unaffected by this artifact is 2005.
- Polar Regions, all MODIS SIN tiles $< v03$ and >14 , demonstrate significant irregularities. With commonly occurring missing data, swath artifacts and prior artifacts present in all dataset years. Example errors for Antarctica in Figure 50.
- A more specific polar issue presents in tiles h10v02 and h11v02, where a wedge shaped feature which does not follow seasonal albedo cycles often occurs. An example is shown in region of interest box 2 in Figure 49. This effect is not always apparent, though when present it is extremely obvious. The effect occurs irregularly throughout all GlobAlbedo dataset years.
- Another specific polar issue occurs in tiles h20v00 and h20v01 in Northern Siberia and in tiles h14v01 and h14v01 over Northern Canada, where snow detection related artefacts occur commonly throughout the GlobAlbedo dataset. An example of this artefact is shown in region of interest boxes 3 and 4 in Figure 49.

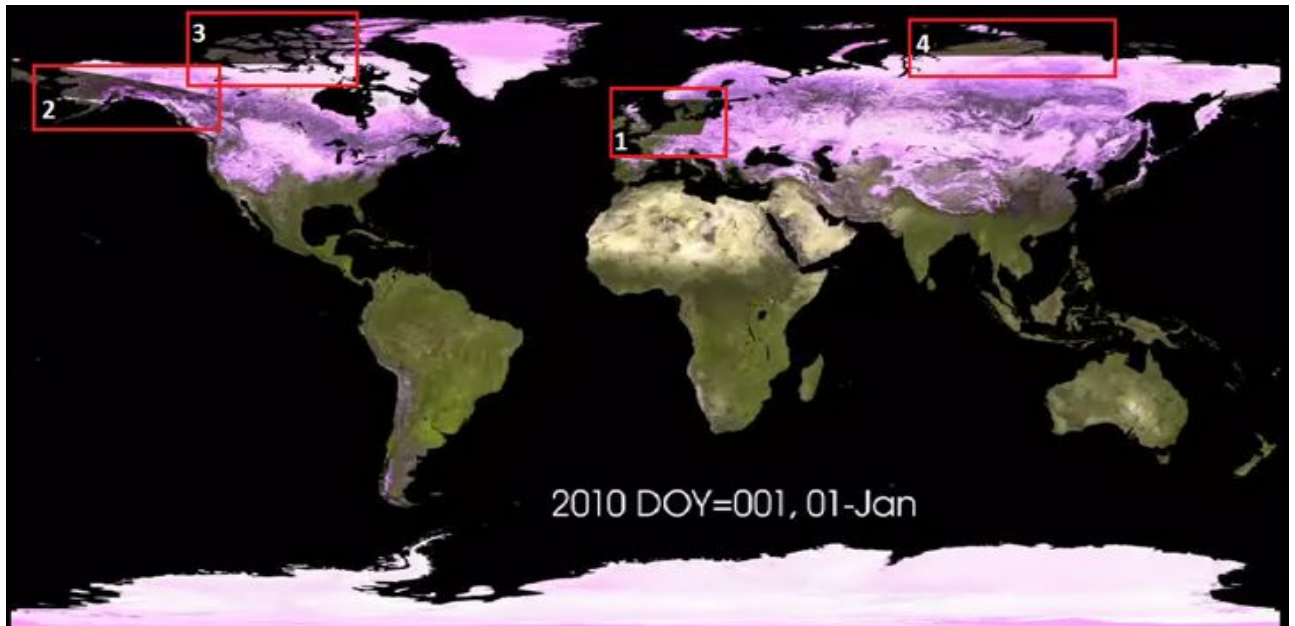


Figure 49. Known issues in the GlobAlbedo dataset. With 4 of the main artifacts identified in the region of interest boxes.



Figure 50. Further issues in the GlobAlbedo dataset. An example of the artifacts found in Antarctica.

11.2 Tower intercomparisons with GlobAlbedo and other EO-derived Blue Sky Albedos

The BroadBand Albedo product described in RD1 was retrieved over 73 tower albedometer sites worldwide (in 23 MODIS SIN tiles) for as many of the 14 years as available. These contained a number of FLUXNET (EuroFlux, North & South America AmeriFlux), US-DoE ARM, US NOAA SURFRAD. The FLUXNET stations are listed in table 11-1 (below).

SITE_Name	Lat	Lon	Tower footprint	Tile	Line	Sample	Source
La Thuile							
AU Tum	-35.66	148.15		h30v12	678.7	43.96	FLUXNET
AU Wac	-37.43	145.19		h29v12	891.1	634.88	FLUXNET
BR Cax	-1.72	-51.46		h12v09	205.9	1027.08	FLUXNET



BR Sa3	-3.02	-54.97		h12v09	361.9	612.26	FLUXNET
BW Ghg	-21.51	21.74		h20v11	180.7	26.61	FLUXNET
BW Ghm	-21.20	21.75		h20v11	143.5	32.87	FLUXNET
BW Ma1	-19.92	23.56		h20v10	1189.9	257.55	FLUXNET
CA Ca1	49.87	-125.33		h09v04	15.1	1106.12	FLUXNET
CA Ca3	49.53	-124.90		h09v04	55.9	1071.54	FLUXNET
CA NS6	55.92	-98.96		h12v03	489.1	545.23	FLUXNET
CA SF2	54.25	-105.88		h11v03	689.5	976.26	FLUXNET
CA SF3	54.09	-106.01		h11v03	708.7	938.34	FLUXNET
CA WP1	54.95	-112.47		h11v03	605.5	648.64	FLUXNET
CZ BK1	49.50	18.54		h19v04	59.5	244.39	FLUXNET
DE Geb	51.10	10.91		h18v03	1067.5	821.63	FLUXNET
DE Hai	51.08	10.45		h18v03	1069.9	787.31	FLUXNET
DE Kli	50.89	13.52		h18v03	1092.7	1022.93	FLUXNET
DE Tha	50.96	13.57		h18v03	1084.3	1025.17	FLUXNET
DE Wet	50.45	11.46		h18v03	1145.5	875.16	FLUXNET
ES ES2	39.28	-0.32		h17v05	85.9	1169.78	FLUXNET
ES LMa	39.94	-5.77		h17v05	6.7	668.63	FLUXNET
FR Fon	48.48	2.78		h18v04	181.9	220.64	FLUXNET
FR Hes	48.67	7.06		h18v04	159.1	558.99	FLUXNET
FR Pue	43.74	3.60		h19v04	750.7	311.61	FLUXNET
GF Guy	5.28	-52.93		h12v08	565.9	874.85	FLUXNET
HU Bug	46.69	19.60		h19v04	396.7	412.84	FLUXNET
IE Dri	51.99	-8.75		h17v03	960.7	552.91	FLUXNET
IT Bon	39.48	16.53		h19v05	61.9	330.53	FLUXNET
IT Col	41.85	13.59		h19v04	977.5	14.27	FLUXNET
IT SRo	43.73	10.28		h18v04	751.9	890.91	FLUXNET
JP Mas	36.05	140.03		h29v05	473.5	385.27	FLUXNET
KR Kw1	37.75	127.16		h28v05	269.5	64.79	FLUXNET
NL Ca1	51.97	4.93		h18v03	963.1	363.97	FLUXNET
NL Lan	51.95	4.90		h18v03	965.5	361.91	FLUXNET
NL Loo	52.17	5.74		h18v03	939.1	421.96	FLUXNET
PT Esp	38.64	-8.60		h17v05	162.7	393.42	FLUXNET
RU Che	68.61	161.34		h23v02	166.3	1060.66	FLUXNET
SE Nor	60.09	17.48		h18v02	1188.7	1045.45	FLUXNET
UK Gri	56.61	-3.80		h17v03	406.3	948.55	FLUXNET
US Aud	31.59	-110.51		h08v05	1008.7	703.37	FLUXNET
US Bn1	63.92	-145.38		h11v02	729.1	729.97	FLUXNET
US Bo1	40.01	-88.29		h11v04	1198.3	284.6	FLUXNET
US Bo2	40.01	-88.29		h11v04	1198.3	284.6	FLUXNET
US FPe	48.31	-105.10		h11v04	202.3	11.26	FLUXNET



US IB1	41.86	-88.22		h11v04	976.3	514.99	FLUXNET
US Ivo	68.49	-155.75		h12v02	180.7	346.56	FLUXNET
US SRM	31.82	-110.87		h08v05	981.1	694.64	FLUXNET
US WCr	45.81	-90.08		h11v04	502.3	864.78	FLUXNET
ZA Kru	-25.02	31.50		h20v11	601.9	1024.79	FLUXNET
US-Bar Bartlett Forest, NH, US	44.0646	-71.2881		h12v04	711.75	1052.56	AmeriFlux
US-Fmf Flagstaff- Managed, AZ, US	35.1426	-111.7273		h08v05	582.39	1036.08	AmeriFlux
US-Fuf Flagstaff- Unmanaged AZ, US	35.089	-111.762		h08v05	588.82	1025.45	AmeriFlux
US-Ha1 Harvard Forest EMS Tower, MA, US	42.5378	-72.1715		h12v04	894.96	818.11	AmeriFlux
US-MMS Morgan, IN, US	39.3232	-86.4131		h11v04	202.58	10.73	AmeriFlux
US-MOz Ozark Site MO, US	38.7441	-92.2		h10v05	150.21	970.15	AmeriFlux
CA-NS1 UCI-1850 Burn Site, CAN	55.8792	-98.4839		h12v03	494.00	570.28	AmeriFlux
CA-NS2 UCI-1930 Burn, CAN	55.9058	-98.5247		h12v03	490.80	572.08	AmeriFlux
CA-NS3 UCI-1964 Burn, CAN	55.9117	-98.3822		h12v03	490.10	582.67	AmeriFlux
CA-NS5 UCI-1981 Burn Site, CAN	55.8631	-98.485		h12v03	495.93	567.46	AmeriFlux



US-UMB Michigan Biological Station	45.5598	-84.7138		h12v04	532.32	81.87	AmeriFlux
US-WBW Walker Branch	35.9588	-84.2874		h11v05	487.77	205.19	AmeriFlux
Bondville, IL, US	40.0062	-88.2904		h11v04	1198.76	284.11	SURFRAD
Boulder, CO, US	40.1256	-105.2378		h09v04	1184.43	1143.3	SURFRAD
Desert Rock,NV, US	36.6232	-116.0196		h08v05	404.72	825.75	SURFRAD
Fort Peck, MT, US	48.3077	-105.1019		h11v04	202.58	10.73	SURFRAD
Goodwin Creek, MS, US	34.2547	-89.8735		h10v05	688.94	685.38	SURFRAD
Penn State, PA, US	40.7203	-77.931		h12v04	1113.06	111.8	SURFRAD
Sioux Falls, SD, US	43.2408	-96.902		h10v04	810.60	1128.55	SURFRAD
Barrow, AK, US	71.3226	-156.6093		h12v01	1040.79	1181.20	ARM

Table 11-1. List of 68 station locations and reference names for the 53 FLUXNET described by Cescatti et al. (2012)* selected for MODIS inter-comparison. The 8 sites highlighted operate the restrictive “La Thuile” data policy prior to 2007 and are therefore not shown here. All other sites operate the Fair Use or Open policy and are shown here.

Following a detailed investigation, it transpires that only one site from the entire BSRN network has useable albedometer data, Tovarere in Sweden. The US stations were carefully chosen by Z. Wang & C. Schaaf of the MODIS team at Boston University to be representative of leaf-on and leaf-off conditions using the approach described in RD19.

The data from the (NSF) AmeriFlux and (NOAA) SURFRAD stations included different instrumental data. The AmeriFlux data only included tower albedometer measurements with no measurements of cloud cover or diffuse vs direct illumination conditions whereas the SURFRAD site included cloud cover and direct and diffuse measurements. For the non-SURFRAD or ARM sites, AOD data derived from VEGETATION using the GlobAlbedo processing chain were employed to calculate the equivalent Blue Sky Albedo values.

The European FLUXNET and US site locations are displayed with GlobCover2005 shown in the background on Google Earth in Figure 51. These cover a variety of forested and non-forested sites. Key characteristics of the US and BSRN study sites are listed in



Title: GlobAlbedo Final Validation Report

Doc. No. GlobAlbedo_FVR_V1.2

[RD32]. In addition, the tower height and footprint is indicated for all the US sites with data supplied by C. Schaaf of the University of Massachusetts at Amherst.



Title: GlobAlbedo Final Validation Report

Doc. No. GlobAlbedo_FVR_V1.2



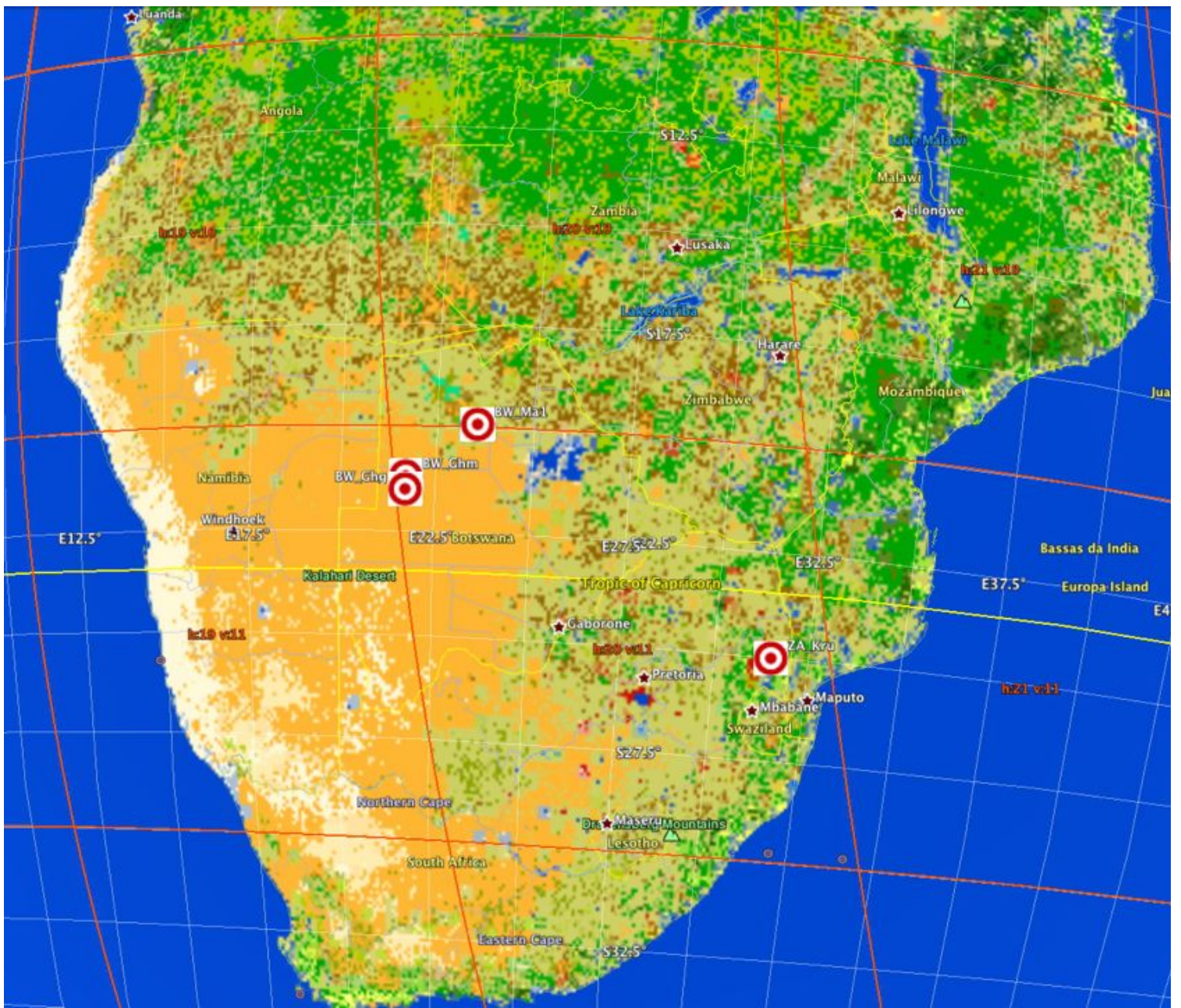




Figure 51. Location of the European (Upper Panel), Africa (Middle Panel) and US (Lower Panel) test sites employed for the validation analysis presented



The GlobCover products from the same year (2005) together with the location of the tower sites are shown below for 3 tiles in the US which were employed.

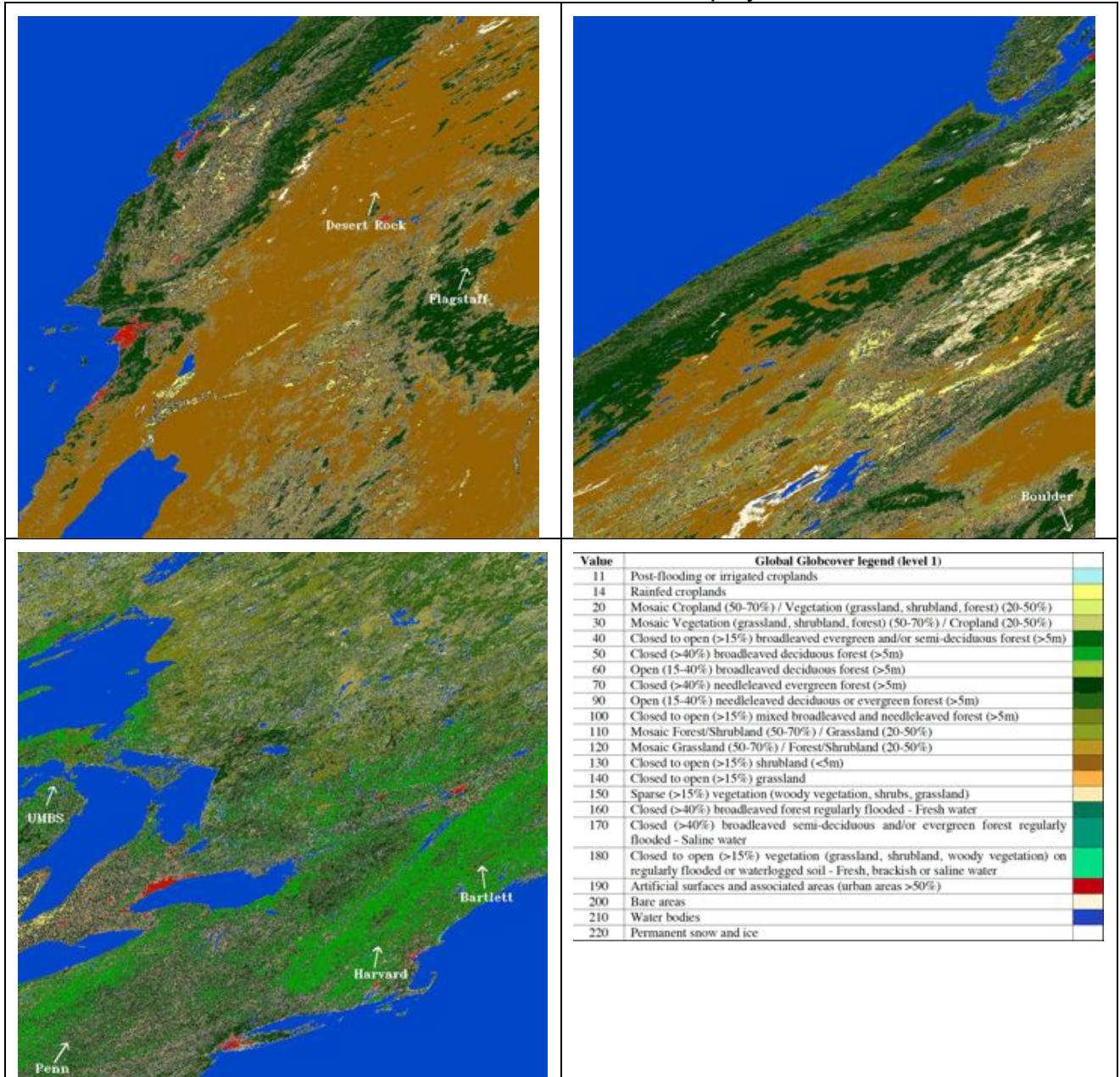


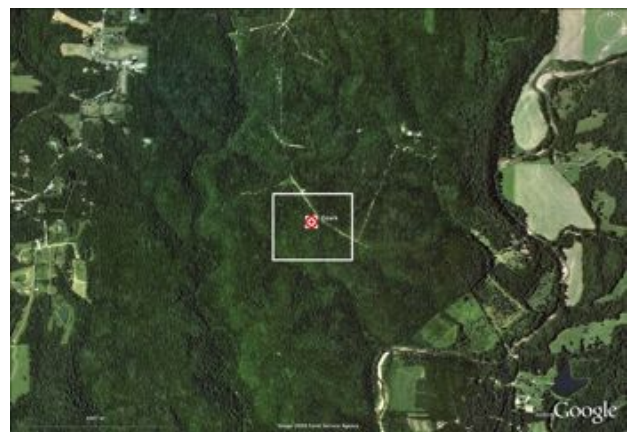
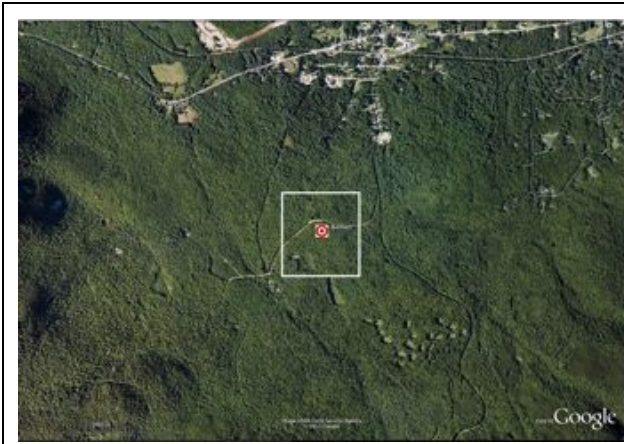
Figure 52. GlobCover maps of 3 validation tiles showing the location of the test sites covering approximately a 1200 x 1200km region. Upper panel shows tiles (h08v05, h09v04 in left and right positions). Lower panel shows tile h12v04 with the GlobCover key (right).



Figure 53. Location of the BSRN Tovarere (upper) employed for the validation

11.3 Methods used

The methods described in the Validation Plan [RD9] were applied given the availability of suitable correlative data. For the albedo product validation, only shortwave (broadband, BB) albedo can be validated. We focused on sites which are “homogeneous” at the scale of 1-3km. The US sites have all been previously studied by the BU MODIS group who have screened the data for outliers and averaged the ground data over 2 hours (11-13 Local Time). The 23 sites listed in [RD32] were analysed. Also, only the shortwave component can be validated as there are no standardised and well calibrated instruments on well characterised sites which operate spectrally in the visible (0.3-0.7 μm) or NIR (0.7-3 μm). Scaling issues were ignored due to the inference of homogeneity. Display of some of these sites in GoogleMaps (see Figure 54) shows that several of these sites appear quite heterogeneous but probably only at sub-pixel resolution (when compared with Landsat which is employed in RD19).



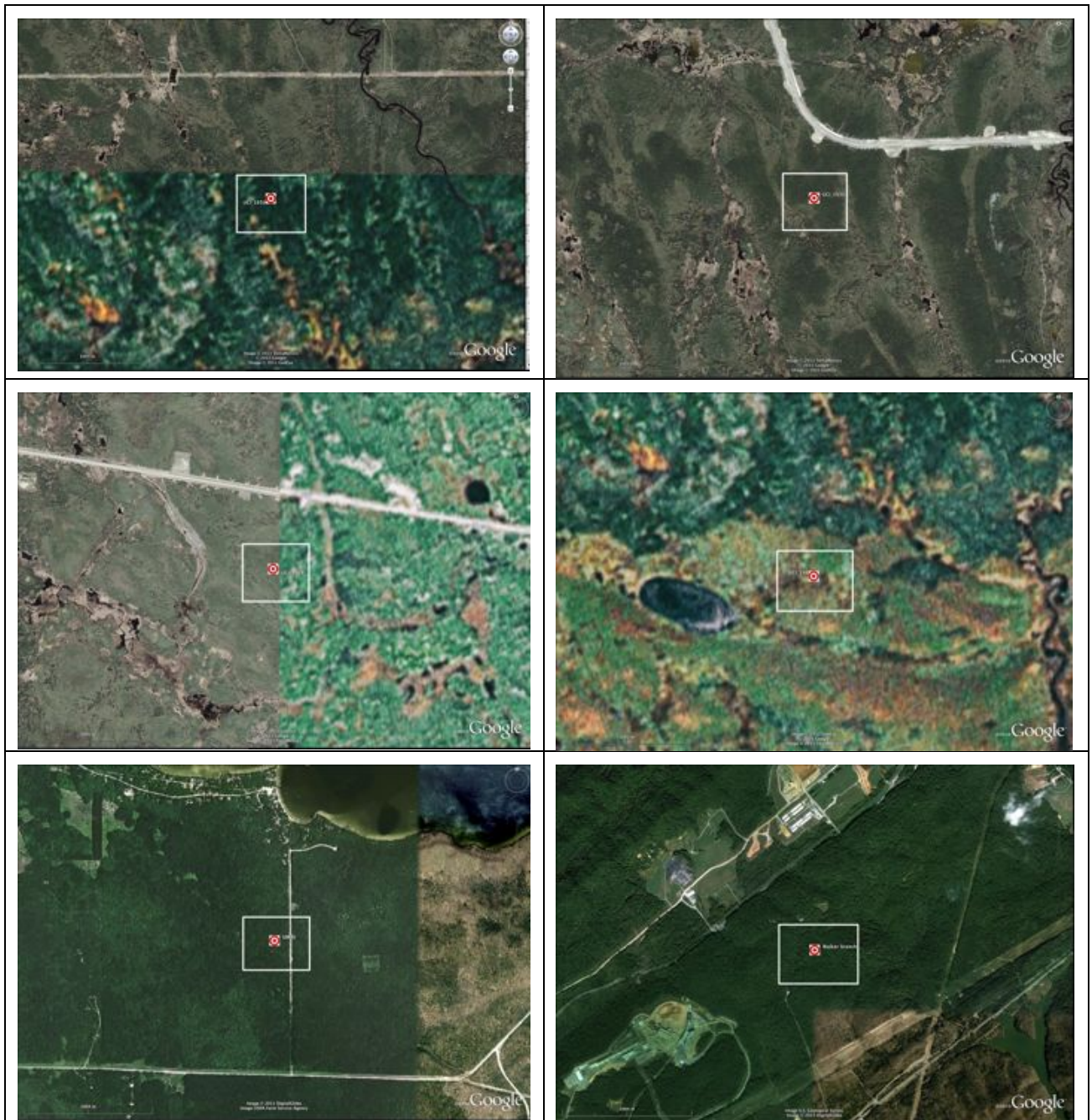
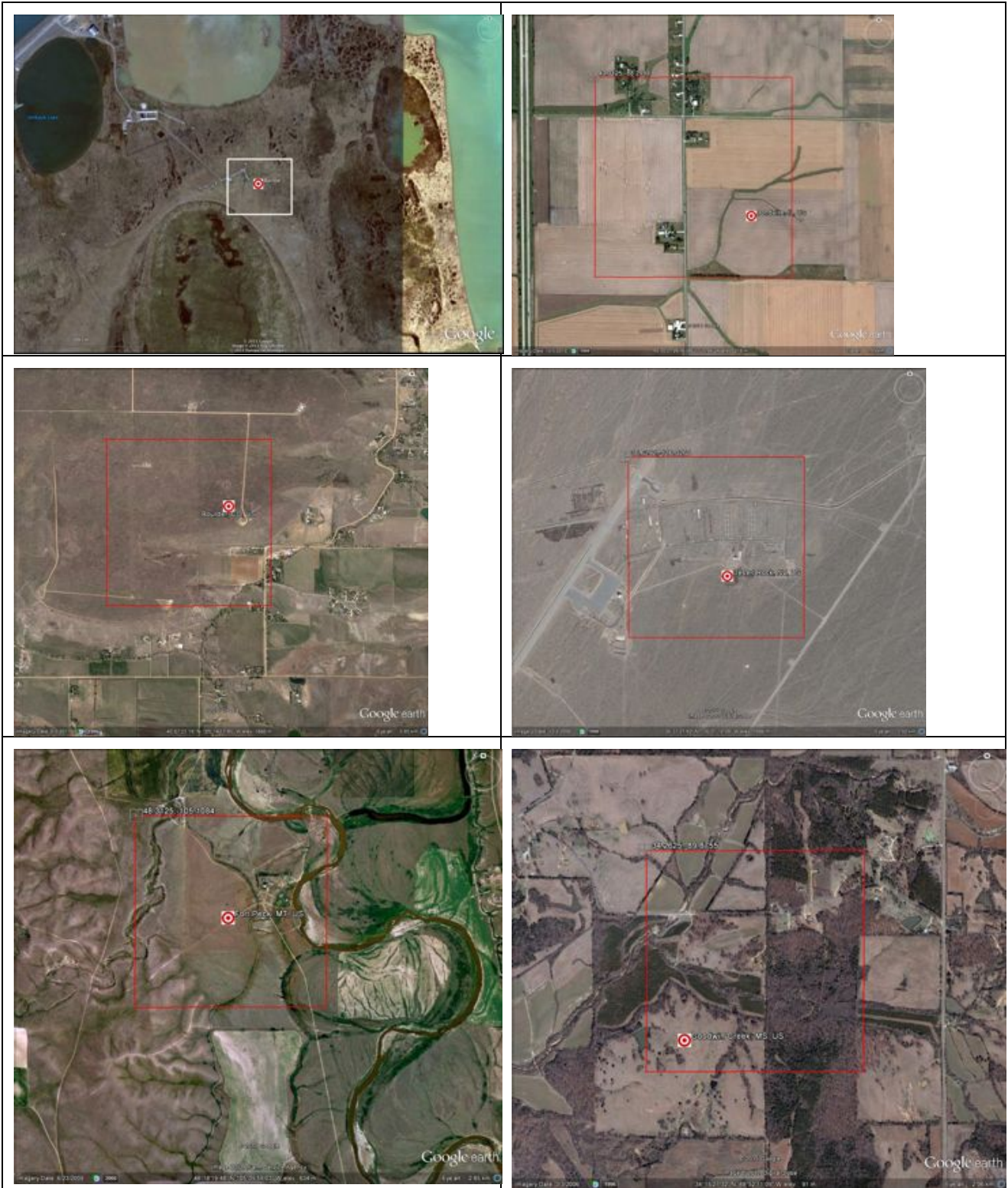


Figure 54. Google Map extracts for the 12 AmeriFlux sites showing 1km pixels centred on the tower site locations. Note that most tower albedometer footprints are << 1km which is smaller than the symbol shown to indicate their locations. Site-names are shown in Figure 52.



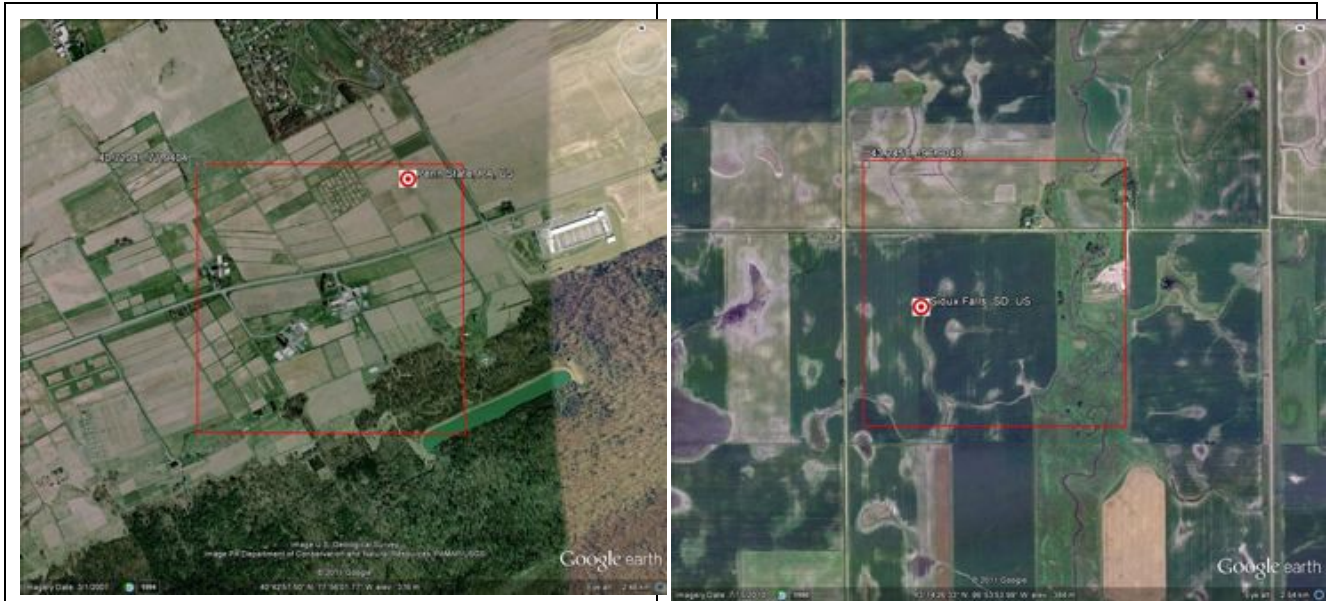


Figure 55. SURFRAD sites from Google Earth showing 1km pixel centred on each tower site. See Figure 10-6 for site names

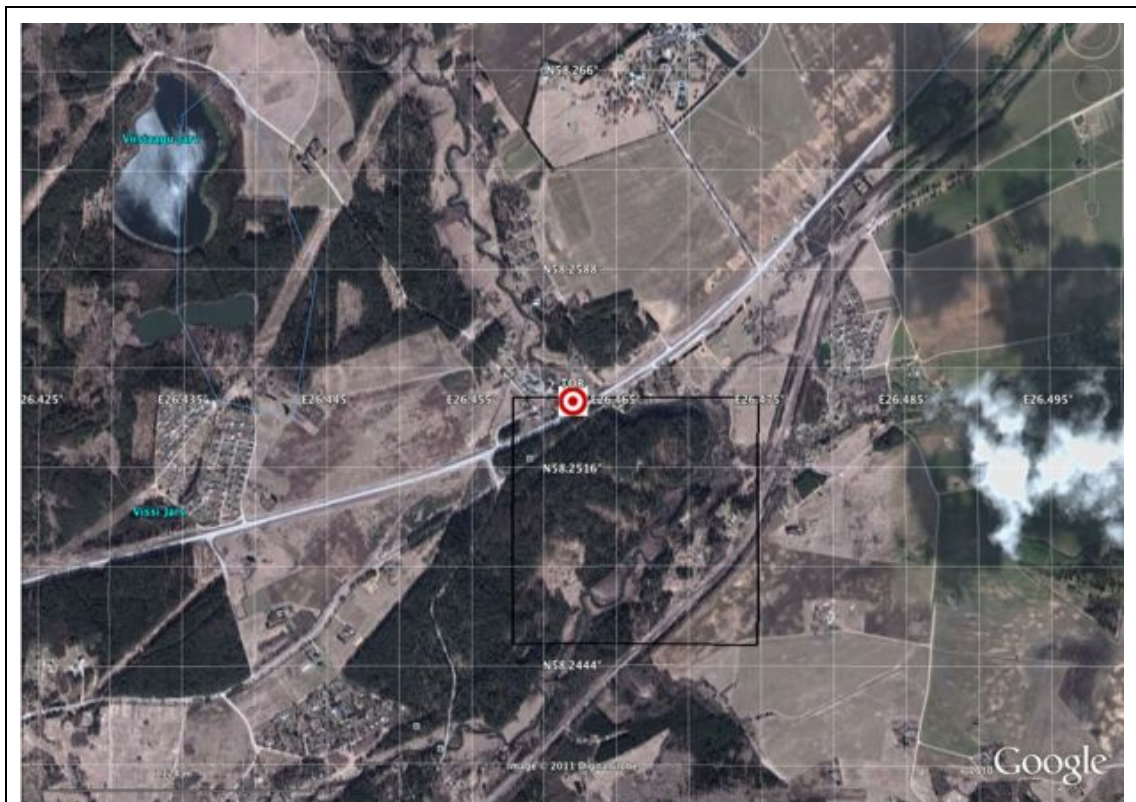


Figure 56. Toravere - The only BSRN site which has reasonably homogeneous texture and albedometer measurements

For each of the non-SURFRAD sites, in addition to averaged ground albedometer (referred to as gnd hereafter) over 2 hours (11-13hrs Local Time), AOD was provided from the GlobAlbedo VEGETATION BBDR product alongside snow cover and cloud fraction.



Using the approach described in [RD20] the sky irradiance component (SKYL) is calculated given the solar zenith angle, the black sky (DHR) and white-sky (BHR) albedos as shown in equation 1 of [RD20]. From this approach the so-called blue-sky albedo was calculated for each date that AOD was available. For each of these dates at Local Solar Noon, the DHR and BHR was calculated as well as extracted from the MODIS priors value. Tests were conducted (not shown here) to look at the effects of averaging predicted Blue-Sky Albedo every 15 minutes compared to one produced from averaging and negligible differences were found between 11-13h LT and Local Solar Noon.

Then plots were produced for all the test sites. The results are shown here for all the EuroFlux, AfricaFlux, AmeriFlux, ARM, SURFRAD and BSRN sites of the tower albedo vs Blue-Sky Albedos calculated from the GlobAlbedo, MODIS Collection 5 (MCD43A3), MISR, MODIS priors and where available METEOSAT from M-05 (0°) and M-07 (63°) and for 2006, the GEOLAND2 albedo retrievals. The SURFRAD sites included instruments to measure the cloud fraction and the direct and diffuse components at the site so that SKYL can be directly computed. In addition, for 8 of these tiles, the albedo values were sorted by land cover using the approach described in [RD22-24]. VIS, NIR and SW albedo histograms were then computed and displayed. Where available, MISR results of BSA are also plotted (these are confusingly referred to as “LandBHR” in the MISR document) as well as their estimated uncertainties.

Triple collocation, which was only briefly referred to in [RD9] has been applied to the entire 11 year time period (2000-2010) and is shown here using global 0.5° x 0.5° MISR, MODIS and GlobAlbedo datasets to demonstrate the principle and what can be learnt. Examples are shown here below.

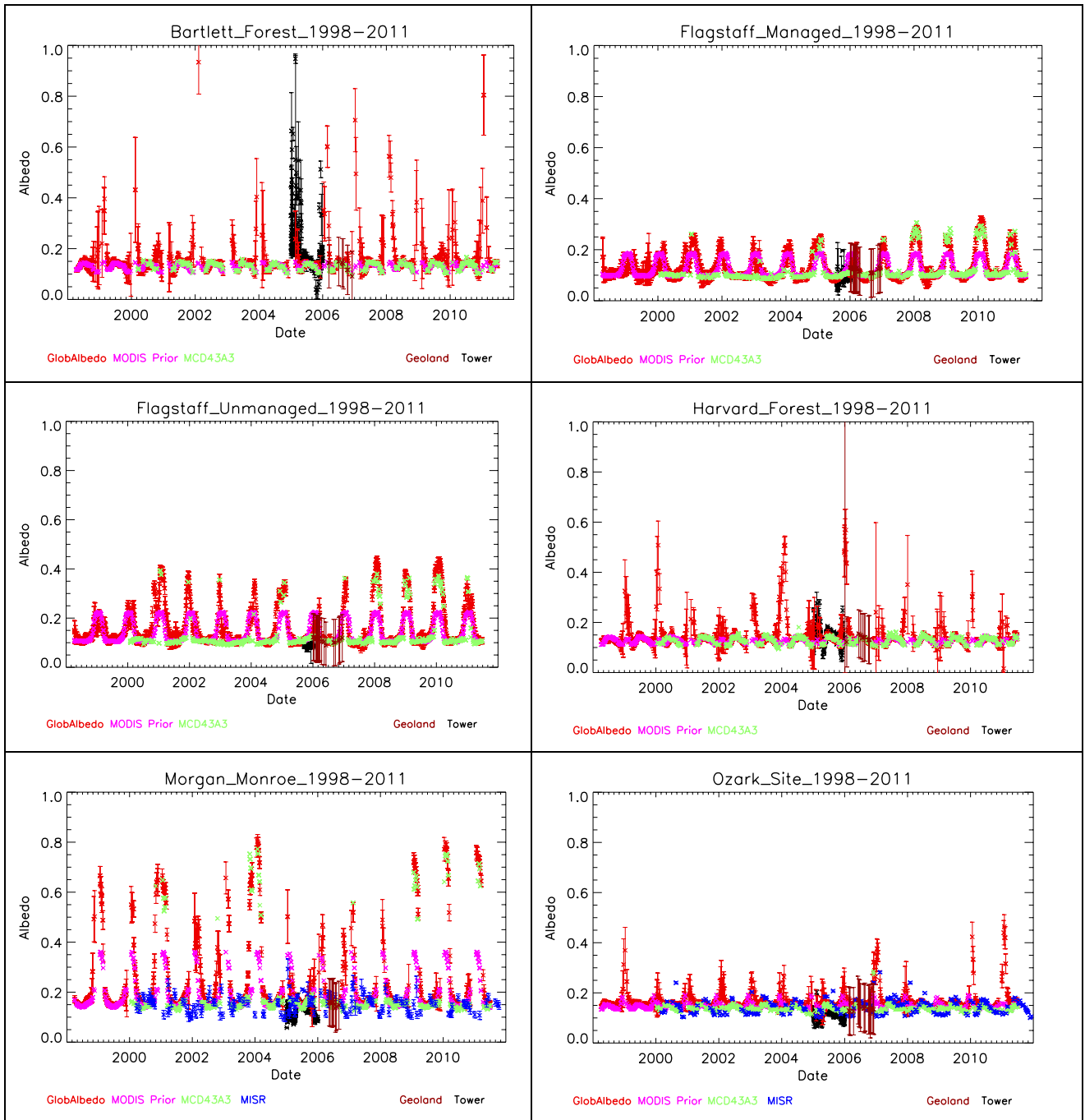
11.4 Analysis

11.4.1 Intercomparison of tower albedos with spaceborne albedos

Starting with the data for the 73 AmeriFlux, ARM, UoA, SURFRAD and BSRN sites, blue-sky albedo values were computed for the 1 x 1 km pixel which covered the tower sites. For each blue-sky albedo estimate, the uncertainty matrix for this pixel was processed into an estimated standard deviation. It should be noted that the ACTUAL position of the tower is usually not the centre of the pixel shown. The corresponding GlobAlbedo pixel is shown where feasible in the above plots from Google Earth.

Starting first with the GlobAlbedo and MODIS Prior Blue-Sky Broadband Albedo in the Shortwave a time series showing all the Ameriflux (Figure 57) and ARM and SURFRAD sites (Figure 58), UoA and BRSN sites (Figure 10-9) are shown. Where MISR instantaneous Blue-Sky Albedo (referred to confusingly as LandBHR) and an associated uncertainty is present, this is plotted as well as the blue-sky albedo calculated from the MCD43B3 MODIS Collection 5 value (at 1km).

For all of the inter-comparisons, all the EO-derived BSA values are very close to each other and the tower albedometer measurements are very noisy aside from their much higher values when snowfall occurs. A number of sites show systematic biases between the tower measurements and all the other EO-derived values, which is difficult to explain.



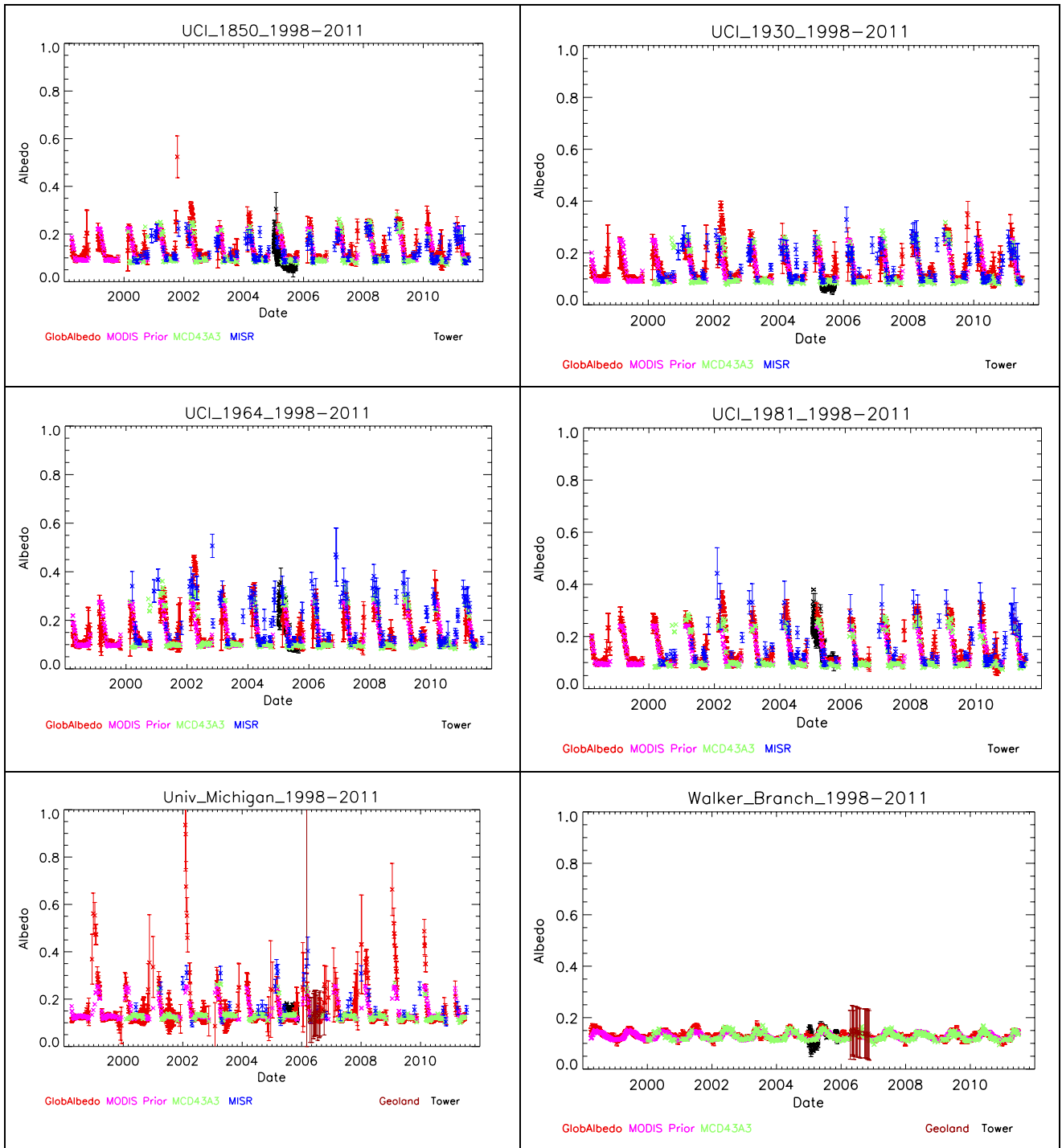
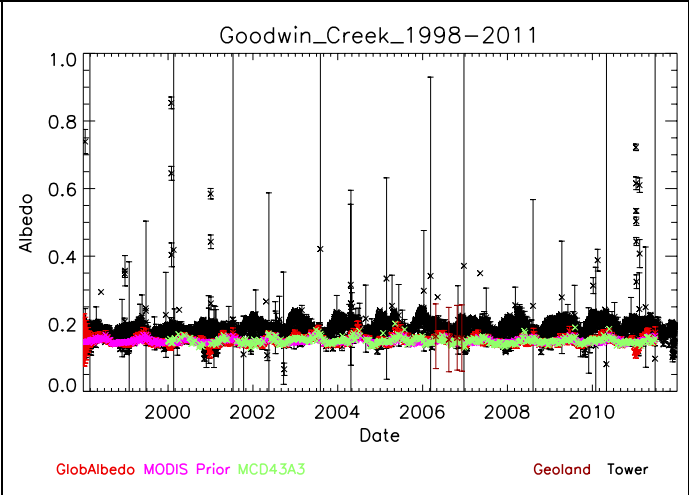
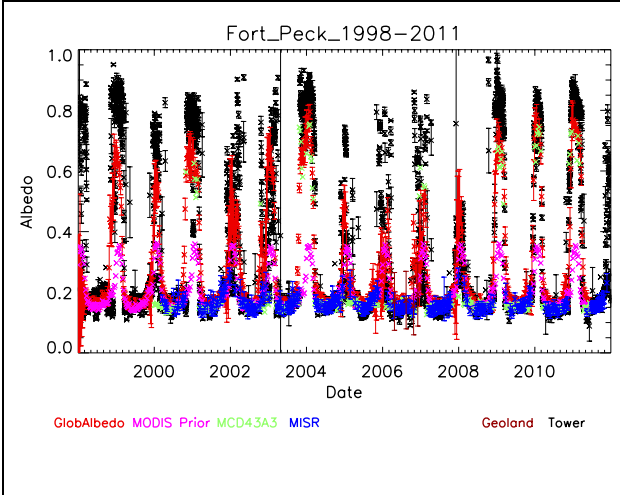
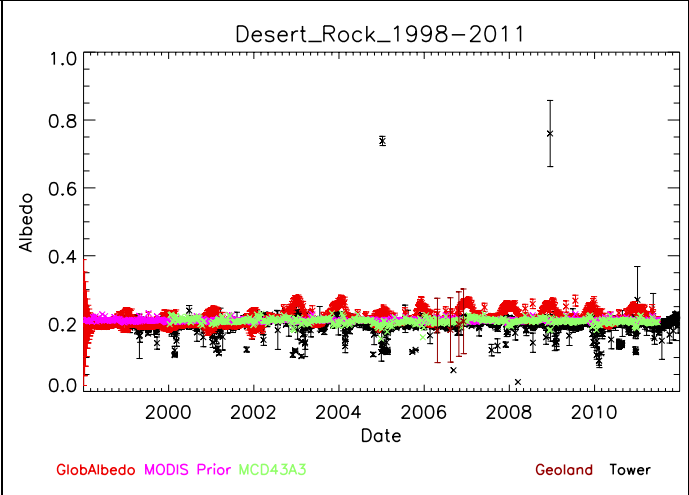
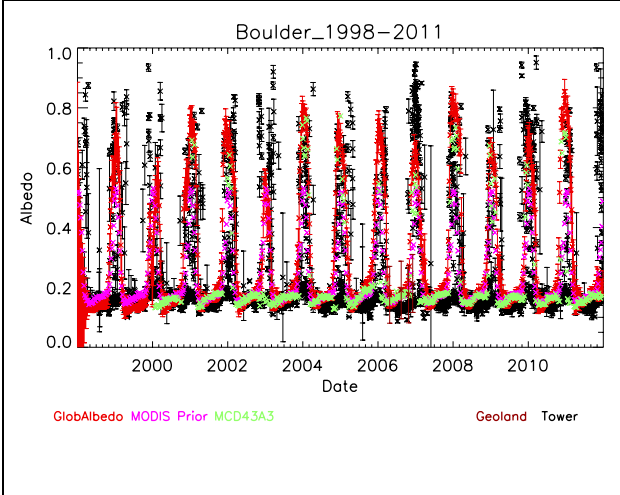
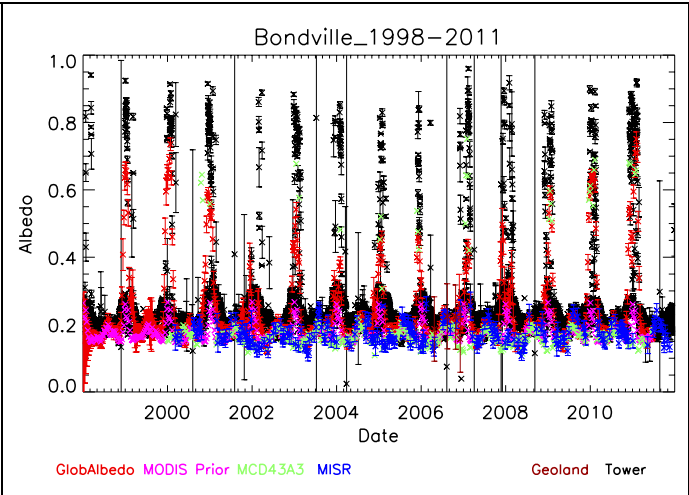
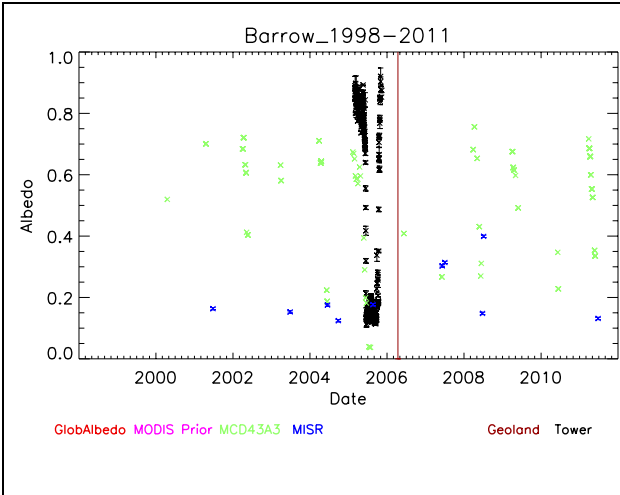


Figure 57. Time series of 1998-2011 12 AmeriFlux Tower albedometer (Tower), GlobAlbedo (GA_BSA), MISR, MODIS priors (MODIS Priors), MODIS collection 5 (MOD43A3), GEOLAND2 (2006 only) Blue Sky Albedos for the named sites.



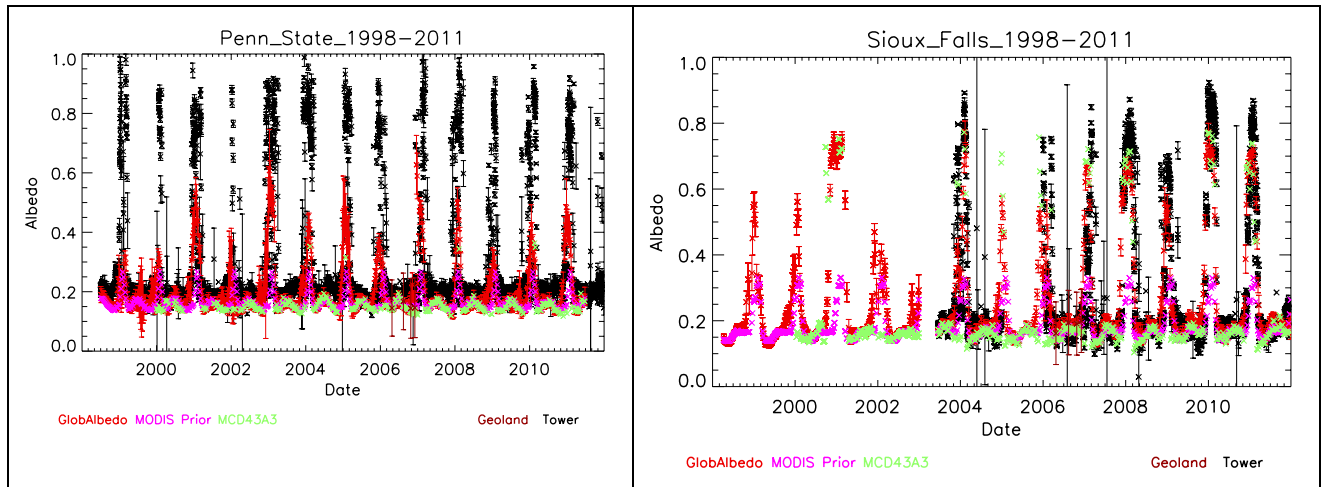


Figure 58. Time series of 1998-2011 of 8 ARM/SURFRAD Tower albedometer (Tower), GlobAlbedo (GA_BSA), MODIS priors (MODIS Priors), MODIS collection 5 (MOD43A3), MISR, Geoland2 (2006) Blue Sky Albedos for the named sites.

These results indicate that for 4 of the 8 AmeriFlux and 7 of the 8 ARM/SURFRAD sites, there is excellent agreement between the EO results and the tower measurements. The remaining AmeriFlux sites all show EO higher than tower. This may be due to the use of the EO-derived AODs to calculate the blue-sky albedos. The results for Goodwin Creek are an anomaly which no explanation at present. The snow albedo results are much better than the 2005 test year results but the EO-derived snow is still lower than the tower measurements. This is most likely due to a spatial resolution effect whereby the tower receives more radiation from the snow under the trees compared with the 1km footprint of the EO measurements. The MISR LandBHR all show excellent agreement with the tower measurements. For a few of the sites, the GlobAlbedo results are closer to the tower results than the MODIS priors or MCD43 but it is probably not statistically significant.

For the Final Product, a new DEM was employed (GMTED2010) with a new land-water mask. Unfortunately, this meant that for Barrow no GlobAlbedo or MODIS_prior data were retrieved.

The tower measurements for Toravere are shown in Figure 59 are slightly higher for most of the year and much higher than any EO retrieval during snow.

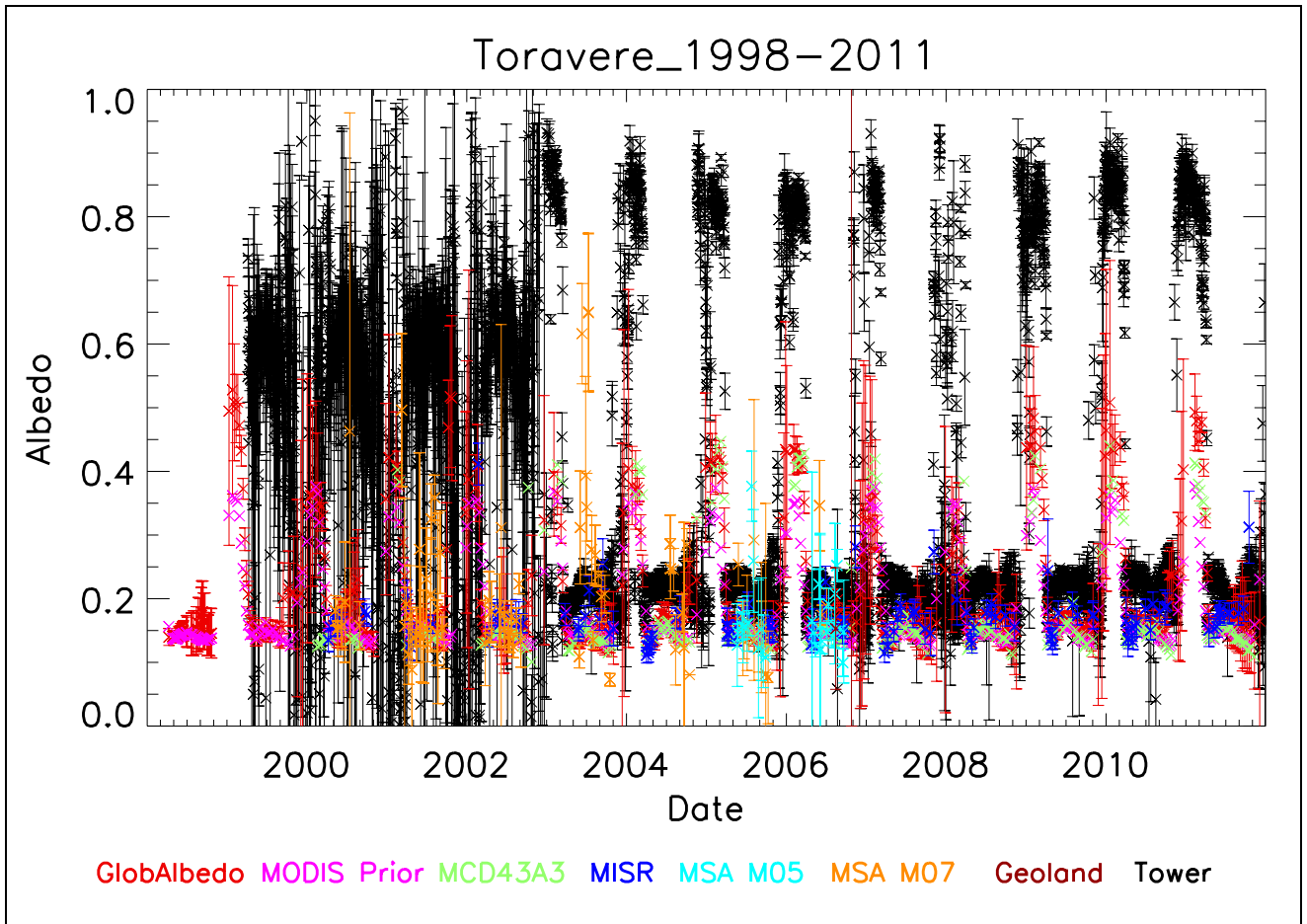
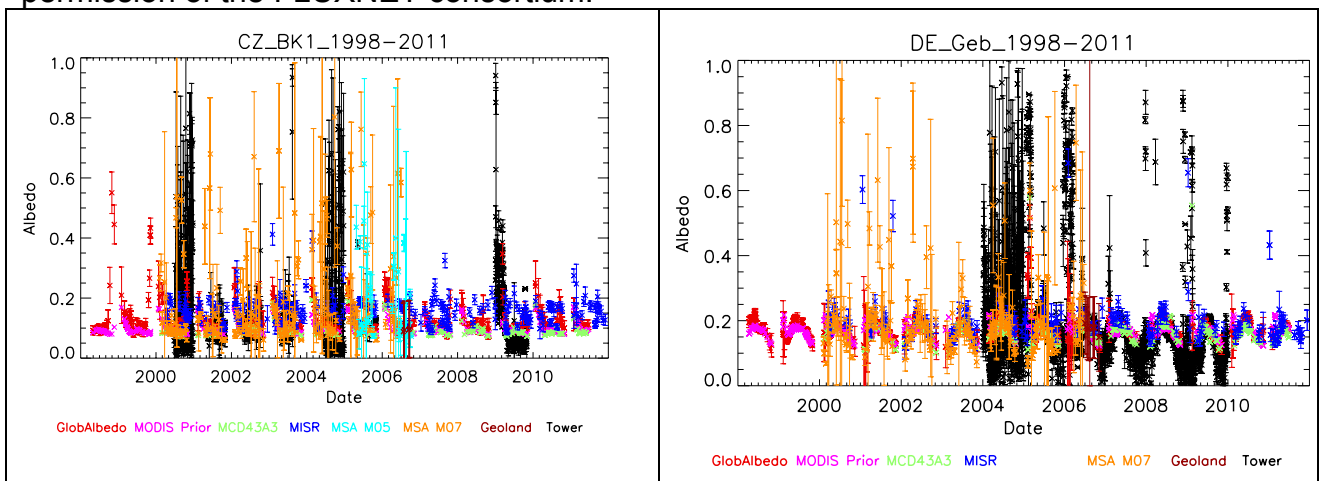
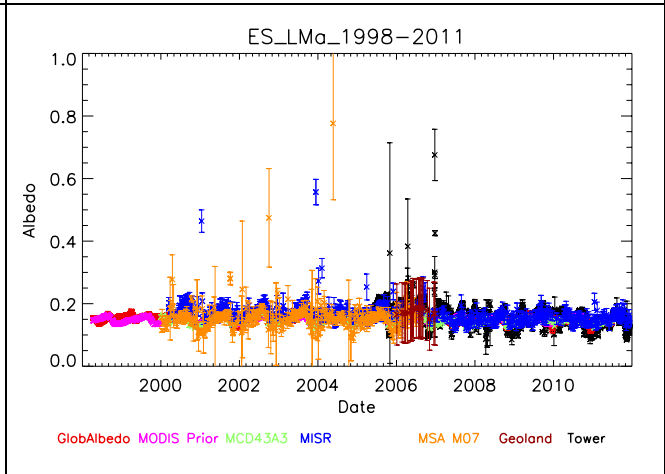
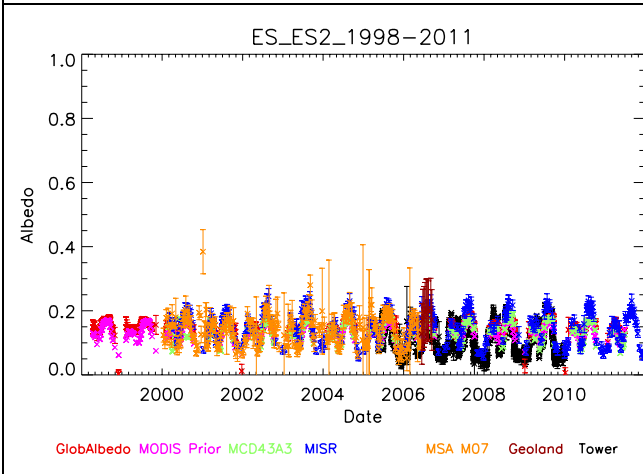
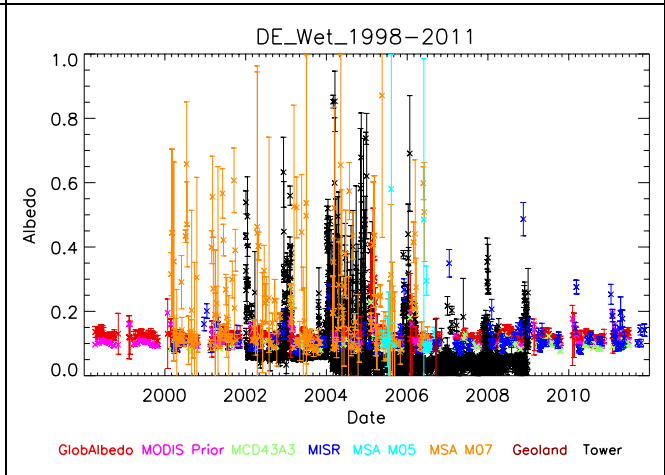
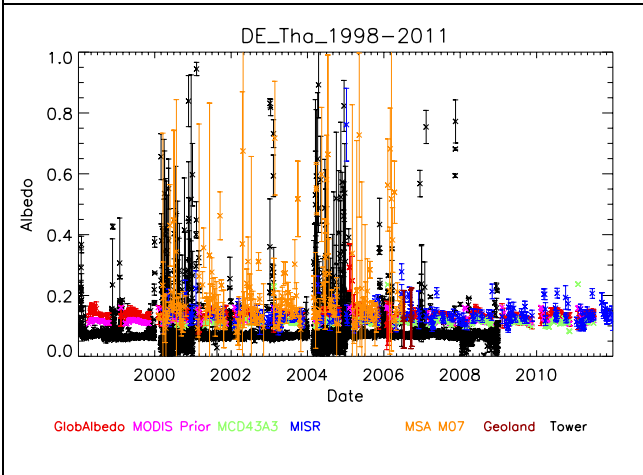
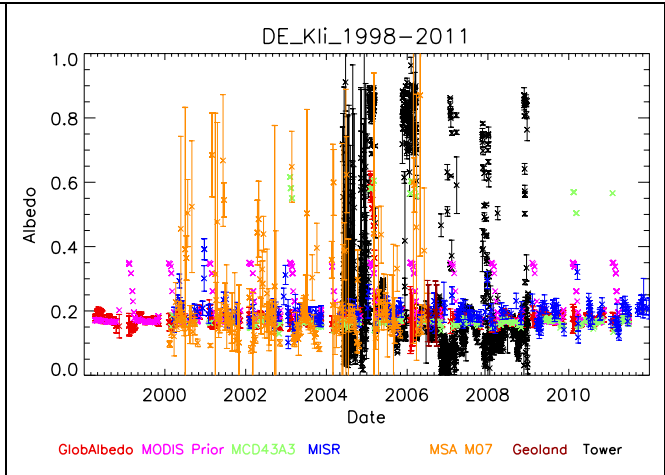
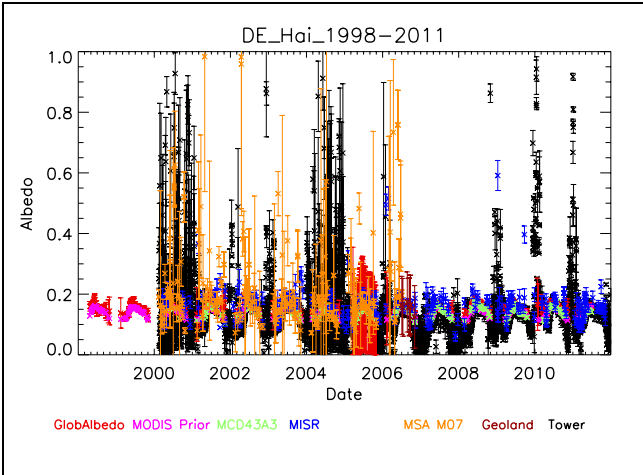
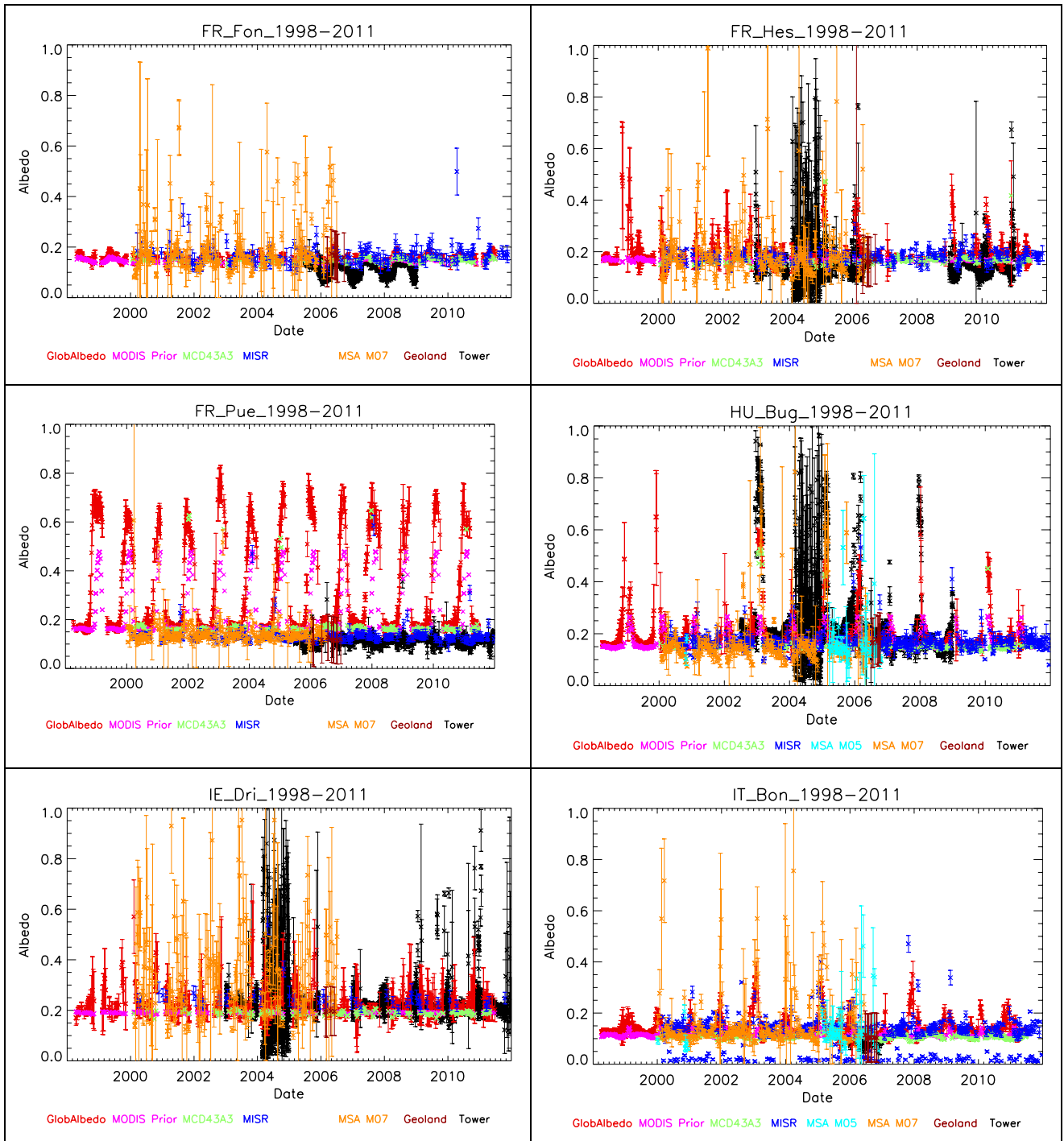


Figure 59. Intercomparison of GlobAlbedo, MODIS priors, MCD43A3, MISR, METEOSAT (M05, 07), Geoland2 (2006 only) and tower albedometer measurements including estimated uncertainties for Toravere

A similar analysis was performed for 20 FLUXNET sites (with data provided by Alessandro Cescatti of JRC Ispra) where METEOSAT data is also available. These are shown below. It should be noted that these plots should not be reproduced anywhere else without the permission of the FLUXNET consortium.







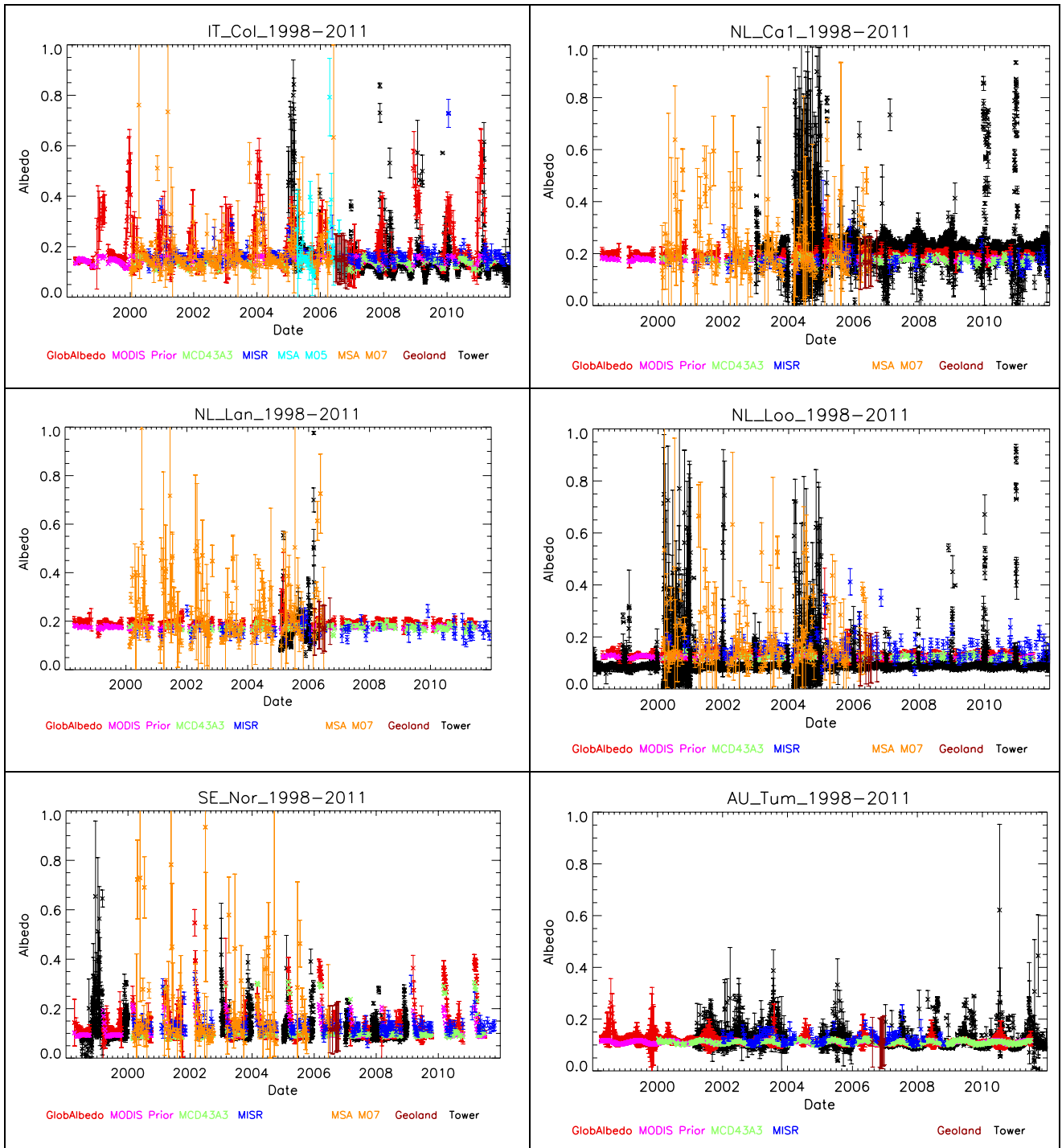


Figure 60. Time series 1998-2011 plots of Blue Sky Albedo from GlobAlbedo (in red), MODIS priors (in cyan), MODIS collection 5 (in green), MISR (in blue), METEOSAT-5 at 0° (in brown) and tower albedometers (in black). The uncertainties are plotted, where available (tower, MISR, GlobAlbedo, METEOSAT)

Once again, for snow beneath trees, the tower albedometers are much higher by usually a factor of 2 compared to the EO-derived values. This is probably due to the fact that the tower albedometers see a lot more ground than those from space. METEOSAT values



also diverge from many of the rest of the other EO values. This especially the case for CZ_BK1, DE_Kli, HU_Bug, FR_Pue, FR_Fon (in winter), SE_Nor and IE_Dri. There is also high noise in the 2004 tower data, even though this was supposedly filtered.

All the tower Blue Sky Albedo (BSA) measurements from all years were compared against corresponding GlobAlbedo, MODIS, MODIS prior and MISR values. These are shown in Figure 68 below. Note the higher correlation for the GlobAlbedo vs Tower than all the other EO datasets. Note also that most of the points do cluster along the one-to-one perfect correlation but the least-squares is too sensitive to noise outside. There is a hint that GlobAlbedo BSA measurements may be unduly affected by aerosol and/or cloud in the 0.25-0.8 range and some of this might come from the MODIS prior as there is no hint of this in the MCD43 datasets.

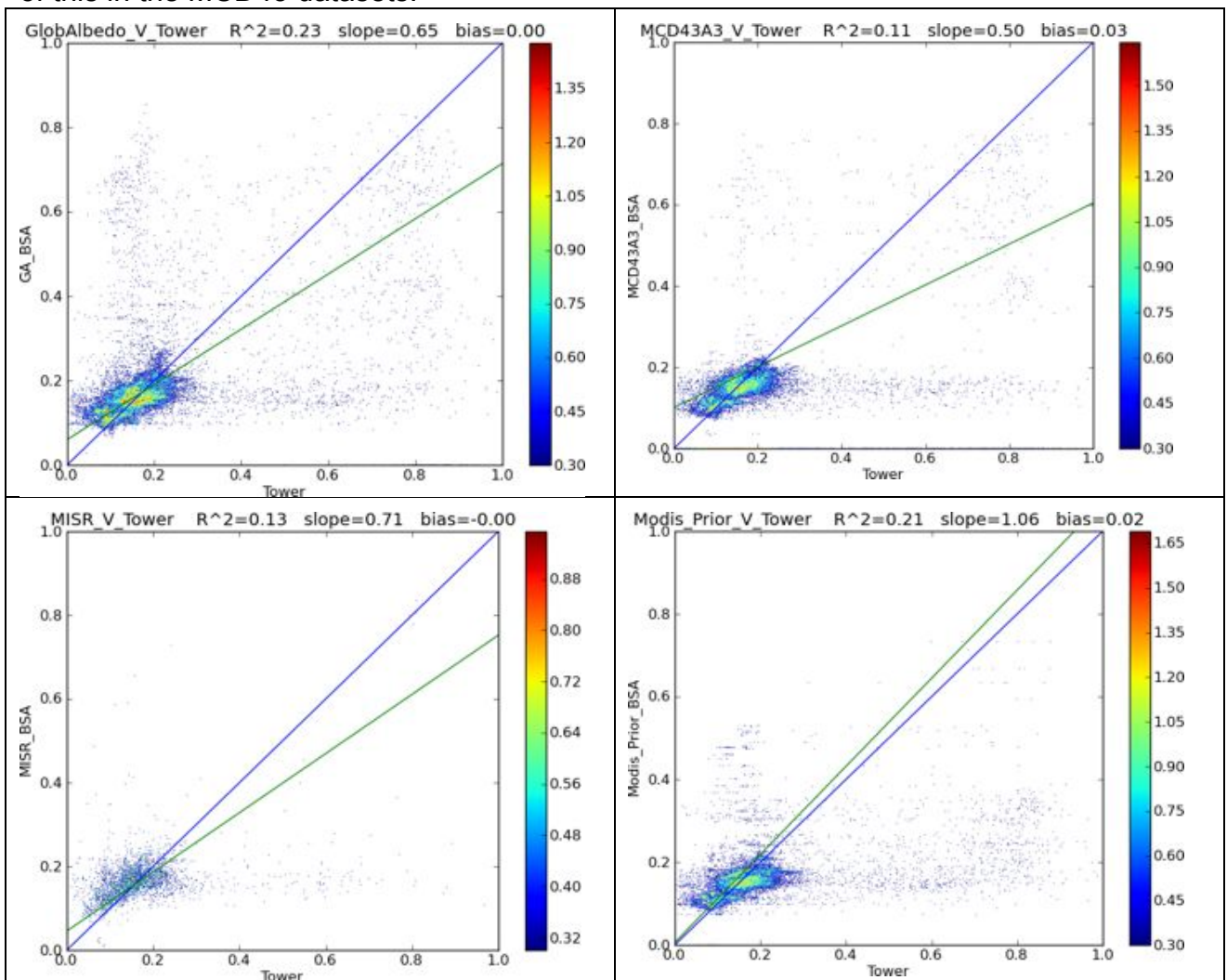


Figure 61. 2D scatterplots and corresponding perfect correlation (blue line) and linear least-squares regression (green line) along with correlation value and slope



11.4.2 GlobAlbedo uncertainties compared with differences with tower values

Given the large inter-comparison dataset, it is feasible to examine how the product uncertainties (for GlobAlbedo and MISR) might map to actual differences with the tower, assuming that the tower measurements represent some kind of “ground truth”.

Taking all the corresponding tuples of matched-up data, an analysis was performed of the EO-tower vs uncertainties, which are shown in Figure 62 below. Neither the GlobAlbedo nor the MISR data are significantly correlated between the estimated uncertainties and the actual differences. The least-squares regression is too poorly correlated to be statistically significant. Note the much smaller range of uncertainties for the MISR data and the lack of any correlation between difference and MISR product uncertainty. Note also the order of magnitude difference between the GlobAlbedo uncertainties and those derived for MISR.

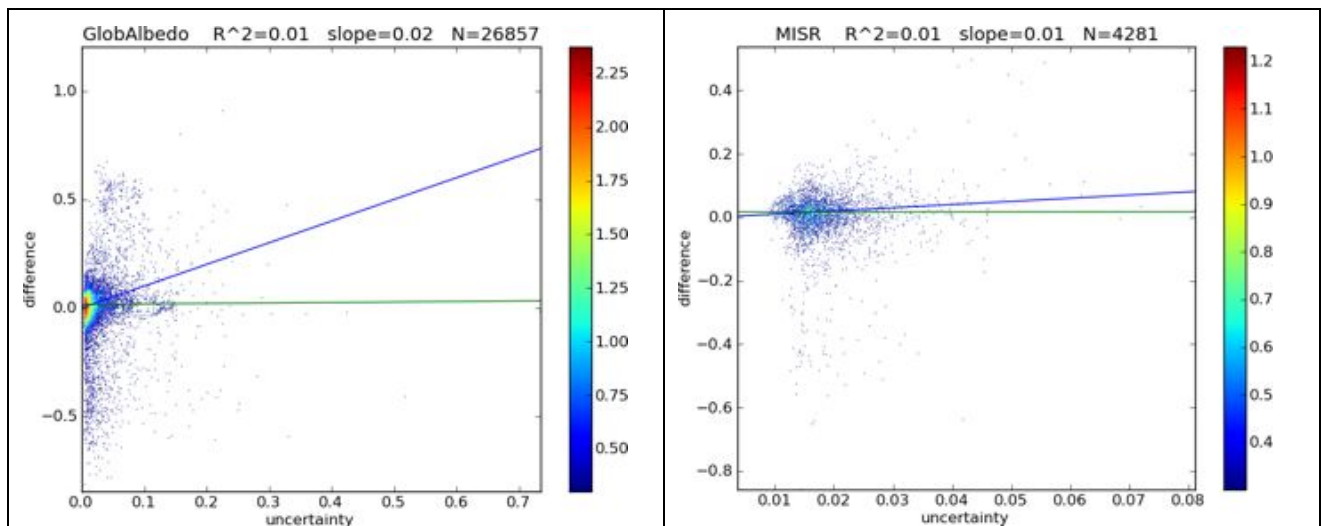


Figure 62. Difference in BSA value for all tower match-ups vs product uncertainties for GlobAlbedo (left) and MISR (right)

The large range of uncertainties hints that there might be an issue with increases in uncertainties as a function of GA BSA values. This is demonstrated clearly in Figure 63 below. This shows there is a clear correlation between GA product uncertainty and GA BSA value with only a hint that below 0.2 that there is a correlatio between GA product uncertainty and differences with the tower measurements.

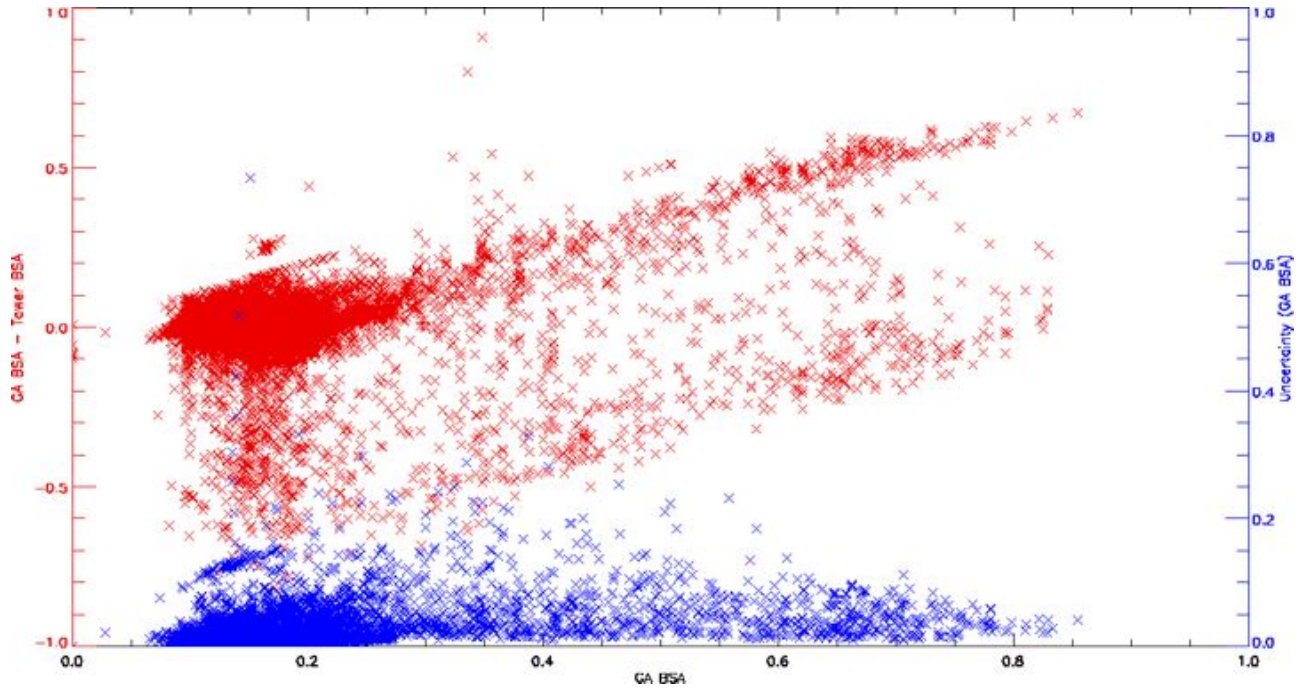
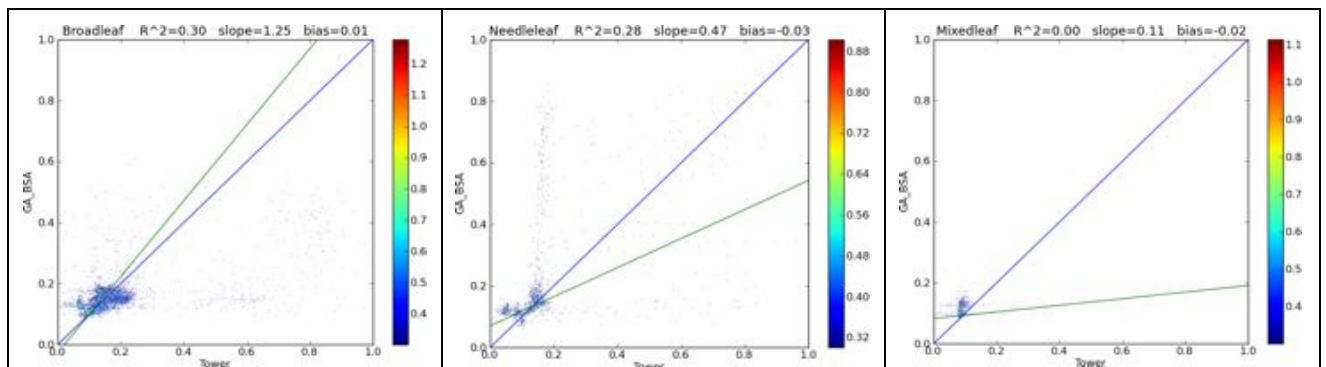


Figure 63. Three-way plot of GlobAlbedo Blue Sky Albedo (BSA) vs both differences with tower (shown in red) and uncertainties estimated in the GA product.

11.4.3 GlobAlbedo values as a function of land cover

For all tower sites the majority land cover class over the tower site was used to classify the albedo values as a function of land cover (bare, broadleaf, grassland, mixed leaf, needleleaf, sparse and water) to compare albedos derived from GlobAlbedo with the tower values. This is shown in Figure 64 for these 6 land covers. Broadleaf and Needleleaf as well as grass all indicate statistically significant correlations. The feature above $GA_BSA \geq 2$ is shown by the needleleaf only.





Title: GlobAlbedo Final Validation Report

Doc. No. GlobAlbedo_FVR_V1.2

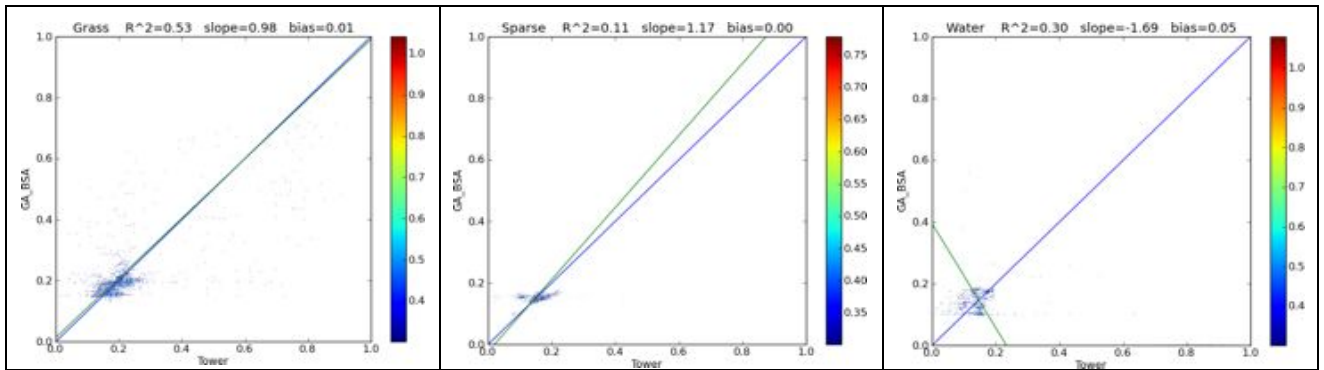


Figure 64. GlobAlbedo Blue Sky Albedos vs Tower measurements for 6 major land cover classes along with their least squares linear fit values

Employing the VIS, NIR and SW albedos calculated by the GlobAlbedo processing chain, 2D scatterplots of VIS vs NIR (and 1D histograms of SW, not shown) have been processed for all of the major land covers (bare, broadleaf, grassland, mixed leaf, needleleaf, permanent snow, sparse, urban and water) observed for all of the areas shown before. An example of this was shown in RD23 for MODIS Collection 4 products, which was re-produced as Figure 7.4-4 in RD9.

Firstly, an example of a false colour composite of VIS, NIR, SW is shown in Figure 65 alongside the GlobCover map at the same resolution and map projection.

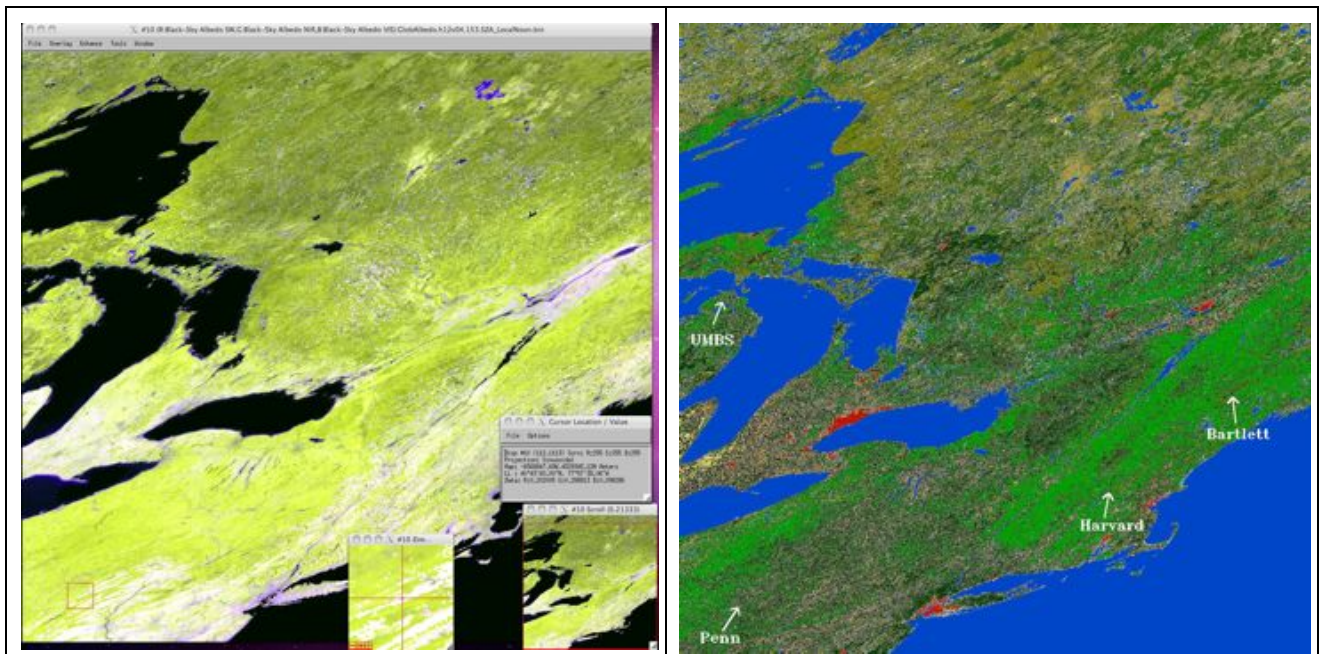
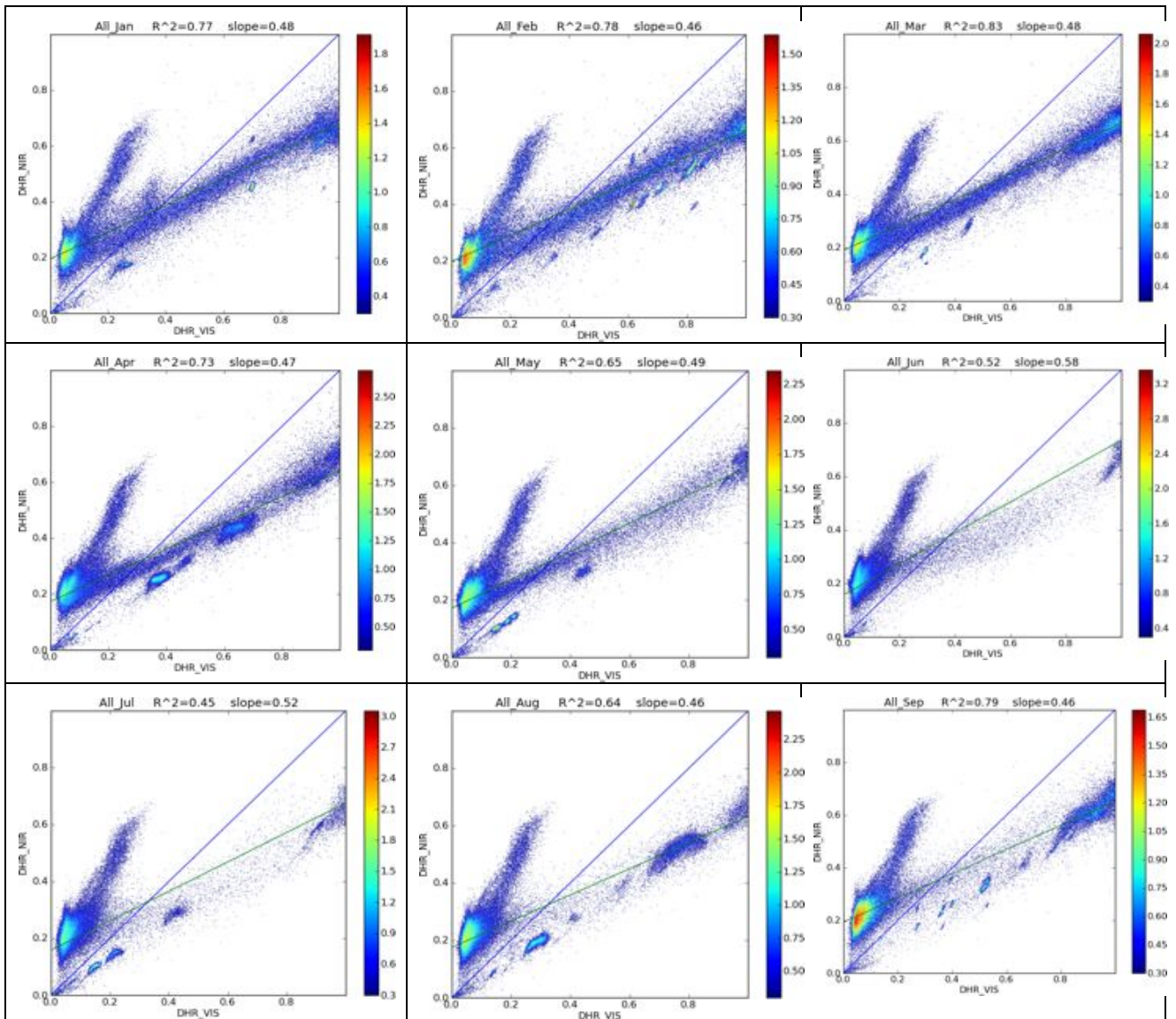


Figure 65. GlobAlbedo FCC (False Colour Composite) of VIS, NIR and SW for DoY=153 (2005) alongside land cover from the GlobCover (2005) dataset resampled onto the GlobAlbedo grid showing the validation site locations.

For each significant land cover class within each tile, a 2D histogram of VIS vs NIR white-sky albedo is plotted for all 12 months through 2005. The resultant plots display snow



effects in January 2005 as well as reflecting the phenology of the vegetation with the central cluster increasing in albedo values in the NIR as the vegetation growth continues. Plots for different vegetation types (e.g. deciduous, evergreen) show very little difference in albedo behaviour. An example of these plots for every month in 2005 is shown in Figure 66 including snow effects in January 2005. The long tail of the off-axis (higher NIR) values are mostly for the BARE class, the dense cluster at the bottom of this axis is mostly from broadleaf and the diagonal (flatter) features are mostly from needleleaf. A number of clusters here across the diagonal appear to be water body features.



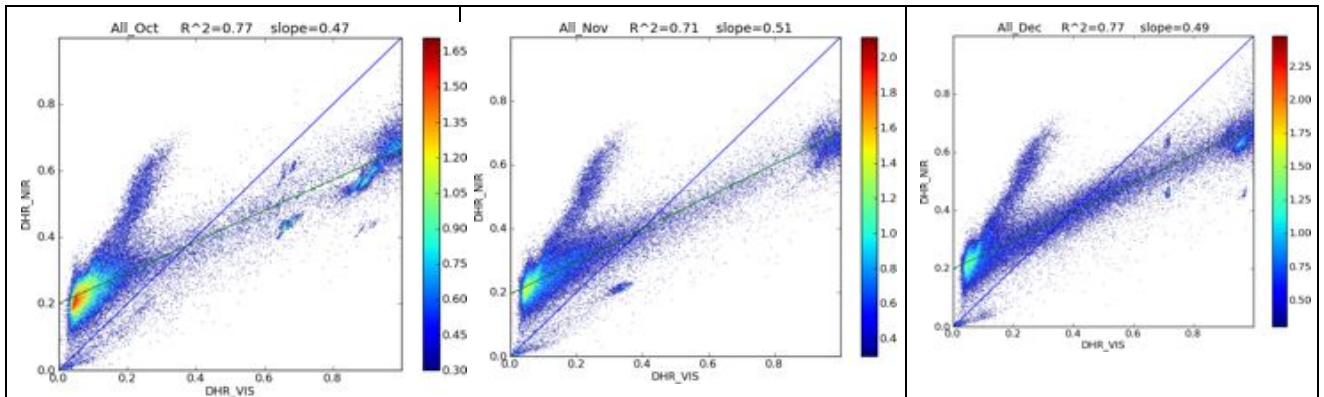
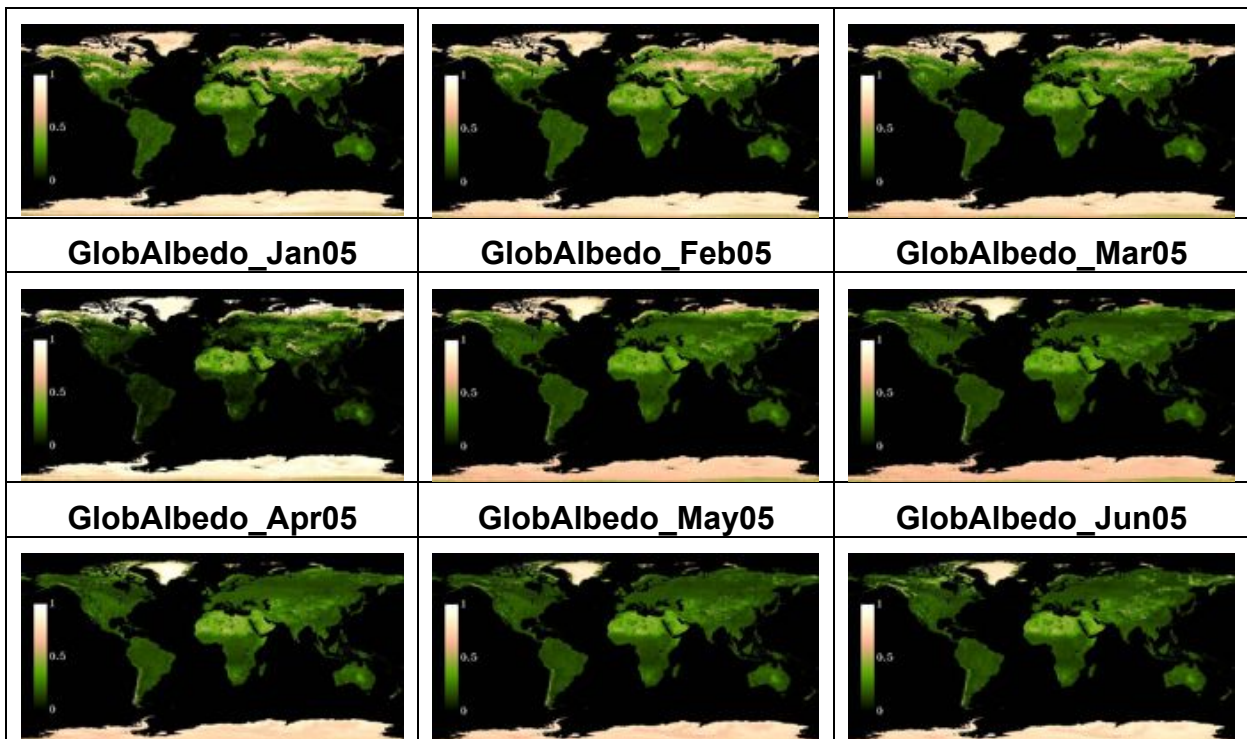


Figure 66. 2D scatterplots of VIS vs NIR for ALL GlobCover Land Cover Classes for every month for all areas between $\pm 60^\circ$ of latitude.

11.4.4 Intercomparison of global albedo results with MISR and MODIS

Using the 0.5° monthly products for GlobAlbedo and MISR and creating a monthly product for MODIS collection 5, the BHR is plotted for every month in 2005 and is shown in Figure 67.

For each and every point-pairs, as shown in Figure 68, an assessment of the statistical correlation (using Pearson measures) was performed for each and every month. The results indicate good agreement, as expected, between MODIS and GlobAlbedo with R^2 values over 0.85. The results for MISR are less good, with $R^2 \leq 0.6$ but given the large number of points still statistically significant at the 5% level. MODIS vs MISR are all close to perfect correlation.





Title: GlobAlbedo Final Validation Report

Doc. No. GlobAlbedo_FVR_V1.2

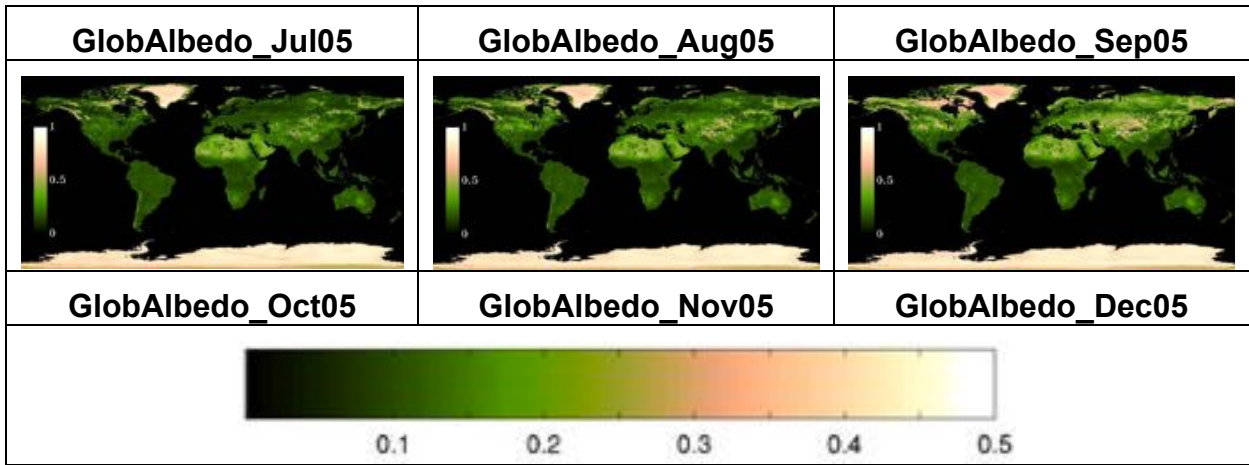
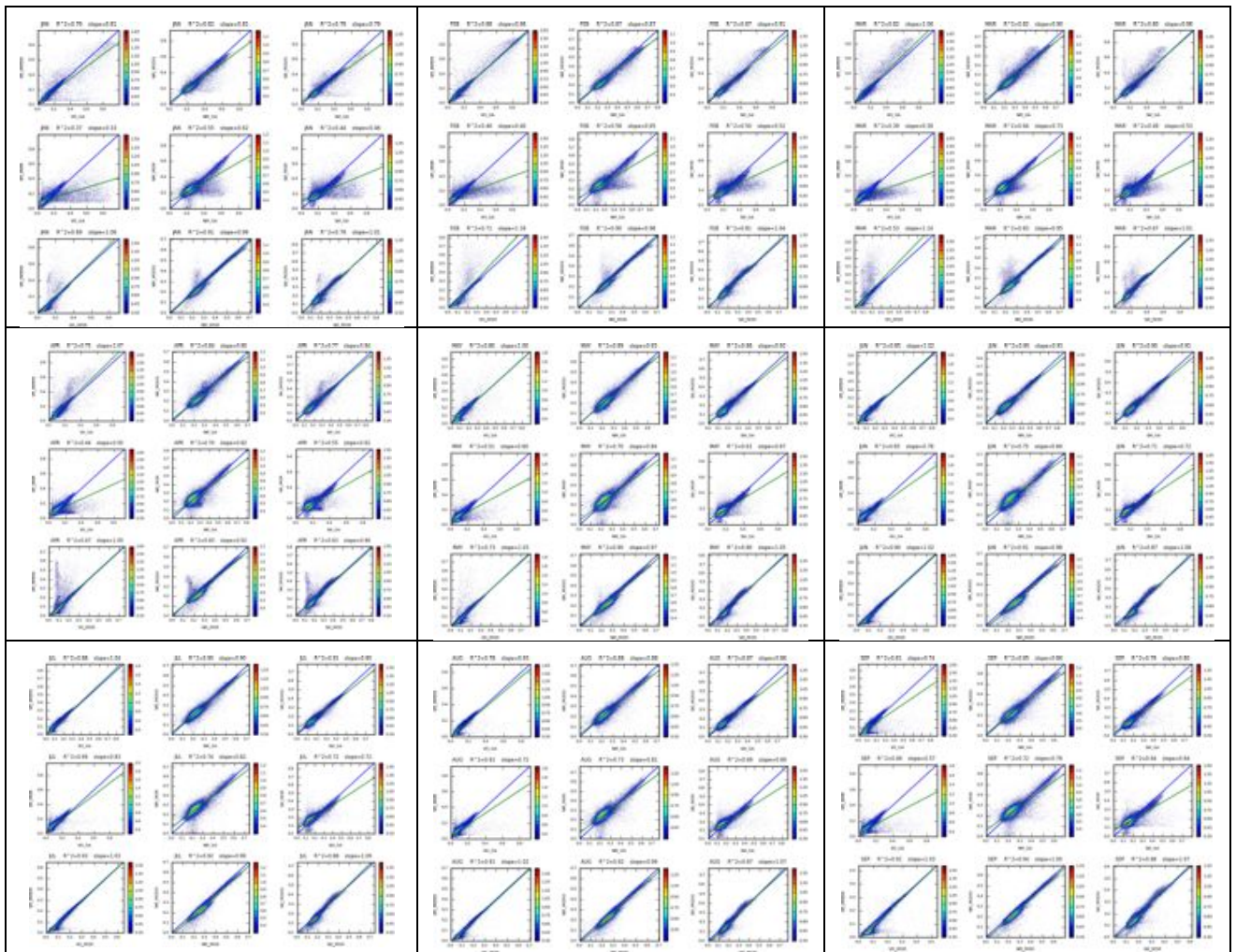


Figure 67. Collage of GlobAlbedo monthly BHR shortwave albedos for every month in 2005 on the same scale.



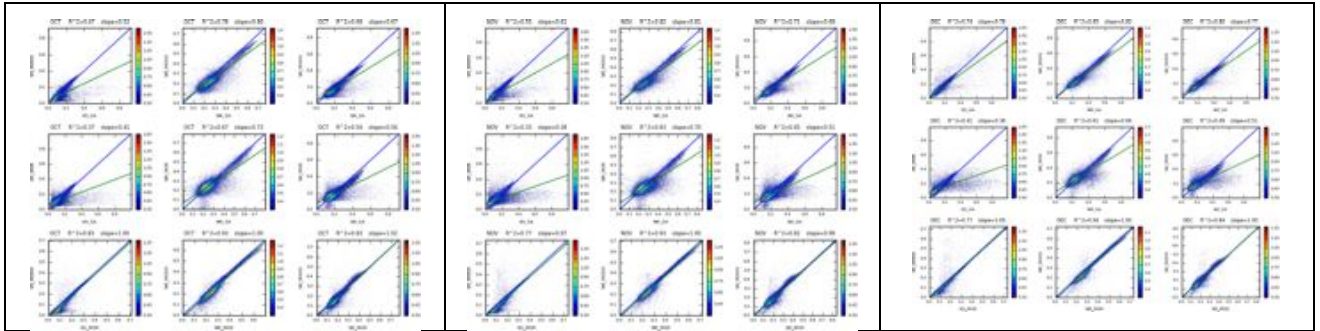


Figure 68. 2D scatterplots of GlobAlbedo vs MODIS (VIS, NIR, SW), GlobAlbedo vs MISR (VIS, NIR, SW) and MISR vs MODIS (VIS, NIR, SW) for every month in 2005.

11.4.5 Triple Collocation to uncover systematic errors

RD26-29 describe the triple collocation technique developed by the meteorological and oceanic community and only recently applied to land surface biophysical variables. This technique requires a very large quantity of triple collocated data for the largest time range possible. This technique has been applied to the global products at 0.5° for GlobAlbedo, MODIS and MISR for the entire time period from 2000-2011 where all three datasets are available and is shown in Figure 69 with corresponding variance histograms in Figure 70.

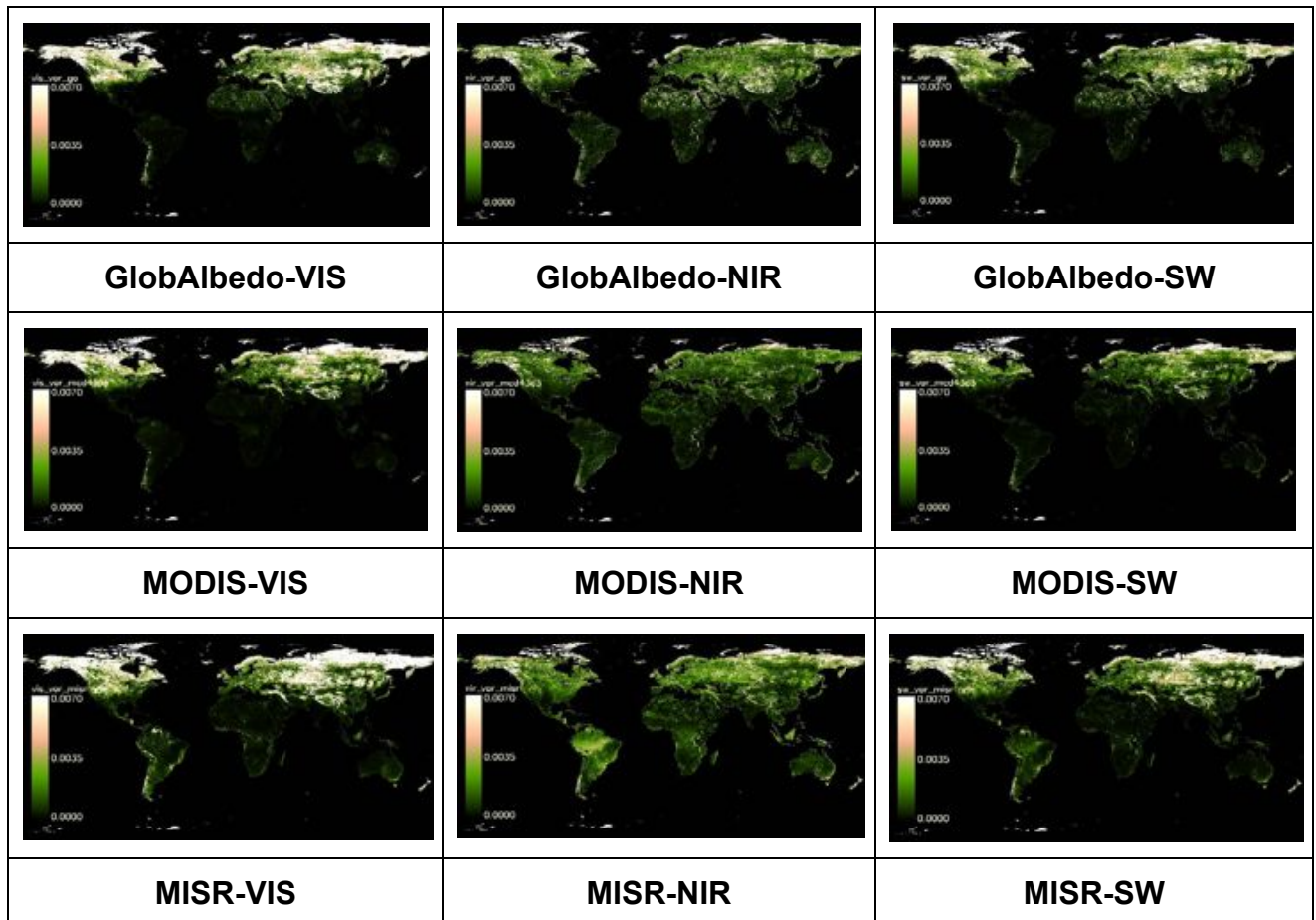




Figure 69. Variance maps for GlobAlbedo (top row), MISR (middle row) and MODIS (bottom row) for Visible (left column), NIR (middle column), SW (right column) using the Triple Collocation technique for all months from 3/2000-3/2011

Using all 144 months as the input, variance maps were calculated for each of the products which are shown in Figure 69. Intriguingly, these variance maps look as if the variance increases from left to right of the composite. The most noticeable difference is for South America which has much higher variance in MISR at SW than either GlobAlbedo or MODIS. The highest variance appear to be where there are the largest problems in differentiating clouds from snow beneath trees at high latitudes. Variance is also much higher at NIR wavelengths.

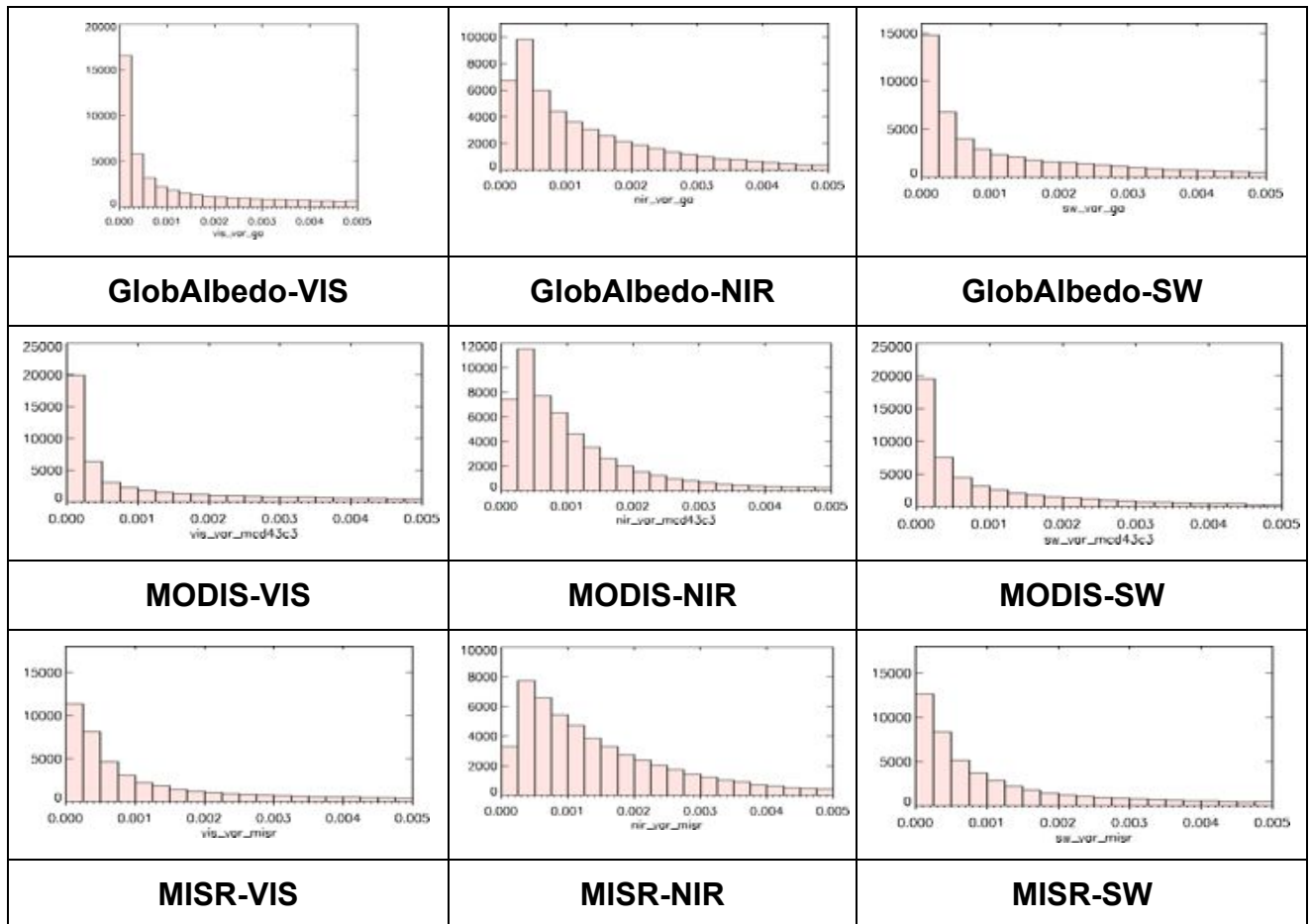


Figure 70. Histograms of Variance for GlobAlbedo (top row), MISR (middle row) and MODIS (bottom row) for Visible (left column), NIR (middle column), SW (right column) using the Triple Collocation technique for all months from 3/2000-3/2011



11.5 Validation summary

GlobAlbedo products have been assessed for 73 tower albedometer sites against instantaneous MISR and composite (8-day) MODIS as well as global products on monthly time-steps against MISR and MODIS. Preliminary conclusions are:

- GlobAlbedo Blue Sky Albedos show clear seasonal cycles and generally agree very well with MODIS, MISR and Geoland equivalents. METEOSAT albedos appear to suffer from noise effects but it isn't clear from where.
- For some tower sites the tower measurements appear to be biased high or low of all the other EO-derived BSA and this is irrespective of
- For “no-snow” and many “snow” products, a few GlobAlbedo-derived Blue-Sky albedo values are in better agreement, than the MODIS priors, with the tower albedometer measurements of the ground area around the towers.
- Snow under trees is significantly under-estimated by all EO-derived albedo values by around a factor of 2 in most cases. The implications of this on climate model parameterisation will be very interesting to assess. It should be noted that in a recent presentation on MODIS Collection 6, snow albedos showed much higher correlation with tower values due to the daily time-step of the 16-day window that MCD43 uses in Collection 6.
- GlobAlbedo albedos are in better agreement with MODIS than MISR. The reason for this is currently not known because the relative entropy does not indicate an overwhelming influence of MODIS priors in the final GlobAlbedo output.
- The estimated uncertainty of each albedo appears to be a reasonable estimate of the actual accuracy. However, the uncertainties are correlated with BSA value in a way not shown by MISR product uncertainties. This deserves further investigation.
- Land cover analysis of albedos indicates that there are differences between bare earth, broadleaf and needleleaf as well as water using visible against NIR broadband albedos for the tiles studied. Tree and grass land cover appears to show higher correlations than other land cover types
- Triple collocation appears to be a potentially useful technique for analysing systematic errors due to issues within the albedos such as residual clouds, snow-cloud contamination and sample numbers. GlobAlbedo, MODIS and MISR monthly BHR shows similar patterns of variance at high northern latitudes.

12 General format

12.1 Ease of data use

The GlobAlbedo data products were straightforwardly ingested into both BEAM and ENVI®. Please see RD1 for further details.



Title: GlobAlbedo Final Validation Report

Doc. No. GlobAlbedo_FVR_V1.2

12.2 Problems encountered

ENVI® does not correctly resample land cover (ordinal) data using majority filtering. This results in an excessive number of zero albedo values when analysing their statistical properties by land cover class. Bespoke software needed to be written and employed.

13 Summary

Validation of intermediate products and the final albedo values has been performed using 11 tiles of GlobAlbedo products at 1km including 73 sites where homogeneous land cover prevails as well as global 0.5° products created for all 12 years (2000-2011). Indications are that the quality of the product is excellent but that the internally estimated accuracy requires further calibration.

14 Recommendations

Further work is required to provide better (and smaller) estimation of uncertainties. Further work is required for the snow products to establish whether this is a pixel masking issue or elsewhere in the processing chain.



Title: GlobAlbedo Final Validation Report

Doc. No. GlobAlbedo_FVR_V1.2

Appendix A: Log of User issues

See UCM-1 report for analysis of user issues.